Doctoral School of Earth Sciences

Relationship between micro-fracture network and karstification in recent (Mecsek) and paleokarst (Gomba) reservoirs

A mikrotörés hálózat és a karsztosodás kapcsolata recens (Mecsek) és paleokarsztos (Gomba) rezervoárokban

PhD Thesis

Author

Márton Bauer

Supervisors:

Dr. Tivadar M. Tóth

Dr. Béla Raucsik

Department of Mineralogy, Geochemistry and Petrology

Faculty of Science and Informatics

University of Szeged

2016

Szeged

Table of Content

List of Figures

List of Tables

Chapter I

Introduction

1.1. The actuality of this research

Exploitation of hydrocarbons (HCs) and water, the two most important fluids for the global economy is connected to subsurface rock bodies. The research of these reservoirs requires both thorough geological knowledge and technical equipment. Fluids (liquids and gases) are basically trapped in pore space of diverse rock types that changes dynamically both in time and space.

The pore space of the rocks is formed by effects of several processes. The porosity is an important derived property of sedimentary rocks that are controlled in part by the textural characters (such as grain size, shape, packing). Because the porosity is a fundamental controlling parameter in the movement of fluids through rocks and sediment, it is of particular interest to petroleum geologists, and hydrogeologists. The porosity (and permeability) also play role in the diagenesis of sediments by regulating the flow through rocks of fluids that promote dissolution, cementation, and authigenesis of minerals.

According to Boggs (2009) classification, porosity may be either primary (depositional) or secondary (postdepositional). Primary porosity can be of three types: (1) intergranular or interparticle pore space that exists between or among framework grains, such as siliciclastic particles and carbonate grains; (2) intragranular or intraparticle pore space within the particles, such as cavities in fossils and open space in minerals; (3) intercrystalline pore space between chemically formed crystals, as in dolomites. Secondary porosity may include (1) solution porosity caused by dissolution of cements or metastable framework grains (feldspars, rock fragments) in siliciclastic sedimentary rocks or dissolution of cements, fossils, framework crystals in carbonate or other chemically formed rocks; (2) intercrystalline porosity arising from pore space in cements or among other authigenic minerals; (3) fracture porosity, owing to fracturing of any type of rock by tectonic forces or other processes such as compaction and desiccation.

The reservoirs, where a fracture system provides storage space and flow paths, have ever growing economic value nowadays. The most common condition of fracture formation is that the rock mass should suffer brittle deformation under its tectonic

evolution. Brittle deformation can evolve only in well-cemented, compacted rocks. Generally, the older rock masses have higher probability to intense deformation and so often contain several fracture generations.

In Hungary, apart from the clastic Miocene and Pliocene sedimentary reservoirs of the Great Plain (like Algyő) the most significant hydrocarbon (HC) deposits are related to the basement metamorphic rocks and granitoids (like Szeghalom, Mezősas, Pusztaföldvár, Battonya), as well as to the Mezozoic carbonates that can be found several kilometres deep (like Szeged, Üllés, Zsana).

The HC explorations started in the Hungarian Paleogene basin in the early 2000s. Reservoir rock types include Paleogene sandstones, limestones, and marls. The principal reservoirs are the Eocene Szőc Limestone and sandstone bodies of the Oligocene Kiscell Formation, some of which are tuffaceous. Productive reservoirs also occur in the Triassic limestones of the basement (Dolton 2006). The most traps in the Paleogene basin are of the structural type, where also traps in the Mesozoic basement beneath the Tertiary unconformity have hydrocarbon potential (Dolton 2006). Although the basement is heavily fractured, the fracture network and its relationship with the various lithologies and positions of the unconformities are poorly known.

One of the most important HC field in the Hungarian Paleogene basin is the Gomba field which is related to the Eocene clastic rocks and the Triassic basement. The production of the Gomba field started in 2003 and actually it has outstanding capacity and plays very important role in the domestic oil production. The field is related to a buried limestone high divided by normal faults, a typical structural form in the basement of the Paleogene basin. So, a detailed lithological and structural knowledge about the Gomba field could lead to localize more similar fields in the region.

1.2. Outlook

1.2.1. Carbonate fluid reservoirs

From geological point of view, reservoirs mean porous, permeable rock masses containing fluids, especially HC or water, in commercial quantities (Ahr 2005). Under appropriate conditions, these reservoirs can develop in several rock types but the highly significant ones are the reservoirs in sandstones and carbonates, both concerning abundance and productivity.

There are several periods in the geological past when carbonates were formed in huge quantity, but the most important reservoirs can be found in the Ordovician and Mesozoic carbonate masses, worldwide. Geographically, most deposits are located in the Middle-East, Libya, Russia, Kazakhstan and North America (Ehrenberg and Nadeau 2005), but the Hungarian ones also have local significance (Dolton 2006) (Fig. I.1).

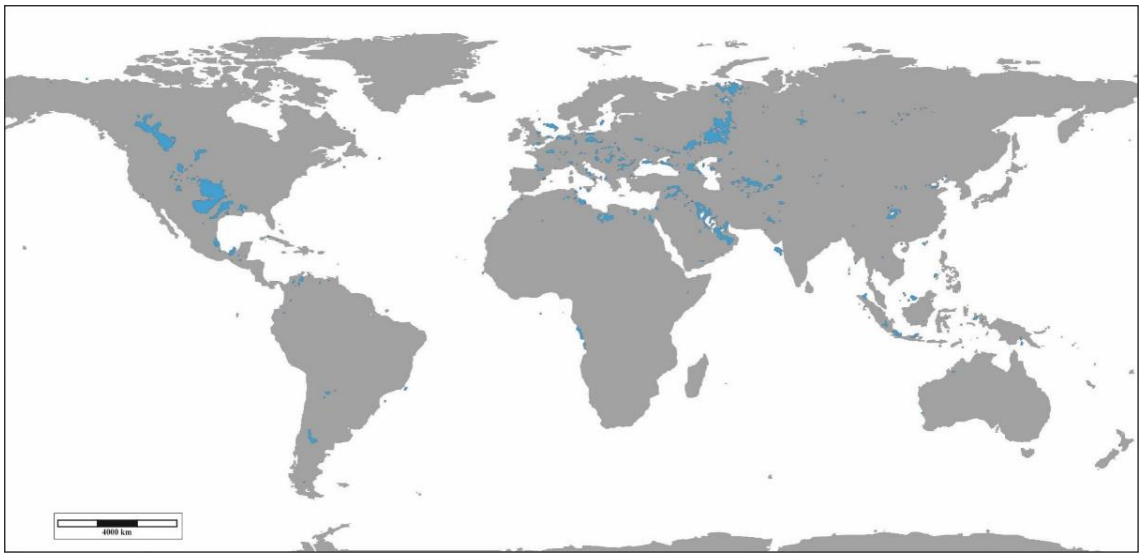

Fig. I.1: Carbonate hydrocarbon reservoirs on the Earth (According to Ehrenberg and Nadeau 2005)

The first exposed field in carbonate rock was the Heide field in Germany in 1856, the yield of which was as high as 1 MMBO (Million Barrels of oil), still, the exploration of the US Lima-Indiana trend in 1884 was the real breakthrough (Keith and Wickstrom 1991). Nowadays about 50–60% of the produced gas and oil comes from carbonates globally (e.g. Rochl and Choquette 1985), moreover the biggest explored oil deposit in the world (Ghawar, Saudi Arabia) and also the biggest known gas site (North Field/South Pars straddling the Quatar/Iran border) are carbonate reservoirs as well.

Carbonate and sandstone reservoir-types differ from numerous aspects. The two main differences lay in the dinamics of the sediment deposition (allochthonous in the case of sandstones and autochthonous in the case of many carbonates) and in the chemical reactivity of the rock-forming minerals as carbonate minerals are much more reactive than sandstone minerals (quartz, feldspar, mica) (Ehrenberg and Nadeau 2005). The chemical activity of the rock forming carbonate minerals (calcite, aragonite and dolomite) has huge effect on the diagenetic processes and the storage capacity, too. While the impact of eogenesis is subordinate in cementation of sandstones, in the case of carbonates it often leads to extensive early lithification which can dramatically change the primary porosity (Ehrenberg and Nadeau 2005).

As a first approximation, the spatial heterogeneity of carbonate reservoirs is higher than that of sandstone ones which results in the fact that production rate of carbonate reservoirs is generally lower. In the carbonate rocks, the several generation of cement phases decrease the effective porosity. An advantage of the carbonate rocks as reservoirs is that they can be heavily fractured which can increase the effective porosity. Recognition of the fracture system is essential for carbonate reservoir studies. Certain features of the fracture system, such as connectivity of the fractures, fundamentally determine the permeability of the reservoir. Spatial density and geometric features of the fractures, like length, aperture and shape can build up huge interconnected reservoir blocks. In another cases fractures can even isolate areas from the hydraulic stream.

An additional important feature of the carbonate reservoirs is that their porosity can be highly modified by dissolution due to diverse acid fluids, like carbonic acid. Dissolution usually takes place along the fractures and widens them. At low flow speed, usually cementation is carried out, while in the case of higher permeability and higher flow speed, dissolution dominates (Singurindy and Berkowitz 2005). This process acts as a positive feedback: the broader the fracture the bigger the degree of widening. In reservoir scales this process will result in zones with extremely high porosity and permeability along the fractures, which, in fact, can be treated as cave voids or cave systems.

According to Shepherd (2009), the carbonate reservoirs can be grouped into the following six typical forms based on differencies in dynamics of carbonate host rock and reservoir-forming processes: (1) organic build-ups including reefs, (2) grainstone shoals on shelves, (3) subtidal and intertidal complexes, (4) leached zones below unconformities, (5) chalk and (6) karst and paleocave systems. Hereafter only the last type will be introduced in detail.

1.2.2. Karstic and Paleokarstic fluid reservoirs

Despite all exploration and recovery difficulties, what mainly comes from the heterogeneity of the karstic reservoir, their economic potential is ever-growing. Plenty of the fields on the American continent (Puckett field/Texas, Late Ordovician, Yates/Texas – Perimian, Golden Lane fields (Mexico) – Lower Cretaceous) and also a high majority of the Chinese stores are in paleokarstic reservoirs (Zhang and Liu 2009). Even if they are essential, karstic and paleokarstic reservoirs play a special role among carbonate reservoirs, mainly because of the special behaviour of porosity and permeability.

According to Zhang and Liu (2009) karstic reservoirs have specific attributes. During the drilling, the ROP (Rate of Penetrating) is typically high but can change suddenly. Also the caliper may increase suddenly, core recovery rate is low and the drill bit blows off occasionally. Partial or total mud loss is also typical during the drilling of paleokarstic reservoirs. Natural gamma and neutron porosity rate is typically high, while the different resistivity values and the rock density show low values. Cores brought to the surface often have steep-angled fractures, dissolved and other weathered surfaces and breccias of different types.

1.2.3. Classification of paleokarsts

Nowadays two approaches exist on how to classify paleokarsts. The earlier one is that of James and Choquette (1988), who have separated three distinctive groups on stratigraphic grounds. The more familiar classification scheme of Esteban (1991) is based on the link between karstification and different order unconformities, i.e. it applies a sequence stratigraphic approach.

1.2.3.1. James and Choquette (1988) classification

- Synsedimentary paleokarst: karstic phenomena of this group are of the same age as the sedimentation process itself, and they are associated with the cyclic formation of the carbonate platform. The karstic surface during the formation is no more than cm/dm range and it is mostly formed on the weakly or not at all lithified sediment. Often the subsurface solution forms are only of micrometer size.
- Local paleokarst can be formed if the edge of the carbonate platform gets temporarily exposed. Depending on exposure time, even significant subsurface forms may be developed but they usually are laterally pinched out within a relatively short distance.
- Regional paleokarst is evolved if a long exposure period is existing. Karstic forms cannot be linked to the sediment formation of the carbonate material in this case. The presence of the solution forms affects large areas both vertically and laterally. These cavities frequently are filled by the dissolution remnants or allogenic debris.

1.2.3.2. Esteban (1991)’s classification

The basis of the Esteban (1991) classification system is presence of unconformities of different orders. Discordance surface means a time-gap which can be originated either due to erosion or due to interruption of sedimentation. Unconformities can be grouped hierarchically depending on the size of the stratigraphic hiatus. Depending on the extent of the hiatus, different types of karsts can form (Table. I.1).

STRATIGRAPHIC DISCONTINUITIES		ORDER	TIME GAP	CORRESPONDING STRATIGRAPHIC UNIT	KARST CHARATHERISTIC
UNCONFORMITIES Composite	Mega - unconformity	1 inter-regional	200	Mega-sequence	**General karst** Longer exposure time Stable minerology Important deep phreatic zone Secondary and fracture porosities predominate Abscence of marine mixing zone effects Presence of hydrotermal mixing
	Super - unconformity	2 inter-regional	4-12	Super-sequence	
UNCONFORMITIES Single	Regional unconformities (sequence-boundaries)	3 regional	~1	Depositional-sequence	
CONFORMITIES	Syntectonic unconformity	3-4	0.01-1	Rotational onlap-offlap	
	Boundary of shoaling cycles	4	0.01	Parasequence	**Caribbean type karst** Short exposure time Minor deep phreatic zone Unstable carbonate minerology Shallow burial Affected by marine mixing
	Bedding planes	5	0.001	Bed	No recognizable karstification

Table I.1: Classification of the unconformities associated to paleokarsts, and the typical karst character. (Based on Esteban 1991)

1.3. The aims and structure of the dissertation

The dissertation studies the connection between karstic forms and the features of the fracture system in a recent and in a paleokarstic reservoir in Hungary. At first, a well-known area with diverse surface and subsurface forms in the Mecsek Mts. is studied. Based on experiences of this surface area, the dissertation also deals with the petrological and reservoir geological features of the important Gomba hydrocarbon field.

This latter region is of high priority in the domestic hydrocarbon production. Its examination started in the late 1990s, while production has been going on since 2003, within the scope of MOL Plc. The first interpretations of the reservoir rocks (unpublished MOL report) introduce the area as a fractured karstic reservoir without understanding the impact of karstification on the reservoir features. Based on these early results, the key aim

of the dissertation is to explore the relationships between the karstification and the microfracture network in the Gomba field.

The work includes two parts. The first section applies the relationship between the fracture parameters and the karst forms in the Mecsek area; the second one is related to the Gomba field petrology and its fracture network. The main questions to answer are the followings.

1) Can the fracture network contribute to compartmentalization a reservoir?
2) How do spatiality of fracture network geometric parameters and the locality of the karstic objects relate to each other?
3) What fracture geometrical parameter has the most important effect on the spatial distribution of the karstic objects?
4) Can fracture system serve as a HC migration pathway in the Gomba field?
5) Has fracture dissolution and karstic processes any effect on behaviour of the Gomba field?
6) How one can localize traces of karstification in the carbonate rocks of the Gomba reservoir?

The forthcoming sections represent a selection of published and submitted papers about the research of the fracture network and karstic phenomena of the Western Mecsek study area as well as about the petrography and fracture network modelling of the Gomba field.

Following this brief introduction (Chapter I), each part of the dissertation represents different, individual stages of the research. Chapter II presents a case study from a well-documented karstic area from the Western Mecsek. In this section the fundamental fracture network features (density, aperture and length distribution) are quantified. Additionally, relationship to numerous observed karstic phenomena, e.g. cave entrance locations, cave passage orientations, doline and doline chain locations is discussed. Chapter III gives a detailed petrological description of the carbonate beds of the available core samples from the Gomba reservoir. In this section, beyond the detailed description of the rock types, a diagenetic history scheme and a genetic model of the fracture generations and vein filling are deducted. Additionally, an attempt is made to reconstruct the main evolution phases of the reservoir and the potential breccia-forming processes are overviewed. Chapter IV presents detailed characterization of the fractures in micro- and macro-scales. The calculated fracture parameters are applied to create Discrete Fracture Network models which describe the fracture network in reservoir scale surrounding two

wells. In Chapter V the main results and conclusions of the research are presented. A reference list of all chapters can be found in Chapter VI.

Chapter II

Modeling microfracture geometry to asses the function of a karst system (Vízfő spring catchment area, Western Mecsek Mountains, Hungary)

Márton Bauer
Department of Mineralogy, Geochemistry and Petrology
University of Szeged, Szeged, Hungary
baumart87@gmail.com

Tivadar M. Tóth
Department of Mineralogy, Geochemistry and Petrology
University of Szeged, Szeged, Hungary
mtoth@geo.u-szeged.hu

Geologica Croatica
Vol 68/4, 11-23 (2015)
DOI: 10.4154/GC.2015.02

2.1. Introduction

Karsts are geologically significant for a number of reasons. Caves have provided shelter, and karstic springs have offered good quality drinking water since the beginnings of mankind. Approximately 25% of the people on Earth use karst water daily or live in or near a karstic region (Romanov et al. 2004). In addition to hydrogeological and environmental aspects, karsts are also significant for hydrocarbon exploration. As conventional hydrocarbon deposits diminish with the growing energy demand, the hydrocarbon industry is paying more attention to the exploration of fractured karstic reservoirs (Lun et al. 2010; Feng et al. 2013).

Karstic evolution is a complex process, and the development of these areas is influenced by many factors in both space and time, which may result in an extremely heterogeneous structure and morphology. The quantity and quality of precipitation, the ever-changing surface and the subsurface geomorphology and biological processes are equally important factors. Lithological and structural parameters are important parameters that are more constant in space and time than biological or environmental factors. In numerous limestone bodies where the syngenetic primary porosity has drastically decreased during diagenesis, the main flow paths are fractured structures that developed through different deformation events. They are linked to other "inception" horizons, whose size, form and permeability can greatly change during karst formation. According to Palmer (1991), 57% of karstic conduits is related to bedding planes, 42% to fractures and 1% to the rock matrix.

One of the main objectives of karst research is to understand the spatial dynamics of karstic processes that increase or decrease pore volume. In the early 1990s, karst system modeling was mainly used to reconstruct individual fracture developments (e.g., Palmer 1991; Dreybrodt and Gabrovšek 2000; Bauer and Liedl 2000). From the mid-1990s, technology enabled 2D models to also be used (Kaufmann and Braun 1999, 2000; Bauer et al. 2002, 2003; Kaufmann 2003a,b; Dreybrodt et al, 2005). We can now construct 3D numeric models, even though this is a complex, several-step process. Three-dimensional numerical models are typically based on three key aspects: a dissolution algorithm, a flow and/or transport model, and an algorithm to reconstruct the spatial geometry of fracture networks. Our paper focuses on the last task.

The aforementioned studies, depending on their purpose, were interested in reconstructing initial fracture geometry (e.g. Jacquet et al. 2004; Kaufman et al. 2010;

Borghi et al. 2012; Pardo-Iqúzuiza et al. 2012). Several works discuss some regular structure or formula to which the spatial net is approached. The development of computer technology has made it possible to realistically reconstruct more complex geometries, such as karstic networks. The fundamental precondition of a near-reality reconstruction is that the input parameters of the model should be based on measurable factors from the known area. Karstic objects are fractal-like objects (e.g., length distribution of caves, (Curl 1986)), so their geometric parameters given in a particular size range can be scaled to both smaller and larger size ranges. It is also notable that, because the quantity and quality of the perceptible factors are variable within a given range, very small and very large forms may not necessarily fit spatial reconstructions. It is best to sample the range of cores, hand specimens and cave passages, and the latter was where Pardo-Iqúzuiza et al. (2012) started. Because more geometric information can be obtained by analyzing microfracture networks in less developed or speleologically less explored karsts (e.g., karstic hydrocarbon reservoirs), we surveyed the parameterizability of these fractures.

Individual fractures that co-occure, such as karstic forms, can appear in a wide range of scales from submicroscopic to 100 m (Allègre et al. 1982; Ouillon et al. 1996; Turcotte 1997) and their features can be compared across different ranges. The structural data of the fractures and microfractures obtained in surface explorations, caves and boreholes can provide important information about large-scale structures, faults and fault-zones. The qualitative features and the values of the measurable parameters (size, spatial density) depend on the petrographic features of the given deformed rock type, e.g., its mineral composition, grain size distribution, structure and former orientation. The physical circumstances in which the deformation takes place also play a vital role; the primary significance of the stress field is substantially modified by the lithostatic pressure, temperature and the rock's fluid content. The resulting fracture system, as a geometric object consisting of individual fractures, is created as the cumulative result of all these forces. Although under the Coulomb criterion it is possible to prove the genetic connection between the stress field and the geometry of the fracture system, the former still cannot be deduced from the latter (Campos et al. 2005). Therefore, the simulation algorithm (dealt with geometry), unlike several others (e.g. Olsen 1993; Renshaw and Pollard 1994; Riley 2004), does not examine the evolutionary process of the fracture network in the given stress field, but aims to reconstruct the complex geometry.

The karstic block of the Mecsek Mountains in SW Hungary has been investigated for several decades. The purpose of our paper is to supplement the experimental (dye

tracing, well data, speleological observations, etc.) modeling results of the fracture system to help understand how the main karst system of the mountains (Vízfő) functions.

2.2. Geological background

The most important rock types for karstification in the western Mecsek Mountains are the diverse Triassic formations, particularly the Anisian Lapis Limestone. The oldest Triassic formation in the area is the Jakabhegy Sandstone Formation (Barabás and Barabásné 2005), which is composed of variations of quartz-cemented, cross laminated polymicritic sandstones and conglomerates, followed by the Hetvehely Dolomite Formation, with a total thickness of not more than approximately 40 meters (Haas et. al. 2002). Next is the Lapis limestone, a highly fractured rock, with relatively high clay and organic content; this formation is thinly layered, sometimes bedded and formed in an inner-ramp facies. Because of the syn-sedimentary deformation events (syn-sedimentary faults) and post-sedimentary faults, the original stratification is highly disturbed and can only be traced in blocks of some tens of meters.

Because of Alpine orogenic movements during the Cretaceous, the whole sequence is strongly folded (Benkovits et al. 1997; Csontos et al. 2002). The study area is located on the northern limb of the main fold (Fig. II.1). The Mecsek Mts. were raised and thrust on its northern foreground and partially folded the young sediments (Sebe et. al. 2008). Although the present structure of the mountains was determined by these Mesozoic movements, the karstic processes were more strongly influenced by younger tectonic events.

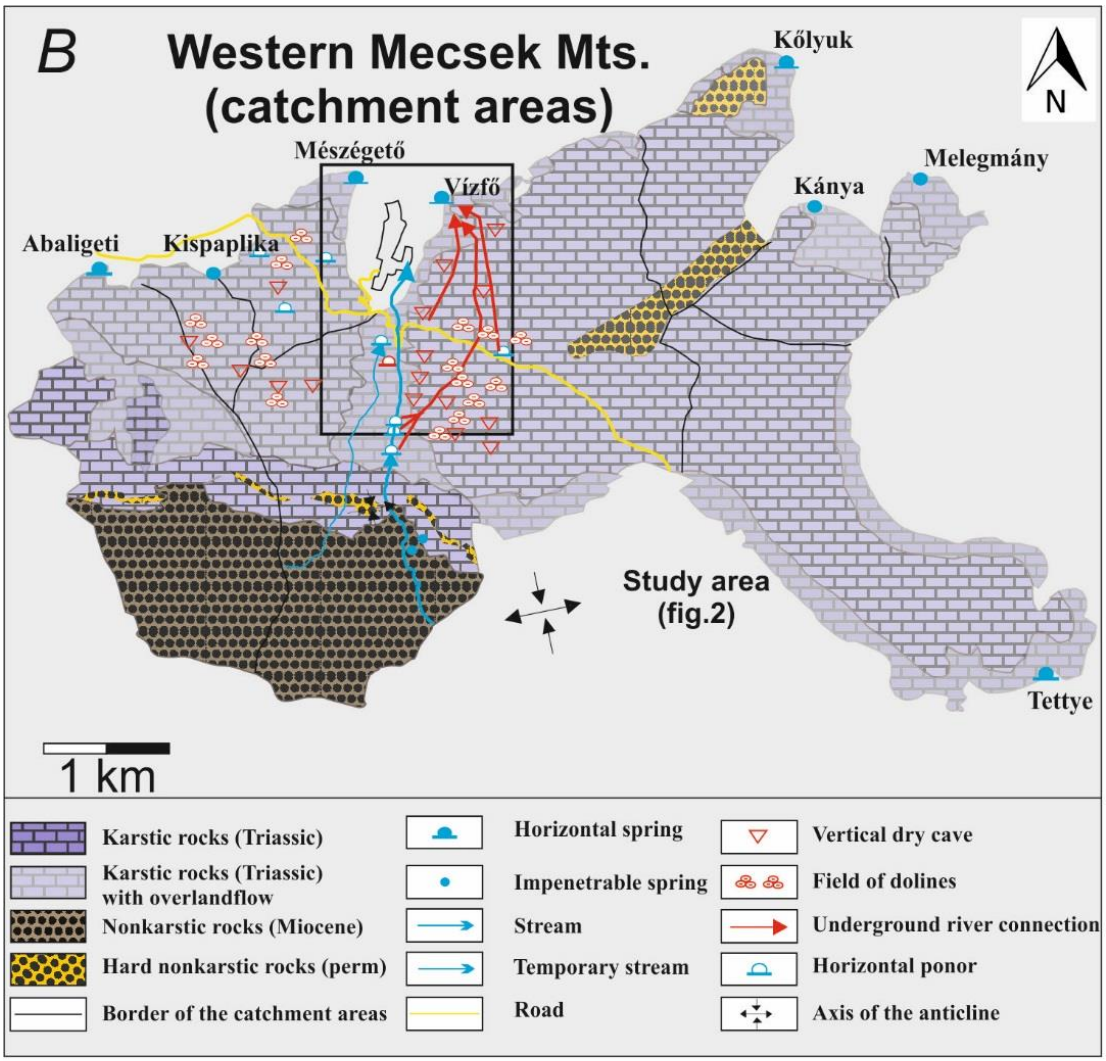

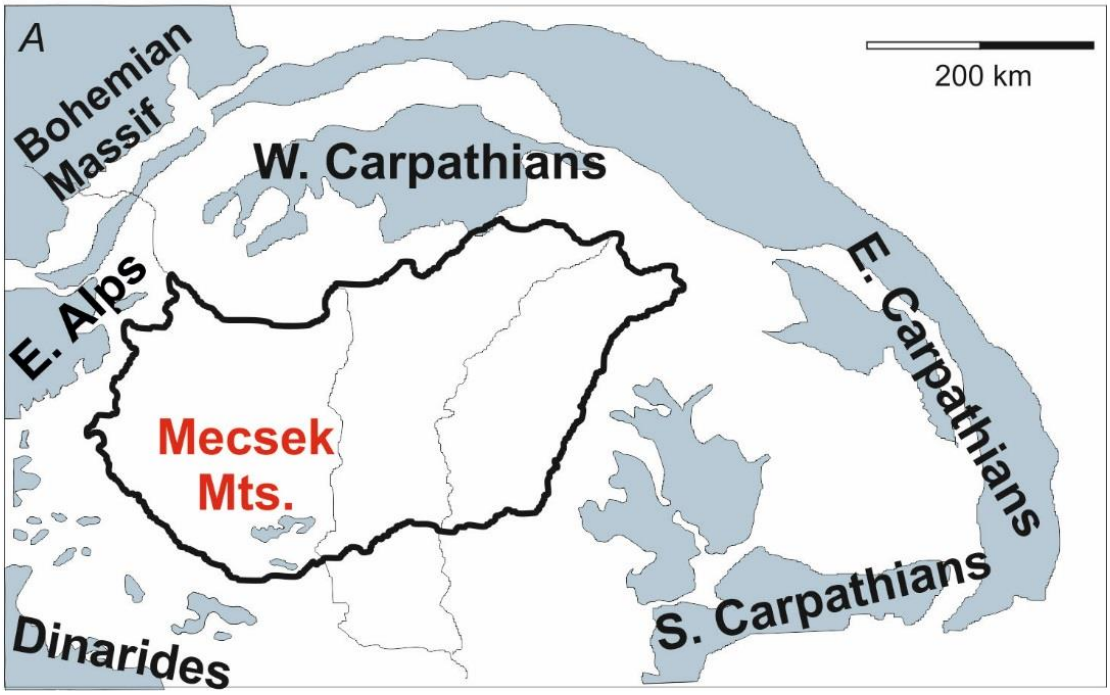

Fig. II.1: Location of the study area and the karst aquifers of the Western Mecsek Mts. (modified after Rónaki 1970).

The NE–SW structural lines, where fissure caves and karstic cavities formed, opened in the Pleistocene in several stages (Szabó 1955). After this tectonic event, N–S and NW–SE structural lines formed. In the early Holocene, a general rise in the region occurred, which resulted in a significant increase in erosion (Szabó 1955). Simultaneously, the karstic water level began to heavily fluctuate, which influenced the valley structure of the western Mecsek Mts. and strongly affected the formation of its caves (Szabó 1955; Lovász 1971; Sebe et al. 2008). The present direction of the largest main stress is NE–SW, which opens parallel fractures and closes perpendicular ones (Bada et al. 2007) and has a strong effect on the relationship of the fracture system. The karst-forming layers now typically dip 20° north and are heavily folded. No thorough survey has been prepared on the hydrogeologic impacts of the structural elements.

The neotectonic and geomorphological evolution resulted in eight catchment areas in the central karstic region in the western Mecsek Mts. (Rónaki 1970) (Fig. II.1). The largest of which is the catchment area of the Vízfő spring. Approximately 30% of the 16 km^2 catchment area consists of non-karstic formations; the Jakabhegy sandstone is the highest relief in the south, while Lapis limestone dominates in the north. Our research area covers approximately 60% of the whole catchment, covering the territory between the Szuadó-valley, the Körtvélyesi-valley and the Vízfő cave (Fig. II.2). Data from the most important caves are summarized in Table II.1.

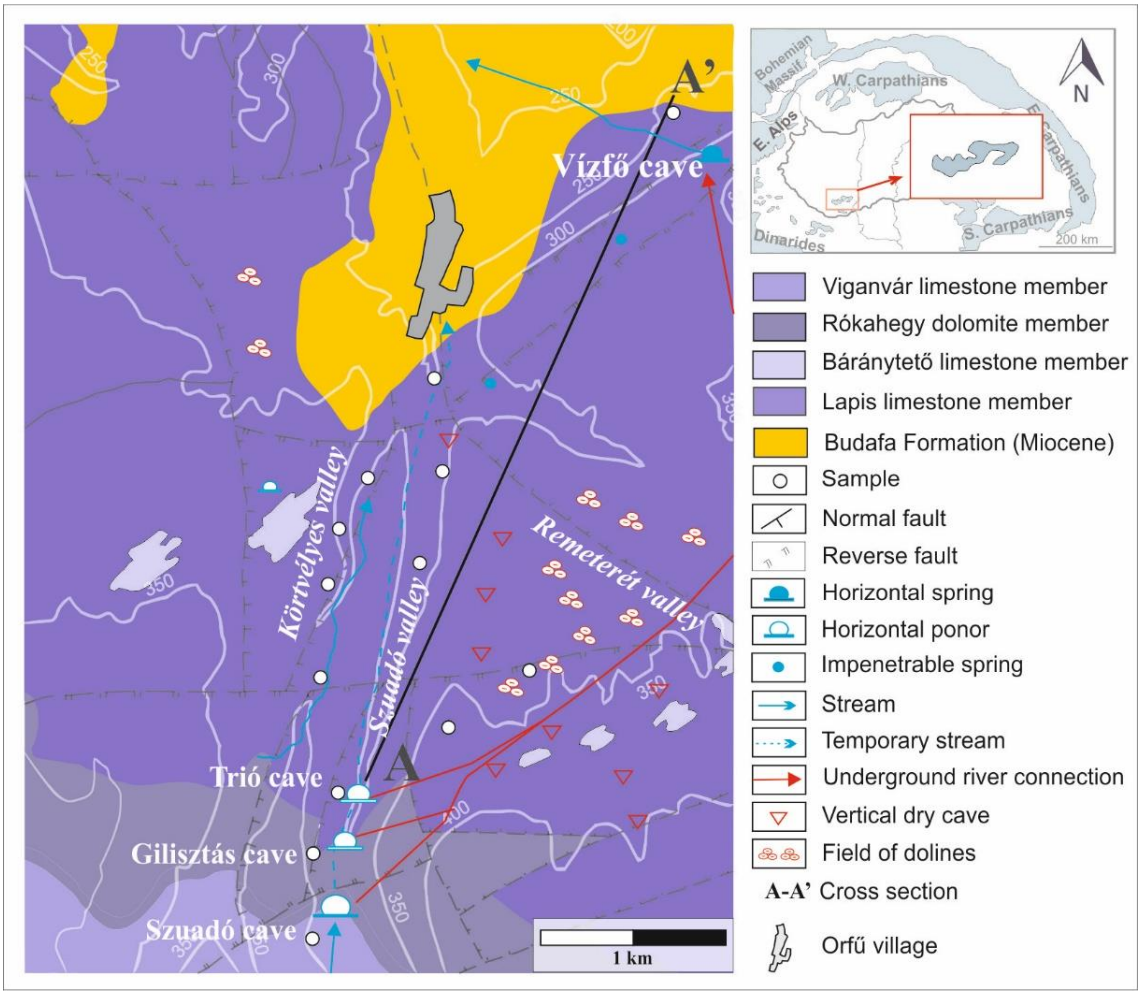

Fig. II.2: A simplified geological map of the investigated area (modified Konrád et al, (1983) - Unpublished)

According to Szabó (1955), the karst phenomena in this catchment area formed in several individual stages and the valley formation and the subsurface karsts started to develop simultaneously. There are 73 discovered cave entrances in the 16 km^2 large drainage area. After several decades of speleological research, it is now clear that most of the caves and cave parts (passages, halls) are oriented northeast (Fig. II.3) and numerous caves have siphon endpoints. The spatial distribution of these caves, however, is uneven, similar to that of dolines. Lipmann et al. (2008) found that dolines concentrate in the central part of the area, defining NE–SW oriented chains for structural reasons. The shapes of individual dolines were not determined by structural effect, but rather by micromorphological and microclimatic circumstances. The average annual precipitation is approximately 600–650 mm, higher than the Hungarian average, which is the result of the strong Mediterranean effect. The least amount of precipitation occurs in January, and the most occurs in June, although there is a second peak in the autumn.

There are two permanent surface water courses in the area: the Orfű-creek in the Szuadó-valley and the Körtvélyes-creek in the Körtvélyesi-valley. Their average rate of flow is 52 m^3/day and 17 m^3/day, respectively. The water from both creeks is directed to the Vízfő spring through sinkholes, but our experience shows that a large amount of water leaks underground through the fracture network from the creek beds. Little information can be found on the path of the water through the sinkholes. The test results are shown in Table II.2. The average flow rate of the Vízfő spring is 420 m^3/day, but can exceed 100,000 m^3/day during a flood.

Name	Length	Depth	Distance from Vízfő spring	Entrance Asl	End Point Asl
	[m]	[m]	[m]	[m]	[m]
Vízfő cave	330	-1	0	211	329
Trió cave	255	-55	2550	297	242
Gilisztás cave	133	-51	2650	301	250
Szuadó cave	345	-52	2800	303	251

Table II. 1: Tophographical data of the main caves in the study area.

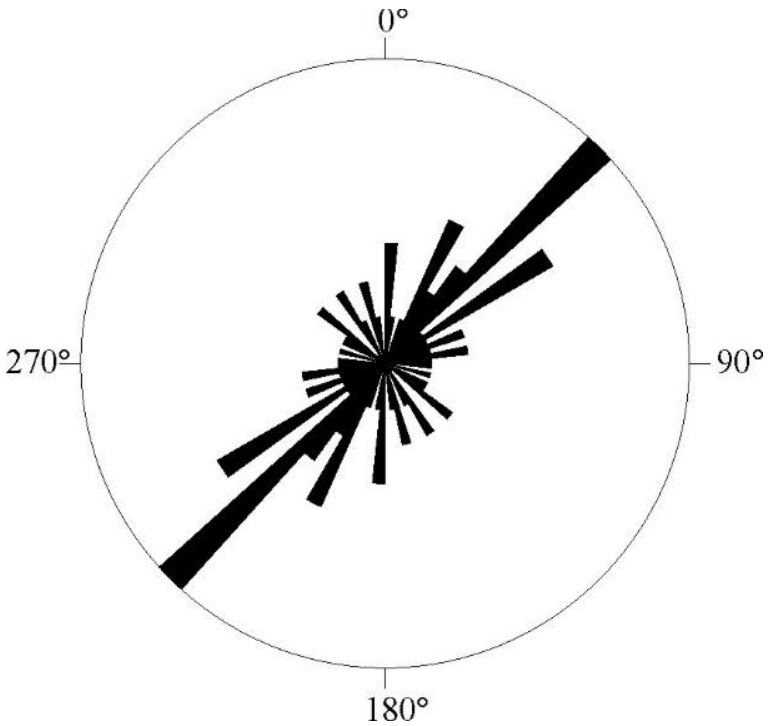

Fig II. 3: Orientation of the largest cave passages in the study area (N=55).

Sinkhole	Date of tracing	Precipitation difference	Straight distance to Vízfő spring	Injected fluoressceine	Inflow rate	Average outflow rate	First arrival	Transit time	Flow velocity
		[mm]	[m]	[g]	[l/m]	[l/m]	[hour]	[hour]	[m/day]
Szuadó-cave	1960. Aug.	N.D	2800	700	350	2250	210	120	320
Gilisztás-cave	1996.March	-13	2650	N.D	3500	N.D	24	12	2650
Trió-cave	1998. April	-41	2550	100	250	4100	90	12	680
Gilisztás-cave	2000. Jan.	46	2650	200	500	3600	65.6	28.5	970
Szuadó-cave	2001. Jan.	46	2800	200	350	3600	82.5	31	815
Gilisztás-cave	2000. March	-40	2650	N.D	700	3600	32.3	18.5	1969
Asl: Above Baltic Sea level									
Precipitation: Difference of the previous three mounth precipitation sum and the long term average precipitation at the same three mounth (1973-2013)									
N.D: No Data available									

Table II. 2: Results of the tracing works in the Szuadó-valley.

2.3. Methods

Individual fractures can be interpreted as 2D surfaces of finite extension, usually bent in multiple and very complex ways, but can mostly be approached by planes (Chiles and de Marsily 1993). In our case, we followed the circle representation in both the parameterization of fractures and further simulation. The geometric parameters clearly describe individual fractures as the spatial position of the circle's center, the radius and orientation (dip, strike). For a fracture system, this can be interpreted as a function of the spatial density of the center points and a distribution function typical of the radius and dip-strike value-pairs. The hydraulic description of the fracture system needs positive volume of the individual fractures; therefore, circle plates without thickness were replaced by flat disks with apertures (parallel plate model, Witherspoon et al. 1980). Discrete fracture network modeling requires characterizing the geometry of individual microfractures, which was completed using the methods described below. Abbreviations used to describe the fracture network geometry are summarized in Table II.3.

Abbrevation	Meaning
l	Length of a fracture in 2D
a	Aperture of a fracture
α	Dip of a fracture
β	Strike of a fracture
N	Number of fractures
D	Fractal dimension in general
E, $F\text{-}N(L)=F*L^{-E}$	Parameters of length distribution functions
A, $B\text{-}a = A*L+B$	Parameters of the aperture function
k	number of cases on the histogram

Table II. 3: Abbreviations of the individual fractures and fracture network parameters.

2.3.1. Field work

We first localized all outcrops on the surface and subsurface, recording their GPS coordinates. The orientation (α, β) of each individual fracture was measured using a compass after the outcrops had been cleaned. Next, 5 MP photos were collected from representative sections of the outcrops. In 9 cases, hand specimens were also collected to investigate their microfracture systems in laboratory conditions. Using the photos, thousands of individual fractures were digitized from hand specimens using ArcView software. Digitized images were used to detect the length distribution, aperture and the relative position of the fractures

2.3.2. Data processing

Based on previous studies, the distribution of fractures lengths (measured on 2D surfaces) follows a power law distribution, which can be approximated by a straight line on a $\log(N(l)) - \log(l)$ plot (e.g. Yielding et al. 1992; Nieto-Samaniego et al. 2005). Calculating the frequency distribution is the first step for the precise definition the power law functions. Because the number of cases on the histogram can have a great influence on its shape, this number was defined as

$$k = 2 * \mathrm{INT}(\log_2(\max(l)) \qquad (1)$$

Neither the shortest nor the longest fracture sets fit on the expected line. Both biases come from representative problems at extreme sizes, so they were left out of the subsequent analysis. Outlier data were selected using Grubbs test.

Measuring the fracture aperture is an uncertain task. Although there are accurate and accepted methods in the literature (e.g., MicroCT, MRI), these techniques require special laboratory equipment. Applying these approaches is impossible in the field. In many cases, the distance between the opposite fractures walls could not be measured correctly because of the irregular and rough walls. The aperture of the individual fractures was measured at least three times at three different points (typically four or five). To evaluate the data, the average values of the measured data were used.

Although there were many uncertainties, previous investigations suggest that the aperture follows a power law distribution similar to the length (De Dreuzy et al. 2002;

Ortega et al. 2006). In addition, a linear correlation exists between the length and the aperture of the individual fractures (Barton and Larsen 1985; Vermilye and Scholz 1995; Gudmundsson et al. 2000; Gudmundsson 2001). The aperture of a single fracture can be described by the following equation:

$$a = A * L + B \tag{2}$$

The two parameters (*A, B*) can be determined by computing the linear regression between the measured length and the aperture data.

The spatial distribution of fractures was analyzed using the fractal dimension of the midpoints of the digitized fractures. There are numerous methods to calculate the fractal dimension, such as Mass Radius, Cumulative Intersections, Vectorized Intersections, Convex Hull Intersections, Convex Hull, etc. We applied the Box Counting algorithm (Mandelbrot 1983; Mandelbrot 1985) to characterize the fracture network following the suggestions of Barton and Larsen (1985) and Barton (1995). The Benoit 1.0 software was used, which demands 1 bit (black and white) images of the fracture midpoints. Two breakpoints typically appear on each point set generated using the Box Counting algorithm. Points below the first one belong to very small box sizes, while those above the second one come from the largest boxes. The two point classes have no geological meaning and are only derived from the applied approach. A regression line was fit between the two breakpoints in each case.

2.3.3. Mapping

Fracture parameter maps were generated to spatially extend the data measured in discrete points to the whole study area. All maps were computed using Surfer 8.0 using the linear kriging approach because there were not enough points to thoroughly fill variography calculations. The grid cells were 40x40 m.

2.3.4. Modeling

The RepSim code was used for 3D fracture network simulations many times (M. Tóth et al. 2004; Vass et al. 2009). RepSim code has been applied for building the DFN (Discrete Fracture Network) model because it follows the box-counting algorithm to locate

fracture centers and uses the measured D, E and orientation data for simulation. This is a DFN modeling software that uses the fractal geometry behaviour of fracture patterns and is based on the previously mentioned parameters. Although many papers suggest that, the assumption of circular shaped fractures is more likely to validate in massive rocks, there is absolutely no data to use polygonal or ellipse approach for the individual fractures. Although the simulated system consists of a myriad of discrete flat cylinders, hydrodynamic parameters (porosity, intrinsic permeability tensor) are calculated for a given grid net for hydrodynamic modeling. The size of the grids is defined following the REV (representative elementary volume) concept of Bear (1972); the volume, above what the calculated porosity does not change remarkably. Following the approach of M. Tóth and Vass (2011), REV is defined at the grid size where the variation coefficient of porosity becomes stable. It is important to note that porosity, permeability and REV calculations relate only the fracture system and the model ignores the effect of the bedding planes.

2.4. Data

Measured fracture length data follow the expected power law distribution in each studied locality, so the *E* and *F* parameters needed for modeling were derived. Similarly, a box counting calculation was successful in each case, and the *D* parameter, representing the spatial distribution of fracture midpoints, was computed in all 11 study points. The results from the parameter calculations are in Table II.4, and the evaluated data of a typical sample are in Figure II. 4. The results from the aperture measurements show some deviation from the assumed linear relationship, likely because of dissolution for a few microfractures. Most fractures lie along the trend line (Fig. II.4/e, f) if the strongly dissolved fractures were ignored during the linear regression calculations (c.f. Equation 2). Parameter maps calculated using normal krigings are illustrated in Fig. II.5.

Sample	n	D	E	F	A	B
Sárkány-valley_1	198	1.45	-1.94	10.78	0.004	0.93
Körtvélyesi_1	40	1.28	-1.28	5.71	0.002	0.436
Körtvélyesi_2	109	1.84	-0.67	4.23	0.22	0.486
Vízfő-cave	59	1.35	-0.41	2.89	0.10	0.701
Trió-cave	861	1.69	-2.03	13.35	0.008	1.53
Szuadó-valley_1	107	1.84	-0.94	6.10	0.004	0.829
Szuadó-valley_2	85	1.37	-0.76	4.15	0.014	0.438
Szuadó-valley_3	40	1.33	-0.49	3.51	0.007	0.071
Szuadó-valley_4	87	1.35	1-42	6.99	0.035	0.112
Nagykaszáló_1	88	1.54	-1.82	3.65	0.032	0.034
Nagykaszáló_2	53	1.45	-1-13	5.22	0.091	0.265
n: number of the digitized fractures						

Table II. 4: Measured geometrical parameters of the fracture network.

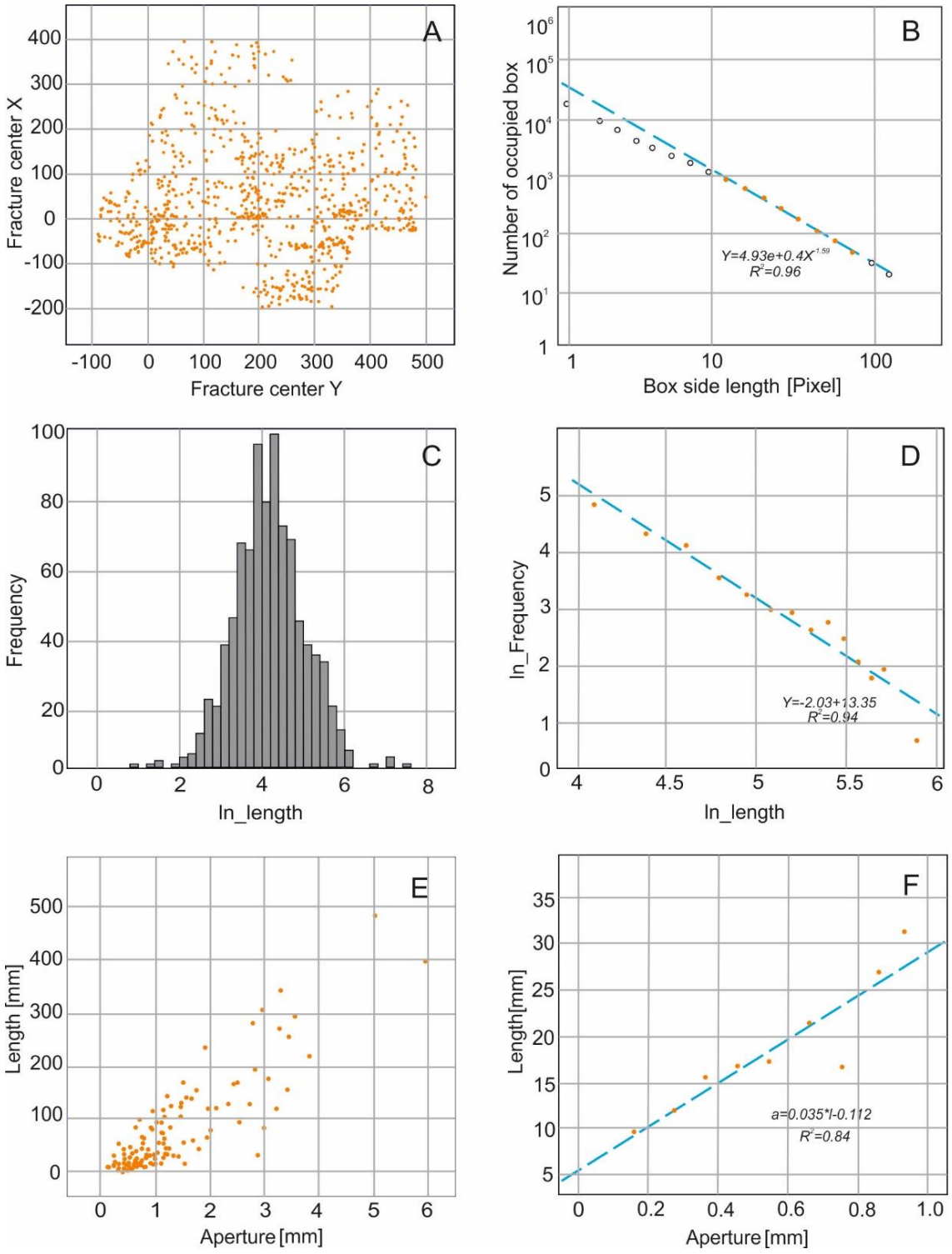

Fig II. 4: Processing methods of a typical sample. A, B) Result of the box-counting analysis of fracture midpoints. C, D) Frequency distribution of the fracture length values and the corresponding linear regression function. E, F) Relationship between the aperture and length values, and the same relationship without the extremely dissolved fractures (applied software: SPSS 20).

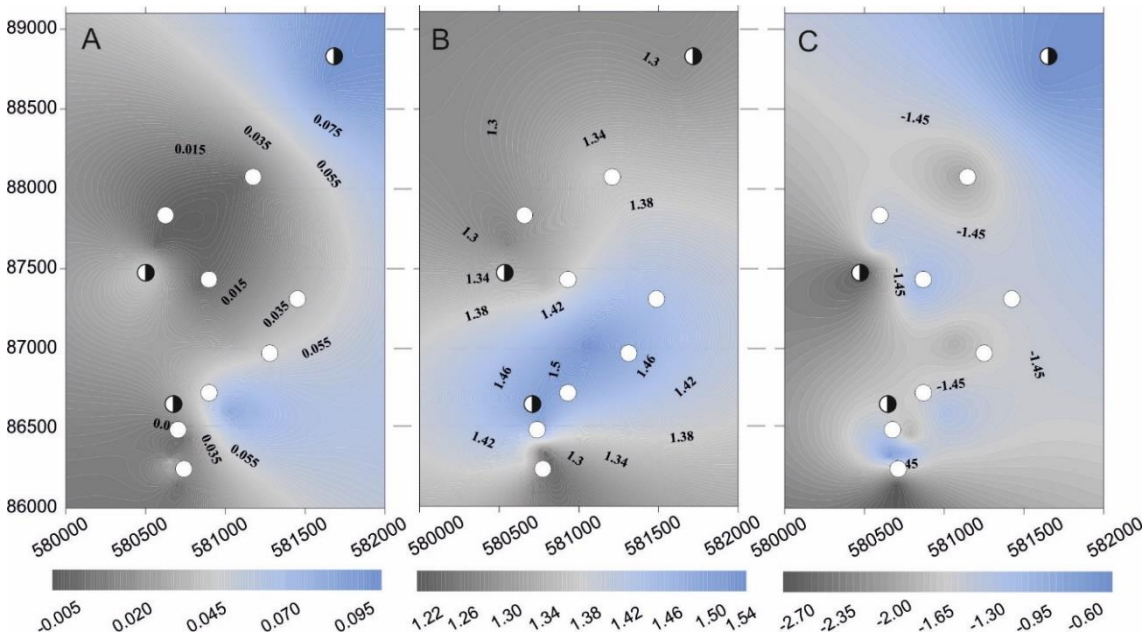

Fig II. 5: Spatial distributions of the measured parameters. A: Map of the E parameter. B: Map of the D parameter. C: Map of the aperture. White circle = sampling locations; black circle = cave entrances.

2.5. Discussion

2.5.1. Simulated fracture network

At the beginning of modeling, we defined the primary cell edge as 10 m, which was halved during the iteration process until we reached a minimal cell length of 1 m. This method required four iteration steps, during which we generated approximately 113000 single fractures. For each midpoint, a single fracture was chosen from the 1–50 m length interval using the calculated length distribution. Altogether, 10 independent fracture network models were computed and evaluated.

In each case, the generated model forecasted two fields of dramatically different behaviors: a highly fractured zone, which has at least one well-commutating fracture group (Type 1) and a zone, which has no well-communicating fracture cluster at all (Type 2) (Fig. II.6). The connectivity of a fracture group can be defined by the proportion of the interconnected fractures. It essentially depends on the *D*, *E* and the orientation values of the fracture network (M. Tóth and Vass, 2011). In this paper a fracture group was considered well-communicating if it contains more than 5% of all simulated fractures from the modeled volume.

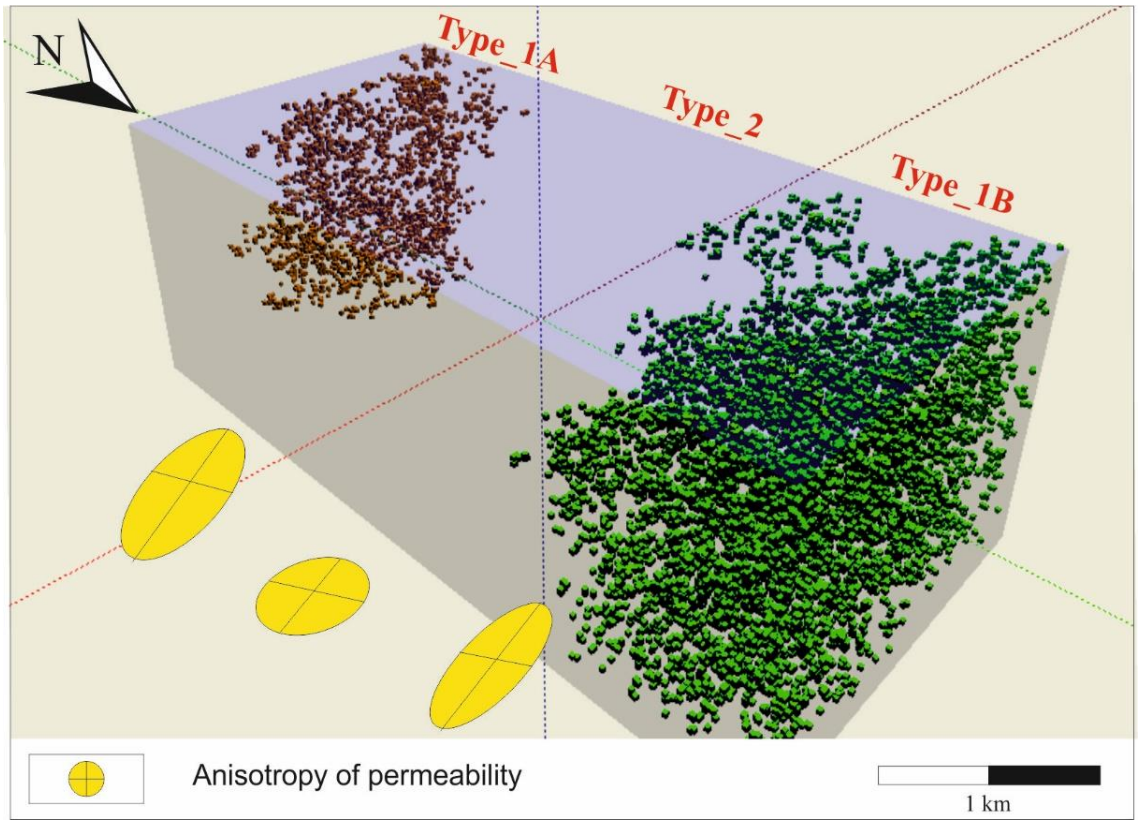

Fig II. 6: Calculated communicating fracture groups, and the horizontal segments of the permeability anisotropy ellipsoids in the three differently fractured domains.

Two large, independent fracture groups were rendered probable in the area. One on the southeastern part contained approximately 10% of all of the fractures (Type 1a), while another communicating system in the north contained approximately 5% (Type 1b). Both zones had relatively low *D* values (~1.26) and relatively low *E* values (<1.00), suggesting that the fractures were relatively long. In the Type 2 zone, geographically surrounded by Type 1a and Type 1b areas, even the largest fracture networks consist of no more than approximately 0.1% of all fractures. This region is characterized by high *D* values (~1.6) and high *E* values, which suggests that, even if a dense fracture system was typical here because the network is dominated by short fractures, the number of communicating subsystems is subordinate (Fig. II.7).

To test how well-connected the Type 1 systems are, each fracture with a length below a certain threshold was diminished to model the possible role of vein cementation. As the simulation of cementation goes on, the size of the communicating clusters decreases evenly. Even if fractures with apertures of 120 mm (L = 20 m) are closed, a remarkably large communicating fracture group can be rendered probable, suggesting a mature 3D fracture system is present both in the northern and southern part of the study area.

The variation coefficient calculated from the average and standard deviation data of porosity for different grid sizes stabilizes at approximately 0.6, so we defined the REV typical of Type 1 zones in the corresponding 50 m. The fractured porosity for fractures of at least 1 m (aperture 8 mm) for this REV is 6.8%, which is considered good porosity for Triassic reservoirs. If we also include other possible porosity types (solution, along bedding, etc. (Choquette and Pray, 1970), however, this area seems to have outstanding porosity. The permeability tensor calculated for the representative volume shows significant NE-SW anisotropy of 1.37 with an average value of $8*10^{-11}$ m^2. This direction does not depend on the orientation of the particular fractures but is closely connected to the anisotropy of the fracture density (Fig. II.6).

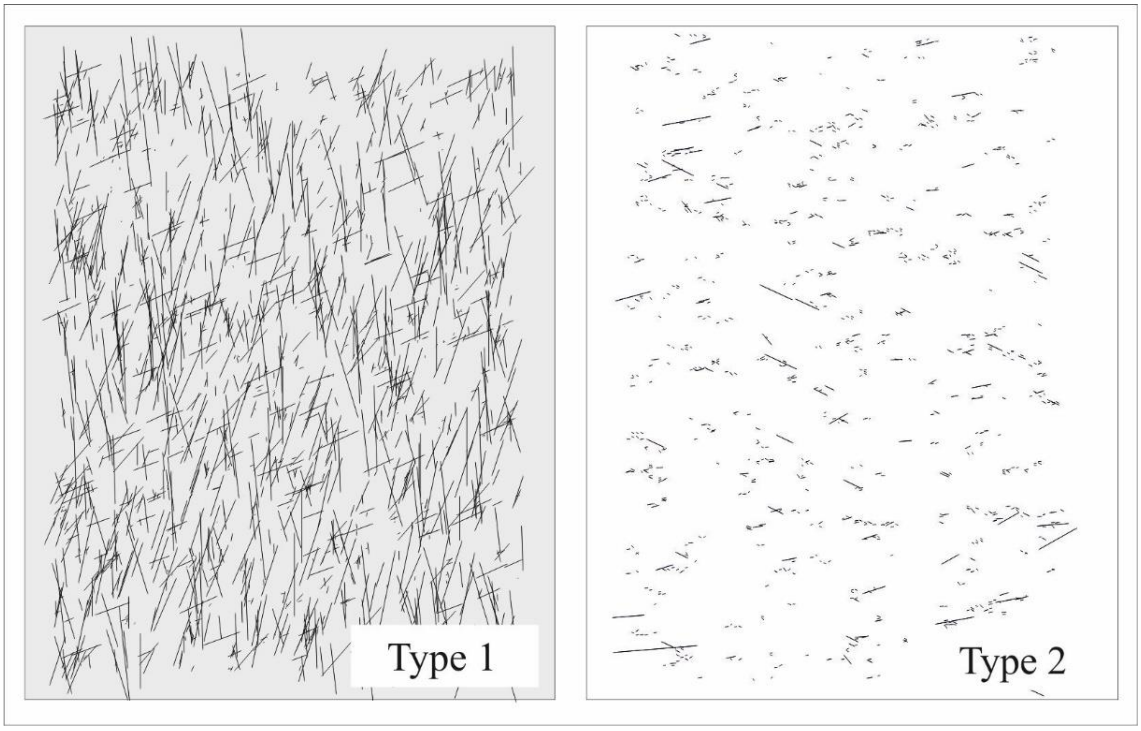

Fig II. 7: Typical horizontal sections of the different types of the simulated fracture networks (scale independent).

In Type 2 zones, the biggest connected fracture group in the models only generates 0.01% of the fractures, while plenty of small fracture groups are evenly distributed. REV is defined as 70 m for this area. The fractured porosity calculated for a volume above REV is < 0.001%, which means that this zone has neither storage nor conducting capacities. That is why we believe that the slight NE–SW permeability anisotropy typical of this area has no practical geological effect. The calculated average fractured permeability of $6*10^{-13}$ m^2 must be even smaller because the fractures do not define a connected network.

According to the previous statements, one can see that the fracture system of the examined area and its hydrodynamic features (porosity, permeability) are not uniform. The northern and southern parts of the area have outstanding effective fracture porosity, while in the middle, it is practically negligible.

Considering the hydrodynamics and karst formation of the area, however, it is extremely important to know the joint features of the three different zones. The REV calculated for the whole area is approximately 90 m, which is rather high compared to other case studies (e.g. Wu and Kulatilake 2012). This increase in size is because linking the two types of areas results in a substantial growth in the standard deviation of porosity. The fractured porosity above this REV is 2%, which is an average effective porosity value in the whole studied karstic reservoir. Using other methods, Vass (2012) obtained similar results for the catchment of the nearby Tettye spring, whose lithological and structural environment is the same as ours.

2.5.2. Geological and morphological consequences

Although the dominating Lapis limestone has different varieties, there is no evidence for different dissolution abilities. Additionally, current and palaeo-climatic parameters do not differ either; there are no places with local maximum and minimum values of precipitation. There are no substantial differences in the elevation of the study area, so we can assume that the main factors influencing epigenic karstic formation (soluble rock, precipitation of appropriate quality and quantity) affected the whole area to the same degree. There can be a crucial difference in the state of deformation of the rocks, which can affect the present surface and subsurface morphology as well. The modeling results suggest that the spatial distribution of the rate of brittle deformation is extremely heterogeneous in the area.

The NE–SW orientation manifested in fracture density maps is also shown by structural geological surveys performed on a larger scale in the wider area of the Mecsek Mts. (Csontos et al. 2002; Lipmann et al. 2008; Konrád and Sebe 2010). This renders the genetic link of micro- and macro-structures probable, so our observations are coherent with the statement that fracture patterns follow a scale-invariant pattern and can be modeled by fractal geometric approaches (Yielding 1992; Korvin 1992; Nieto-Samaniego et al. 2005; M. Tóth 2010).

Although this research did not target the analysis of the fracture-system genetics, the spatial distribution of the different fracture systems is still closely related to well-known tectonic events. We found that when the short fractures in the model were blocked (e.g., mimicking cementation), the size of the fracture system in the southern part of the area (system Type 1a) decreased from south to north. Our measurements showed that the basic difference between the northern and southern regions of the study area, compared to the central region, was the length distribution of the fractures. One reason for such a crucial spatial variability of fracture lengths may be the complex tectonic evolution of the region. The deformation response to the given stress field systematically changed when moving away from the anticline axis of the western Mecsek Mts. (Fig. II.1). Relatively few, but larger fractures formed near the axis, while a denser fracture system of smaller fractures formed (Type 1a) further away. The fracture system in the south seems to be fold related, but the northern region is related to the fault system that created the Orfű basin (Type 1b) (Fig. II.8).

Gabrovsek et al. (2004) and Singurindy and Berkovitz (2005) observed that the net efficiency of karstic processes is significantly higher in well-fractured zones where the permeability and flow velocity are much higher inside a given rock mass. In these regional processes doline formation, karren formation, or even cave formation may be enhanced. In the less fractured zones, fractures are cemented and karsts typically do not form. In intensely fractured zones, a positive feedback process occurs. During this process, the more apertured fractures have larger soluble surfaces, which enhance solution processes, so the karst formation process speeds up (Jakucs 1971; M. Tóth 2003; Filipponi et al. 2009). Structural control like this is well-known in several karstic areas (Billi et al. 2007).

The above results suggest that the relationship between different karstic forms and the fracture systems should be independently studied for the three diverse fracture patterns.

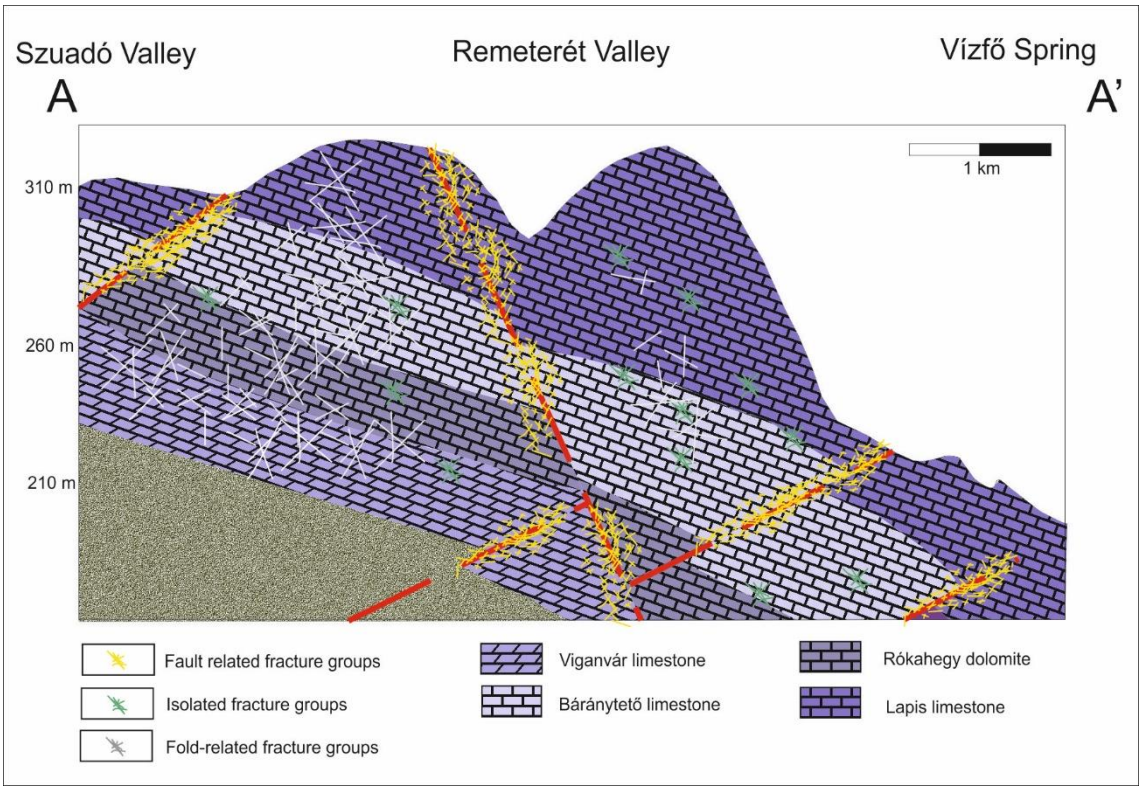

Fig II. 8: Cross-section along the A–A' line (see Fig. II.2) with the conceptual fracture systems.

2.5.2.1. Type-1

These areas can be characterized by a communicating fracture system with high permeability and porosity values. We can expect significant solution forms in this type of area. There is no difference in the karstic phenomena between Type 1a and Type 1b and all known large caves are all Type 1. These caves (e.g., Trió cave, Szuadó cave, Gilisztás cave, Vízfő cave, Fig. II.2) formed through solution along fractures and erosion. Tectonic preformation substantially influenced and is influencing cave formation today. Although the regional flow gradient follows to the north because of the position of the anticline, all of the aforementioned caves are NE–SW oriented, corresponding to the orientation of the permeability anisotropy previously calculated. Dolines are relatively rare in these two zones (Lipmann et al. 2008).

2.5.2.2. Type 2

Singurindy and Berkovitz (2005) discuss that in areas of low porosity and permeability, cementation processes dominate. In the central zone of the study area, this statement is supported by the lack of significant (longer than 50 m) caves. The orientations

of all known small cave-entrances and immature vertical caves do not follow the permeability anisotropy. The very low rate of underground karstic processes is because the zone has little fractured porosity and no ability to conduct water.

In this zone, the number of dolines is remarkably high (Lipmann et al. 2008), but NE–SW orientations are atypical. As these dolines are neo-formations (Lipmann et al. 2008), we think that the geometrical features of micro-fractures must have determined the initial stage of doline and doline-chain formation according to Singurindy and Berkovitz (2005). The relatively high number of individual fractures (D=~1.6) can be the main reason for the high doline number. Although the there are many dolines in this area, these are very immature because probably of the low permeability of the fracture system, which conclusion is coherent with that of Singurindy and Berkovitz (2005). Additionally, a significant part of the small caves in the area are linked to dolines from a solution origin. Czigány and Lovász (2006) emphasized the definite NE–SW orientation of the doline chains without any orientation of the particular dolines. This agrees with the orientation of the large structural elements throughout the study area, while the microfracture networks are immature.

2.5.3. Theoretical model

The two large fracture groups (Type 1) found in the southwestern and northern part of the study area can be identified with the spatial location of the most important caves. The model predicts the largest communicating fracture system near the Szuadó valley caves, while the second largest communicating zone is predicted to be near the Vízfő cave (Fig. II.9). In the case of the Szuadó valley sinks, the fracture model assumes a connected fracture system exists, which suggests that the Szuadó, Gilisztás and Trió caves are directly connected. This does not necessarily mean the connection can be passed through by people. Radon gas exploration was used for the Szuadó valley sinks (Koltai et al. 2010) to explore the connection. The series of measurements was not successful, as it could not prove or exclude connections. This issue still requires more research as earlier explorations did not target the relationship of caves to each other.

There is a hydrological connection between the sinks and the spring areas (Gila 2000), although no passages have been found between the two highly fractured regions. Only a certain amount of water leaking into the karst moves along the fracture planes. Without these planes, a large volume of water may move along bedding planes (Kaufmann

2003a; Kaufmann and Romanov 2008). A typical example is the initial section controlled by planes in the Szuadó valley sink caves (e.g., Trió cave), which can carry as much as several hundreds of liters of water per minute (unpublished). In these caves, these sections are typically oriented north, so the strongly northerly average plane inclination on the northern wing of the anticline contributes to the northeast run of the caves. We observed that, after a short initial section of the sinks, the flow tracks connect to mature fractures. The flow rate does not grow along the planes during floods, but even small fractures have significant flow rates. Although the karst and speleology literature provides information on a large number of caves with important galleries following the bedding planes, the cave evolution in the Mecsek Mts. depends mostly on the fracture network and fault system. The beddings are scared by syn- and post-sedimentary faults, fractures and folds, so their lateral spreading is smaller than a few tens of meters.

Although there are no flow-place measurements (in fractures, faults or on bedding planes) of karstic water, passage features in the Vízfő spring between the sinks and the spring were examined by dye tracing tests (Gila 2000; Szőke and Ország 2006; Rónaki 2007). Although these surveys have shown a quick appearance time and thus a strong hydrological connection, because of the very high deviation of the first arrivals, these passage feature estimations are extremely uncertain (Table II.1). Despite the quick appearance, each dye tracing test experiment showed some slowing features in the hydrological system. Gila (2000) and Szőke and Ország (2006) assumed that slowing by siphons or storage lakes occurs because the transitional time is not stable; it can be short or long. The previously discussed model that predicts the coexistence of different fractured zones in the area implies that the slowing factor between the sinks and the springs should not be a series of siphons or storage lakes, but that the poorly connected fracture system is responsible for this phenomenon. The slowing rate of the middle zone must depend on the quantity of the received water. The extremely rainy period in 2010 is a good example of this. In 2010, there was a fluctuation of more than 50 m in the water level of the Szuadó valley caves, while in the other part of the karst, around the spring, the water level did not even reach 5 m (unpublished). Using the current fracture model, in the Type 2 zone, the fracture network is unconnected and the bedding planes alone are responsible for water flow. As soon as they became saturated, further tapping was impossible along bedding planes where there is low permeability. The middle zone then slows and diverts the flow from a northern to a northeastern direction. The fact that the karstic water arriving at the southern border of the non-communicating zone has to turn to the northeast is a very

important element in the hydrogeological system and the development of the cave orientations.

To sum up, our model suggests that in the catchment of the Vízfő cave between the Szuadó valley caves and the Vízfő spring, a zone should exist where cave maturity is significantly underdeveloped compared to its vicinity because of tectonic preformation. This zone plays an important role in the hydrology of the area as it greatly decreases the permeability between the sinks and the spring, and practically diverts flowing waters to a northeastern direction.

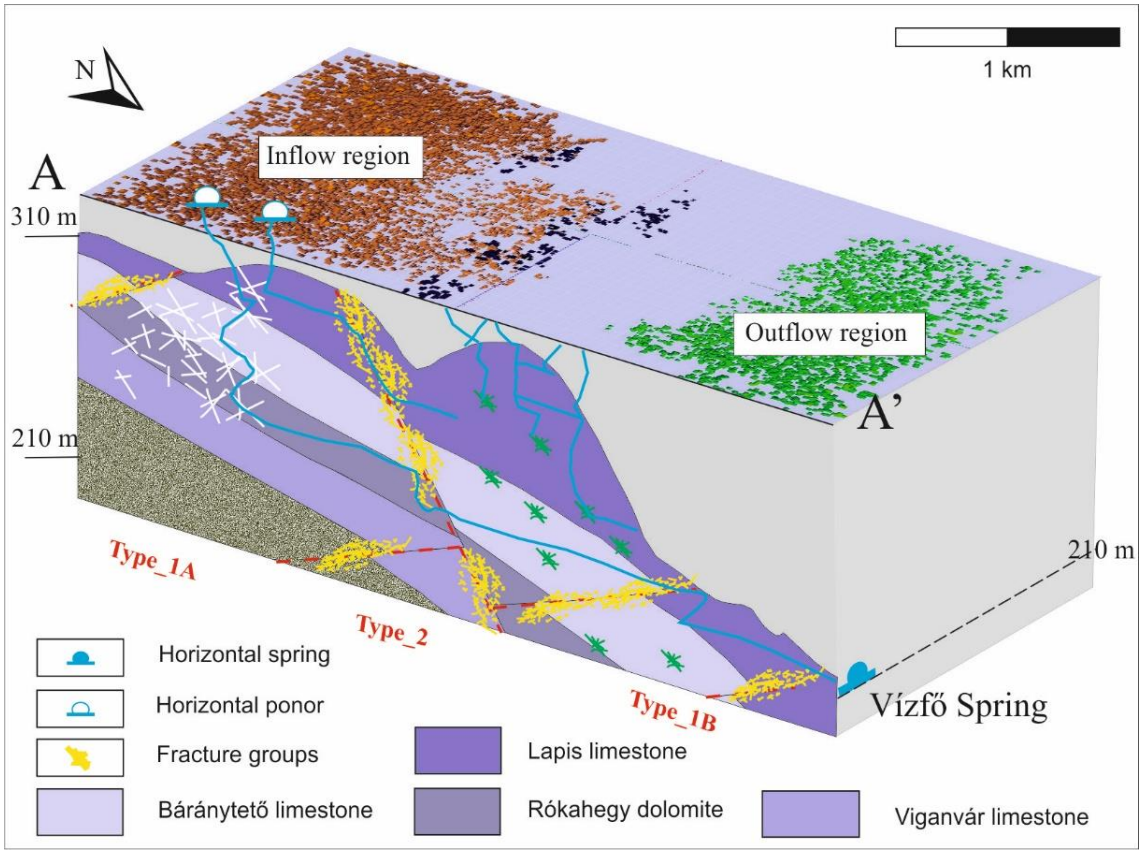

Fig II. 9: Effect of the fractures and bedding on the hydraulic behaviour of study area. The main conductive zones are fault related fractures (yellow), and according to the DFN model, there is an unfractured, bedding only, hydrological connection between the inflow and outflow regions.

2.6. Conclusions

- Through the study and modeling of the microfracture network in the examined area, the vicinity previously considered homogeneous can be divided into three distinctly different zones which differ in fracture network connectivity, porosity, permeability and type of karst development.

- In the study area, the REV calculated on fractured porosity is approximately 90 m, but for the well-fractured sub-areas, this volume is much smaller (50 m).
- There are direct fracture geometric connections between the sinks of Szuadó valley (Szuadó, Gilisztás and Trió caves), but they are not necessarily passable by people.
- We have increased the knowledge of the karstic development in the area with new elements by studying the microfracture network and applying the previously discussed simulation method. This method makes it possible to simulate fractures at a reservoir scale using point-type data (even drills). This can be extremely important to learn about hydrocarbon and geothermal reservoirs.

Chapter III

Petrology and Paleokarst features of the Gomba hydrocarbon reservoir (Central Hungary)

Márton Bauer
Department of Mineralogy, Geochemistry and Petrology
University of Szeged, Szeged, Hungary
baumart87@gmail.com

Tivadar M. Tóth
Department of Mineralogy, Geochemistry and Petrology
University of Szeged, Szeged, Hungary
mtoth@geo.u-szeged.hu

Béla Raucsik
Department of Mineralog,y Geochemistry and Petrology
University of Szeged, Szeged, Hungary
raucsik@geo.u-szeged.hu

István Garaguly
Department of Mineralogy, Geochemistry and Petrology
University of Szeged, Szeged, Hungary
garagulyistvan@gmail.com

Central European Geology
In-press (2016)

3.1. Introduction

More than 60% of the world's oil and 40% of the gas reserves are stored in fractured carbonate reservoirs. The pre-Cenozoic basement of Hungary has a significant volume of carbonate rocks, which are excellent reservoirs at places. There are six Total Petroleum Systems known in the Pannonian Basin Province (Kókai and Pogácsás 1991, Dolton 2006). One of the most complex and most important ones is the Paleogene Petroleum System, which is located in the Hungarian Paleogene Basin in the central part of Hungary (Fig. III.1). The study area is the Gomba field in the west part of the basin. The field has Triassic carbonate and Eocene-Oligocene detrital reservoir rocks, complex structural and sedimentary traps and source rocks of supposedly Pliocene age. Hydrocarbon exploration and production from Gomba began only at the end of the 90s (Dolton 2006), but today, it is one of the most productive areas in the country.

Although the production history is not long, the geological and geophysical research has a far reaching past. The structure of the region is well-known from geophysical investigations, but the petrography of the Triassic reservoir is less known because of the few cores and the very restricted number of analyses. Nevertheless, the production history clearly shows that the available geological and fractured reservoir models do not fit well enough to explain past production and predict future trends. Thus, it is essential to improve our understanding the geology of the area.

Based on the available reports and unpublished information, the carbonate part of the reservoirs may have paleokarst features (e.g., paleo cave facies, large caverns or collapse structures), which can significantly modify the porosity and permeability of the reservoir. Karst processes may increase or decrease porosity, modify migration pathways by cave passages or collapse structures and thus significantly change the hydraulic behaviour of the complex reservoir. Nevertheless, it is very problematic to localize the effect of karst processes in the subsurface even though there are numerous works on understanding the hydrodynamic role of paleo-caves by several authors, including Lucia (1968, 1995, 1996), Candelaria and Reed (1992), Lucia et al. (1992), Fritz et al. (1993), and Loucks (1999), Loucks at al. (2004). Based on these works, there are some typical paleo-cave formations are recognizable not only by well-log analysis but also in cores or thin sections.

Our goals are to observe, document and interpret the petrographic features of the Triassic carbonate rocks and their microfracture network in the study area based on an

analysis of the core material. The main aim is to recognize the evolutionary history of the Triassic beds from the early diagenetic processes to the present day, recognize the main hydrocarbon migration pathways and estimate the effects of the karst forms in the reservoir.

3.2. Geological settings

The investigated area is located in the northern part of mid Hungary, in the western part of the Hungarian Paleogene Basin, which is subdivided into three parts by Nagymarosy (1990). The Gomba field belongs to the southern Buda Paleogene unit. According to the Pre-Cenozoic Basement Map of Haas et al. (2010) the region is located at the boundary of the Transdanubian Range Unit (TRU) and the Mid Hungarian Unit (MHU) (Fig. III.1). The boundary between the TRU and MHU is defined by the Balaton Line, a significant transversal fault zone, while the position of the boundary of the TRU and the Bükk Unit to the north is rather problematic. Though the boundary is unequivocally inferred by seismic studies (Szalay et al. 1976; Szalay et al. 1978), supposed Bükk type lithologies were penetrated also by deep wells on the opposite side of the hypothetic tectonic zone (Benedek 2009).

The Mesozoic sequence of the MHU is hardly known, but it greatly differs from the typical Mesozoic formations of both the TRU and the Bükk Unit. A close correlation with the Dinarides and the Southern Alps was suggested for the lithologies of the MHU (Haas 2004; Schmid et al. 2008). The relationship is discussed by numerous authors concerning both sedimentologiy and the tectonic aspects (Árkai 1983; Kovács et al. 2000; Schmid et al. 2008).

While the Mesozoic rocks in the MHU are unknown at the surface, the formations of both the TRU and the Bükk Unit have been studied in detail from outcrops. The closest outcrops in the TRU to the investigated reservoir are located in the Buda Mts., where Ladinian dolomitized platform carbonates (Budaörs Dolomit Formation), Carnian–Norian platform dolomites and limestones (Dachstein Limestone Formation) and cherty basinal limestones (e.g. Mátyáshegy Formation) represent the Mesozoic sequence. The limestone and dolomite bodies in the Buda Mts. contain significant karst cavities and caves formed primarily by epigeice (Wein 1977; Nádor and Sásdi 1991) and young, still active hypogene processes (Kriván 1959; Kraus 1982; Nádor 1991). Paleokarst features of Mesozoic-

Tertiary carbonates of the Buda Hills were studied by Korpás and Juhász 1990, Esteban et al. 2009, Győri et al. 2011, Poros et al. 2012).

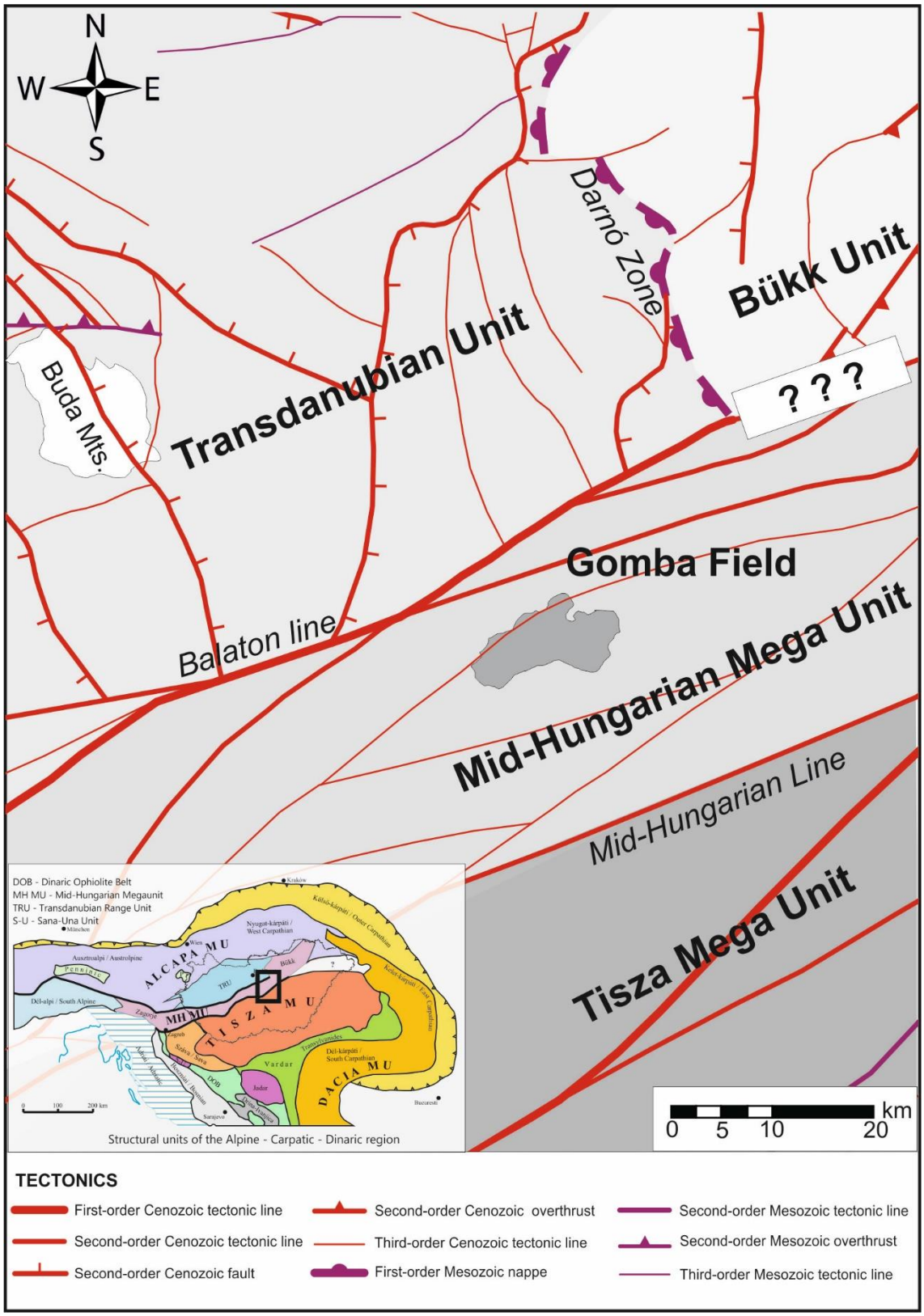

Fig. III.1: Geological settings of the investigated area. (Based on Haas et al 2010)

As far as the Bükk Unit is concerned, the limestone-dominated sequences are recrystallized and generally reached anchimetamorphic grade (Árkai 1983) with the degrere of metamorphism decreasing from the NE to the SW. According to the present lithostratigraphic concepts, the different Middle to Upper Triassic platform carbonates in the Bükk Unit are assigned to the Bükkfensík Limestone Formation (Haas 2004). A peculiar, non-metamorphosed variety of these almost pure carbonate rocks is restricted to the NE part of the Bükk Mountains, called the Kisfennsík Limestone Member. The unit most likely forms a small thrust sheet (Haas 2004).

The Kisfennsík Limestone consists of predominantly light-grey, whitish-yellow carbonate platform facies limestone. Tidal flat, lagoonal and reefal environments can be reconstructed in the carbonate platform sequence of the Kisfennsík block. The sequence is mainly thick-bedded or massive, containing subordinate finely bedded parts and occasionally cyclic loferites. Syngenetic brecciation is relatively frequent (Pelikán 2005). Although the type area of the formation is located in the NE part of the Bükk Mountains, there are some proven occurrences in the subsurface to the SW of the Bükk Mountains. At the southern part of the Bükk Mts., there is the Berva Limestone. It has very similarly appearance to the Kisfennsík limestone, but it contains much more fossils. It is typical formation in the Southern margin of the Bükk Mts (Less 2005). Early karstification of the Kisfennsík Limestone was proven by Velledits et al. (1999). Karstification of the Berva Limestone is not investigated yet. As neither the Kisfennsík Limestone Member (North Bükk) nor the Berva Limestone (South Bükk Mts) is metamorphosed (Less 2005).

The studied region is characterized by continuous sedimentation from the Eocene to the Miocene with numerous subsequent transgressive and regressive cycles (Benedek 2009). The Eocene strata overlie the strongly deformed Mesozoic structures with an angular unconformity everywhere and variable size of absence of sedimentation (Kecskeméti 1998; Less 2005) as a result, different marly and clayey sediments and carbonate rocks formed. Siliciclastic sequences were also deposited during the Miocene (Tari et al. 1993) (Fig. III.2).

One of the most important events concerning the reservoir's evolution was the development of the Eocene basal Paleogene Clastics, Kosd Formation(?), which predominantly consists of debris of grey claystone, sandstone, limestone and dolomite gravels; occasionally, mollusc-bearing marls are present with fresh water limestone and coal in the upper part of the sequence (Less 2005). The starting member of the formation contains 2–25 cm large boulders and gravels, interpreted as erosional debris from the

underlying Kisfennsík Limestone (Less 2005). During the Oligocene, fine-grained (hemi-) pelagic sediments were deposited, e.g., the Tard Clay Formation and the Kiscell Clay Formation. The former is characterized by high TOC content, having reached the oil window during the Pliocene (5 Ma); therefore, this formation is regarded as a source rock for HC generation approximately 2400 m below the present surface (Benedek 2009).

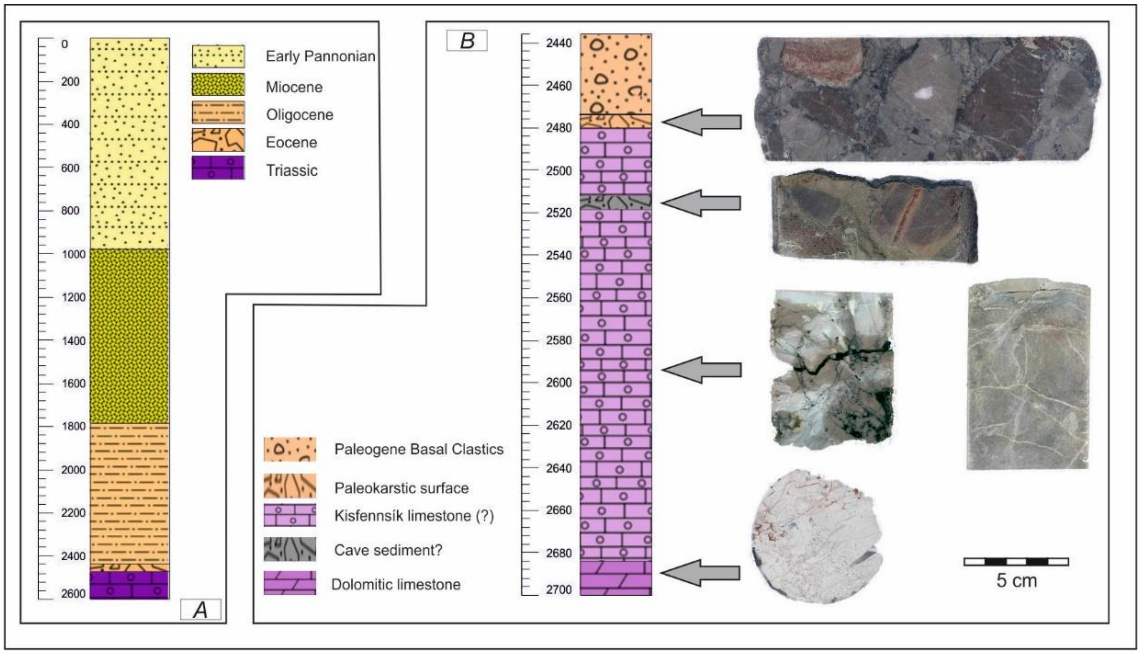

Fig. III.2: A: Idealized stratigraphy of investigated wells. B: The detailed and idealized stratigraphy and the investigated cores.

The reservoir rocks in this area are intensely tectonized. The basin's morphology is controlled by complex fault patterns of predominantly NE-SW strike that were essentially caused by numerous subsequent Eo-Alpine compression phases (Austrian, Pyrenean) and Neo-Alpine (Late Miocene) transversal faults (Csontos and Nagymarosy 1998; Fig. III.1). The Neogene structural pattern of the basin is mainly to the result of these transversal movements; part of the faults can be interpreted as rejuvenated old structures. This complicated fault pattern is supposed to have had a significant influence on the deep basinal hydrological actual and paleo flow system of the reservoir.

Exploration of the Gomba field started at the beginning the end of the 90s. Based on the petrographical investigation of cores and chips, the Triassic carbonate reservoir shows the characteristics of the Kisfennsík Limestone, so the area is interpreted as part of the Bükk Unit. However, the stratigraphic classification is questionable; hence the classification of formations in the current study should be also considered restricted. Similarly to the Kisfennsík Limestone formation, the Berva Limestone is also non-

metamorphic formation, and its South-Bükk range is closer to the examined area, than the Kisfennsík Limestone. Moreover, the classification of the conglomerate covering the carbonate as Kosd Formation is also debatable, thus this structure was named Basal Paleogene Clastics. Up-section, the Eocene debris with high fluid storage capacity is similar to the Kosd Formation.

Based on the present hydrodynamic model, the fractured Triassic carbonates and the Eocene debris behave as a continguous hydraulic system (Benedek 2009). The groundwater beneath the hydrocarbons has a temperature of ~120 ºC with a salinity of ~35‰. As a consequence, it seems possible that the rock body is still under the control of hypogenic karstification following the Cenozoic exhumation related surficial karstification. Understanding the ongoing karstic processes is one of the most important steps in studying the hydrodynamic system of the reservoir.

3.3. Materials and Methods

The occasional total mud loss at certain levels of all (7) boreholes during the drilling process suggests intervals with significant open cavernous pores and extremely high permeability, which explain why a rather limited number of samples could have been collected. Hence, the sampling strategy was to concentrate on core material representing zones of the reservoir as close as possible to the highest porosity horizons. Following a careful macroscopic description, 5x5 cm sized thin sections were made from the available cores. The analysed material and the applied methods are summarized in Table III.1.

	Gomba_1 well	Gomba_ 3 well	Gomba_6 well
Macroscopic core description	12	26	4
Thin section analysis	9	17	4
Computer image analysis	3	17	4
Cathode luminescence microscopy	-	3	-
UV microscopy	-	18	-
Scanning electron microscopy	-	2	-
Raman spectroscopy		18	-
Micro thermometry	-	18	-
X-ray powder diffraction	-	5	8
X-ray fluorescence spectrometry		3	-
Stable isotope analysis	-	14	-

Table III.1: Summarized table of the measurements. 42 cores were examined altogether. On average they were 20 cm long so about 8 m cores were macroscopically examined. Thin sections are 30 μm thin.

3.3.1. Fabric

The rock fabric was observed under an Olympus SZX7 binocular microscope at thin section scale and was classified after Dunham (1962) for the limestone and after Sibley and Gregg's (1987) classification schemes for dolomite. Vein texture classification was made according to Bons (2000). Petrographic Image Analysis (PIA) was used to characterize the breccia samples following Mort and Woodcock's (2008) scheme.

The input images were generated using thin sections by a 6000 dpi resolution slide scanner. The Corel Draw X3, Olympus Stream Essential, ImageJ, and Fractalyse software were used for image analysis and the following geometric parameters were measured.

3.3.1.1. Particle Size Distribution

There is a close relationship between the formation process and the clast size distribution of the breccias, which is why the particle size distribution (PSD) is one of the most generally measured geometric parameters (Jébrak 1997). Numerous structural geological studies showed that PSD follows the

$$N(r) = C*r^{B}$$

power law distribution function at each scale, where N(r) means the number of clasts greater than r in diameter, C is a constant, and B means the gradient of the linear function in logarithmic scale. The calculations were fulfilled using the squared area parameter in pixels according to Blenkinsop (1991).

3.3.1.2. Clast/matrix proportion

To calculate this parameter, the areas covered by clasts and matrix were considered first on the surface of the thin section. The proportion of the clasts and matrix was computed as the thin section area/total clast area.

3.3.1.3. Rotation

Grain orientation was characterized numerically by the variation coefficient of the main axes of the ellipses fitted to the clasts. The ellipse fitting method equates the second order central moments of the ellipse to those of the distribution, thereby effectively defining both the shape and size of the ellipse.

3.3.1.4. Roundness

Roundness is a parameter that quantifies the shape of the clasts. It was calculated using the ImageJ software with the following function: Round=4*[Area/π*Major Axis^2], where Major Axis concerns the fitted ellipse, which is fitted onto the individual clasts using the same method shown before.

3.3.1.5. Grain roughness

The fractal dilation method was used to analyse the roughness of the grains. It was originally developed by Flook (1978) and has been extensively used to measure the D of cellular borders. Dilation has several features that make it superior to other methods. The basic idea in the standard dilation method is that one takes convolution kernels of different

sizes (diameters) and convolves them with the image border. Then the resultant area is divided by the diameter of the kernel and the log of that result is plotted against the log of the kernel diameter. A fractal object gives a straight line with slope S and D = 1-S.

The statistical database built from the above mentioned parameters was analysed by the SPSS 20 software. For extreme data handling, boxplots were used, and the Kolgomorov-Smirnov method was applied for the normality test of the parameters.

3.3.2. Phase analysis

The microtexture of the samples was analysed by an Olympus BX41 polarization microscope. A cathode luminescence microscope was used to characterize the overgrowth of the different constituents and cement minerals. Cathode luminescence microphotographs were taken at the Institute for Geological and Geochemical Research's Centre for Astronomy and Earth Sciences, Hungarian Academy of Sciences, using a Reliotron (cold cathode) instrument mounted on a Nikon Eclipse E600 microscope using a Nikon 4500 digital camera. The cathodoluminescent apparatus was operated at a 7–8 keV accelerating voltage and 0.25–0.63 mA beam current.

A Rigaku Ultima IV X-ray diffractometer was used to determine the mineralogical composition of the insoluble residue. Insoluble residue was prepared by digestion of the calcium carbonate by dissolution of bulk samples with 10 v/v% acetic acid in 20 ºC. When choosing samples to dissolve we have taken care that the samples would not be postdiagenetically fractured. To characterize the clay minerals, oriented specimens were measured on a fraction of <2 μm diameter. Air-dried and ethylene-glycol solvated (16 h, 60 ºC) samples were X-rayed to identify the swelling clay species.

A U-RFL-T type UV fluorescence module and a UMNU2 type filter (exciting filter 420-480 nm, emission filter 520 IF, dichromatic mirror 500 nm) was applied to detect the carbonaceous material in the thin section. This set was installed on an Olympus BX41 polarization microscope. Carbonaceous material analyses were performed on a Thermo Scientific DXR Raman microscope equipped with a diode-pumped frequency-doubled Nd-YAG laser at 10 mW maximum laser power. The samples were irradiated by laser light at a wavelength of 532.2 nm, with the laser beam focused using a 100× objective lens, resulting in a spot size of ~0.7 μm. The backscattered light collected by the microscope objective was filtered via an edge filter, dispersed by a single grating (1800 grooves mm^{-1}) and gathered in a CCD detector cooled to -20 °C by the Peltier effect. The instrument has a

spectral resolution better than 2 cm^{-1} and a spatial resolution of a few cubic micrometres; a 25 μm pinhole aperture was used for each measurement. In every case, 1 mW laser power was used to record the spectra. Sample exposures were obtained by operating the DXR Raman microscope in auto-exposure operating mode, in which the instrument attempts to reach a specified signal- to-noise ratio (S/N) during the measurement (in this case, S/N = 60).

We used UV methods to characterize the petroleum inclusions (from the vein system). During the detection, we used the above mentioned Olympus microscope with an Olympus U-MNU-2 filter cube and an Olympus 100 W mercury light source. We collected 18 spectra during the measurement. To optimize the signal-to-noise ratios, we chose the spectrum of the highest intensity among the collected spectra of the single petroleum inclusions. To facilitate a comparison between different petroleum types, each spectrum was transformed into XYZ chromaticity coordinates and was plotted in the CIE-1931 chromaticity diagram (Smith and Guild 1931). This method was also applied to characterize the crude oil from the Gomba-1 well.

3.3.3. Mineral chemistry

The geochemical properties of the different rock-forming phases (including framework grains and cement) were analysed by XRF and SEM EDS instruments. A Horiba Jobin Yvon XGT 500 micro-fluorescence spectrophotometer was used for the XRF measurements with a 15 keV accelerating voltage and 10 μm aperture size. Mg-content measurements of the calcites were recorded by a Hitachi S-4700 FE scanning electron microscope with an Energy Dispersive detector. All the measurements were made at a 20 keV acceleration voltage.

The carbon and oxygen isotopic compositions of selected textural elements were determined in the Hungarian Academy of Sciences Institute for Geological and Geochemical Research using the following methods. Sampling was conducted by a hand-operated micro-drill, and the recovered powder was put into a 10 ml threaded borosilicate bottle closed down by septum after the volume above carbonate was rinsed by He-gas. Carbonate was exposed with water free phosphoric acid (H_3PO_4) at a stable temperature (72 °C). After the 100% carbonate – acid reaction and after isotopic equilibrium was reached (2 hours), the $\delta^{18}O$ and $\delta^{13}C$ values of the gas exposed from the carbonate were measured by a Finnigan delta plus XP vehicle carrier gas mass spectrometer (Spötl and

Wennemann 2003). The institute applied the international standards NBS-18 and NBS-19 and Carrara lab standards. The results were related to the V-PDB (Vienna-PeeDee Belemnite) standard (Coplen 1996) and given in traditional $\delta^{18}O$ and $\delta^{13}C$ values (expressed in ‰) under the following formula: δ = (Rsample/Rstandard -1) x 1000, where R_{sample} and $R_{standard}$ are the $1^8O/^{16}O$ and $^{13}C/^{12}C$ isotope ratios defined in the sample and the standard (McKinney et al. 1950). The uncertainty of the measurement was better than 0.2‰.

3.3.4. Thermometry

Due to the maturation of the organic matter (OM), significant irreversible modification can take place, which can be detected in Raman spectra. Numerous thermometry methods were calibrated for this phenomenon during recent decades (Yui et al. 1996; Beyssac et al. 2002; Rahl et al. 2005; Lahfid et al. 2010; Zhou et al. 2014). All the calibrated methods calculate the maximum temperature the OM, was subject to, considering the position of the graphitic peak and the amplitude, full width at half maximum (FWHM), and area of 3 or 4 defect peaks. From the above mentioned thermometers, Beyssac et al. (2002), Rahl et al. (2005), and Lahfid et al.'s (2010) methods were used on 18 samples.

The Seasolve PeakFit 4.12 software program was employed to evaluate the Raman spectra. A Gaussian deconvolution approach based on the Voigt-type curve fitting procedure was used to determine the peak position (centre), amplitude, full-width-at-half-maximum (FWHM), full width at base, and integrated area of the bands of interest.

In our case, there is a possibility to determine the formation temperature of the vein filling phases by fluid inclusion thermometry. Fluid inclusion petrography and micro-thermometry were performed on thin sections made from limestone samples. Prior to the analytical procedures, double-polished thick sections (75–150 μm) were prepared from the cores. The preparation of thick sections followed the instructions of Shepherd et al. (1985). The sections were then examined to classify fluid inclusion assemblages following the criteria of Goldstein and Reynolds (1994). Micro-thermometry was carried out using a Linkam THMSG-600 heating-freezing stage mounted on an Olympus BX-41 microscope. The stage was calibrated using synthetic fluid inclusions trapped in quartz. The homogenization temperatures (T_h) have standard errors of ±1 °C. The homogenization temperature was usually determined by the cycling method (Goldstein and Reynolds

1994). The salinities of the aqueous inclusions were calculated from the final ice melting temperatures (T_m(Ice)) and reported in m/m% of NaCl equivalent (Bodnár 1993).

3.4. Results

The results show two different types of carbonates (limestone and dolomitic limestone); there is a thin polymictic breccia horizon in the upper part of each borehole (G1, G2, G3) and there are breccia zones that are involved in the massive carbonate rock body. The detailed results are given for each rock type separated in the following section.

3.4.1. Carbonates

The top of the pre-cenozoic basement is marked by a sharp reflection in the seismic images, but due to the above mentioned total mud loss, the Triassic/Eocene unconformity could not be detected precisely in the sampled core material. The boundary was defined only by well log parameters (porosity, and total gamma). More precise petrophysical measurements are not available because there is no core from this depth.

3.4.1.1. Limestones

Below the unconformity two limestone types can be defined at macroscopic scale: Type A is a light grey, massive oncoidal limestone, and Type B seems to be a leached variety of Type A with a light brown, whitish colour and hygroscopic behaviour. The Type B limestone is very friable and weathered. Because it is known from only 40 cm thickness in one core from one of the bottom of the Gomba 1 well it is interpreted as a stratigraphically irrelevant unit.

3.4.1.1.1. Limestone type A

3.4.1.1.1.1. Texture and grain types

The The Type A limestone is onco-bio-pel-sparite grainstone (Fig. III.3/a, b). It consists of peloids and oncoids with foraminifers, algae, echinoderms and ostracod bioclasts in the centre of the coated grains. The peloids and oncoids are well sorted. The

oncoids are of 1–3 mm, and the peloids are of ~50 μm in diameter with isometric shape. Coating related laminae with microsparitic interlaminar infilling are well preserved. The grain-supported rock texture is observed to have several types of calcite spar filling the intergranular porosity. The samples contain (<1%) authigenic euhedral quartz crystals, which do not show fabric selective distribution; rather, they are dispersed in the sediment (Fig. III.3/d). They always contain calcite inclusions.

3.4.1.1.1.2. Cement phases

The intra-skeletal porosity is filled by microsparite, while the intergranular porosity is filled by an early isopach fibrous calcite cement and a later equigranular blocky calcite cement (BC) (Fig. III.3/c). Fenestral porosity is commonly filled by radiaxial fibrous calcite cement (RFC), but micrite occurs as well. RFC and BC do not show luminescence, but the microsparite has a bright orange luminescent colour.

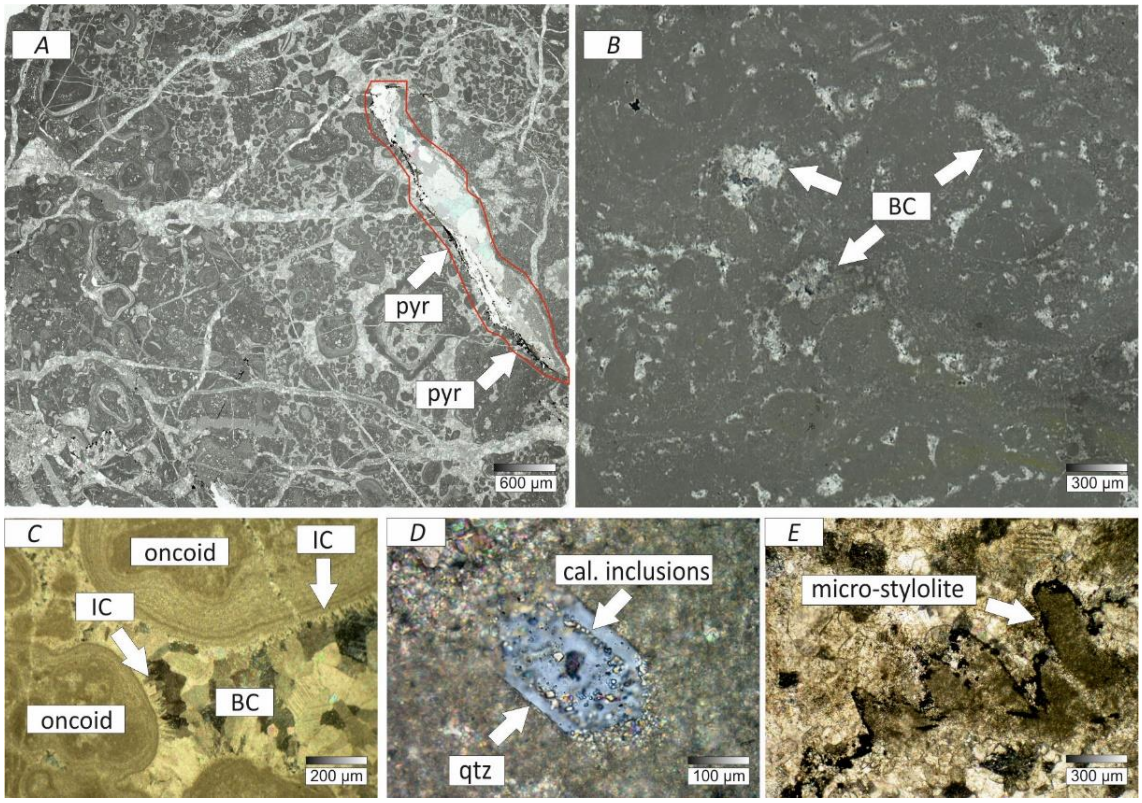

Fig. III.3: A: grainston/packstone fabric of the limestone (Type A). The area included by the red line probably the result of the sulfate reduction; B: Type B; C: different cement types; D: autigene quartz with calcite inclusions, E: Microstylolite ("A", "B", "E" micro photos were taken with planar light and "C", "D" were taken in polarized light)

3.4.1.1.1.3. Microstructure

Based on cross-cutting relationships and vein morphology, four fracture generations (F1; F2; F3; F4) can be defined. The F1 generation can be characterized by syntaxial, symmetric blocky calcite veins (sensu Bons et al 2012) (Fig. III.4/a). Features indicative of growth competition are observable along both sides of the vein walls. The F1 vein generation seems to have been reactivated and encloses the F3 fracture generation. The F2 veins exhibit symmetric syntaxial vein morphology with elongated (150 μm long) calcite crystals (Fig. III.4/b). The distance of the opposite vein walls is equivalently ~200 μm. Textural features of growth competition are not observed; nevertheless, a porosity increase related to dissolution is recognized. Both the primary intergranular and secondary pores are filled by bitumen. Raman spectroscopy measurements confirm presence of organic material through its G (graphitic – 1591 cm^{-1}) and D1 (defect – 1344 cm^{-1}) bands. The F2 filling calcite crystals contain secondary oil fluid inclusions, which have a bright green colour in UV lights. Based on the CL images, the calcite cement growth was a multiphase process. The F3 generation is a narrow (<20 μm), dark coloured anastomosing vein type (Fig. III.4/c) with significant bitumen content. Microfabrics in this vein type are not detectable by petrographic tools because of the presence of the above mentioned bitumen. Locally, the F3 fractures have much larger apertures and enclose ~40 μm sized authigenic, bladed calcite crystals. The F4 vein generation has a symmetric syntaxial vein morphology with an average diameter of >2 mm and consists of blocky calcite. Well-developed growth competition features are visible on the vein walls (Fig. III.4/d). The first calcite generation near the wall is bladed, but there are blocky calcite crystals along the inner side. All the calcite crystals are twinned. There is no intergranular porosity inside the veins, which are lined by micritic carbonate with abundant framboidal pyrite crystals.

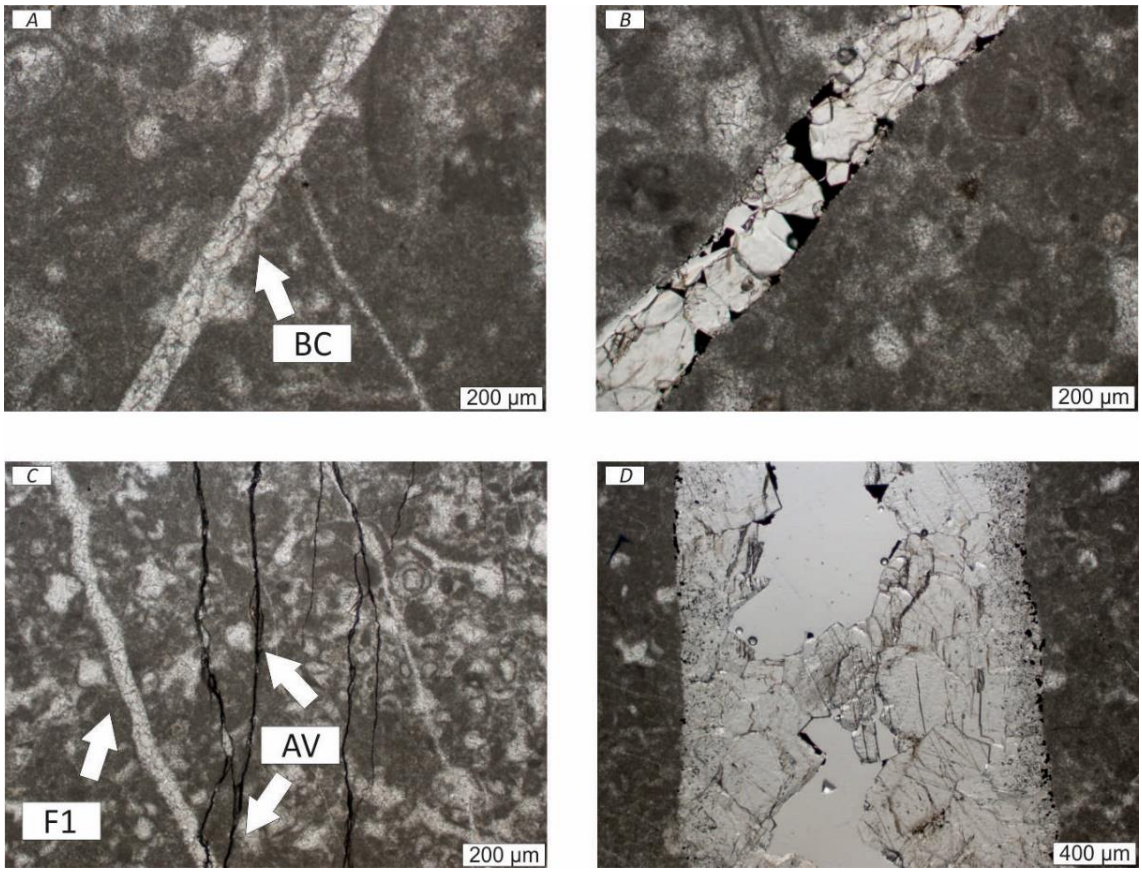

Fig. III.4: Different vein types: A: F1 generation: syntaxial, symmetric blocky calcite vein; B: F2 generation: symmetric syntaxial vein morphology with elongated (150 µm long) calcite crystals; C: F3 generation: narrow (<20 µm), dark coloured anastomosing vein type with significant bitumen content; D: F4 generation: symmetric syntaxial vein morphology with an average diameter of >2 mm and consists of blocky calcite. (All micro photos were taken in planar light)

The vein filling calcite contains many primary and secondary water and oil inclusions. Water-containing fluid inclusions were suitable for micro-thermometry measurement. Based on 16 primary fluid inclusions, the inclusions of aqueous inclusion assemblage undergo homogenization to the liquid phase (LAQ+V→LAQ) between 120 and 140 °C. Based on the average Tm(Ice) value of -2.5 ºC, the calculated salinity of the AQ inclusions is ca. 3.3 mass% in NaCl equivalent (using Bodnar's 1993 method) (Fig III.5).

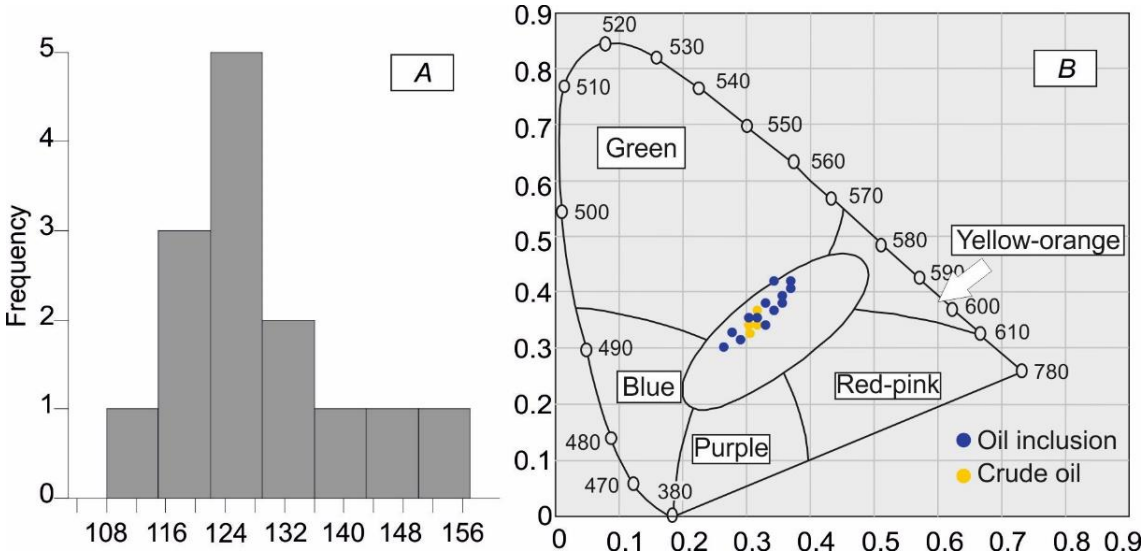

Fig III.5: Results of the micro thermometry and the UV spectroscopy on the fluid and oil inclusions. A: shows the homogenization temperature of the primary water content fluid inclusions (light gray) B: shows the similarity of the UV spectra of the crude oil and the oil inclusions.

Simultaneously to the complex vein system, a well-developed microstylolite system formed with an anastomosing geometry. The maximum amplitude is ~1 mm, and pressure solution films are easily detected on the CL images through their bright orange luminescent colour.

3.4.1.1.1.4. Phase analysis (XRD, Scanning, Raman)

The analysed rock types consist of calcite crystals; other carbonate minerals (dolomite, aragonite) were not detected by the applied techniques.

The most common non-carbonate mineral is pyrite. It has a framboidal form and a bimodal size distribution and fabric position. The smaller sized crystals are related to biogenic components, while the larger ones appear in fractures. The mineral composition of the insoluble residue of the rock is summarized in Table III.2. The results of the thermometry calculations from the carbonaceous material uniformly suggest T_{max}~220 °C. The data are summarized in Table III.3.

	A type limestone[1]	B type limestone[1]	Dolomitic limestone[2]	Breccia[1]
Dolomite	-	-	37%	-
Quartz	-	-	-	???
Illite+Muscovite	~20%	~60-70%	-	~50-60%
Pyrite	~30%	-	-	???
Dickite	~30%	~30%	-	~5-10%
Anatase	~10%	-	-	~5-10%
Gypsum	-	-	-	~5-10%
1: Valid for the insoluble residue				
2: Valid for the Bulk				

Table III. 2: Average mineral composition of the studied rock types

	min	max	average	std.
Rahl et al., 2005	192°C	265°C	226°C	20
Lahfid et al., 2010	210°C	261°C	233°C	11.09
Beyssac et al., 2002a	333°C	382°C	348°C	13.78
Zhou et al., 2014	522°C	599°C	556°C	23.04

Table III.3: Calculated T-max temperatures based on the carbonaceous material (on 18 samples) by Raman spectra

3.4.1.1.1.5. Mineral chemistry

The chemical analysis of the different cement phases by SEM-EDAX do not indicate high Mg-calcite (>4 mol%). Additionally, based on this measurement, there is no detectable difference in the composition of the two different sized pyrite populations; both have a negligible amount of trace metals and can be regarded as pure FeS_2.

Based on the stable isotopic measurements, the carbon and oxygenic isotope composition of the host rock is $\delta^{18}O$: -4.0 (‰V-PDB) and $\delta^{13}C$:+4 (‰V-PDB) (±0.2‰).

3.4.1.1.2. Limestone type B

There is no significant difference between the Type A and Type B limestones regarding their framework composition; Type B limestone is also a peloidal, oncoidal grainstone. There are also no differences in their cement phases.

Based on the results of phase analysis, Type B is similar to Type A. The former is composed of pure calcite crystals; there is no trace of dolomite or aragonite. The amount of the dissolution residue is less than 1 m/m%. A significant difference from Type A appears regarding the mineral composition of the insoluble residue (summarized in Table III.2); the

dickite content of the residue is ~90%, which is much higher than the ~40% in Type A (Table III.2).

3.4.1.2. Dolomitic limestone

3.4.1.2.1. Texture

The allochems are similar to those of the non-dolomitic limestones, suggesting a similar grainstone precursor texture. As a result of the fabric selective dolomitization, a planar-E dolomite (Sibley and Gregg 1987) developed (Fig. III.6/b).

3.4.1.2.2. Cement phases

The primary cement phases in the intergranular space are not recognizable due to the effect of dolomitization, but the abundance of the above mentioned radiaxial calcite cement is much higher than in the case of the non-dolomitic limestone members. In several parts of the samples, large (>300 μm) calcite can be. The shapes of the grains suggest that these calcite pseudomorphs formed after anhydrite crystals but there is not any measurement to prove this. (Fig. III.6/c).

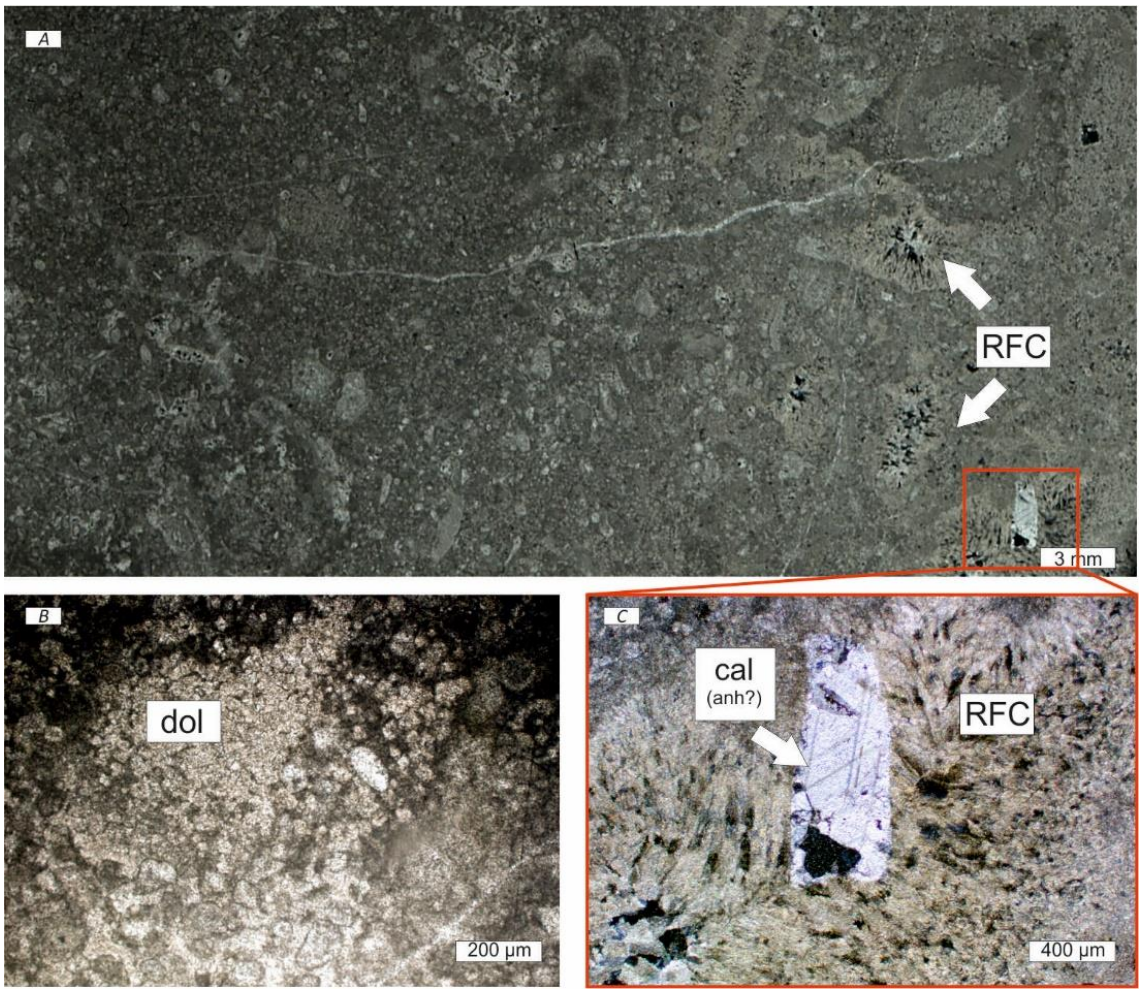

Fig. III.6: Micro phtotos of the dolomitic limestone samples. A shows the fabric of the rock type and the non-fabric selective dolomitization. B: shows the euhedraly dolomite crystals. C: possibly calcite pseudomorphs formed after anhydrite. (All micro photos were taken in polarized light)

3.4.2. Breccia

3.4.2.1. Texture

Breccia zones are defined mainly in the upper few metres of the Triassic carbonates close to the proposed Triassic/Eocene boundary. Subordinately, breccia horizons are detected inside the carbonate bodies in deeper zones as well. Based on the observations, the breccias at different horizons are rather similar, so their descriptions are summarized.

The studied breccias have a polymictic composition (Fig. III.7). Lithologically, the most common clast type is the above characterized limestone. Subordinately, laminated calcrete clasts and those common in the overlying Eocene sequence (i.e., metamorphic rocks, siltstone) occur. The average grain size of the different clast types is different. The limestone clasts are larger (cm scale), while the others are smaller than a few millimetres in

diameter. The roundness for both the carbonate and non-carbonate clasts follows a normal distribution based on the Kolmogorov-Smirnov test, but the roundness of the majority of the carbonate grains is smaller than that of the non-carbonate grains (Table 4; Fig. III.8). The variation coefficient of the main axis of the clasts (0.69) shows a chaotic texture. The packing density of the clasts is very variegated; grain to grain contacts are typical, but in some cases, there is more than a centimetre of space between the floating grains. The matrix content of the breccias is significant (> 60%). Based on all these descriptive and numerical textural parameters, the breccia in question can be characterized as chaotic breccia (Mort and Woodcock 2008). The results of the image analysis are summarized in Fig. III.8.

	Min	Max	Average	STD
Area (mm^2)	0.04	92	5.96	14.16
Rotation	1.5	175	92	43
Roundness	0.21	0.97	0.63	0.17
Roughness	1.04	1.14	1,08	0.02
PSD= -***1,0072***x + 9,3316 (R^2 = 0,9437)				

Table III.4: Results of the image analysis. All parameters had been measured on 332 grains

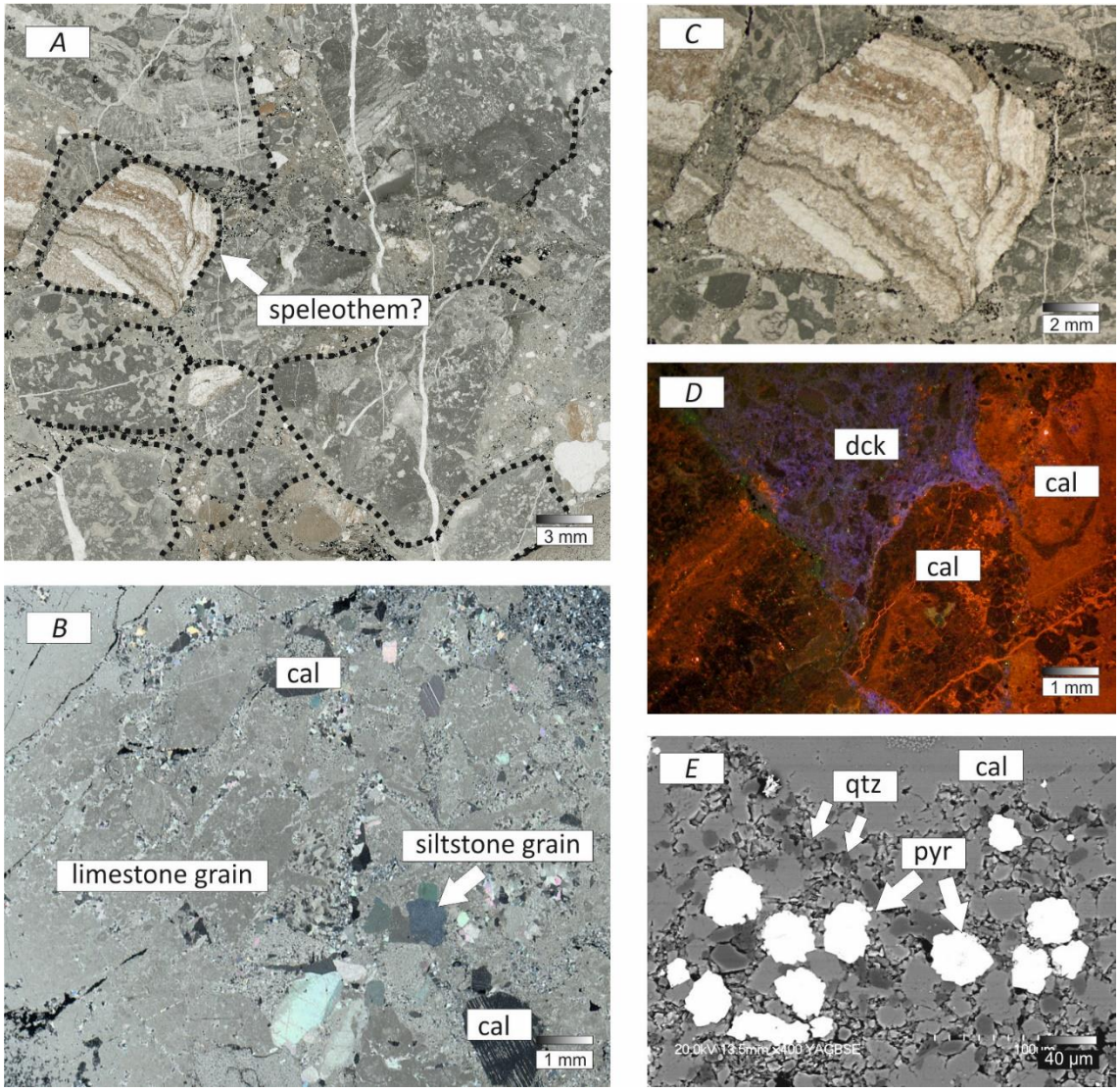

Fig. III.7: Photomicrographs from breccia samples. A: fabric of the breccia from the Triassic-Eocene boundary (2472 m), B: fabric of the breccia from the deeper zone (2520 m); C: laminated calcrete clast from the studed breccia; D: cathode luminescence photo from the matrix; E: framboidal pyrites from the matrix of the breccia; dot line shows the common presence of pyrites ("A" and "C" micro photos were taken with planar light and "B" was taken in polarized light. "E" is a back-scattered electron image) Abbrevations: dck: dickite, cal: calcite, qtz: quartz, pyr: pyrite.

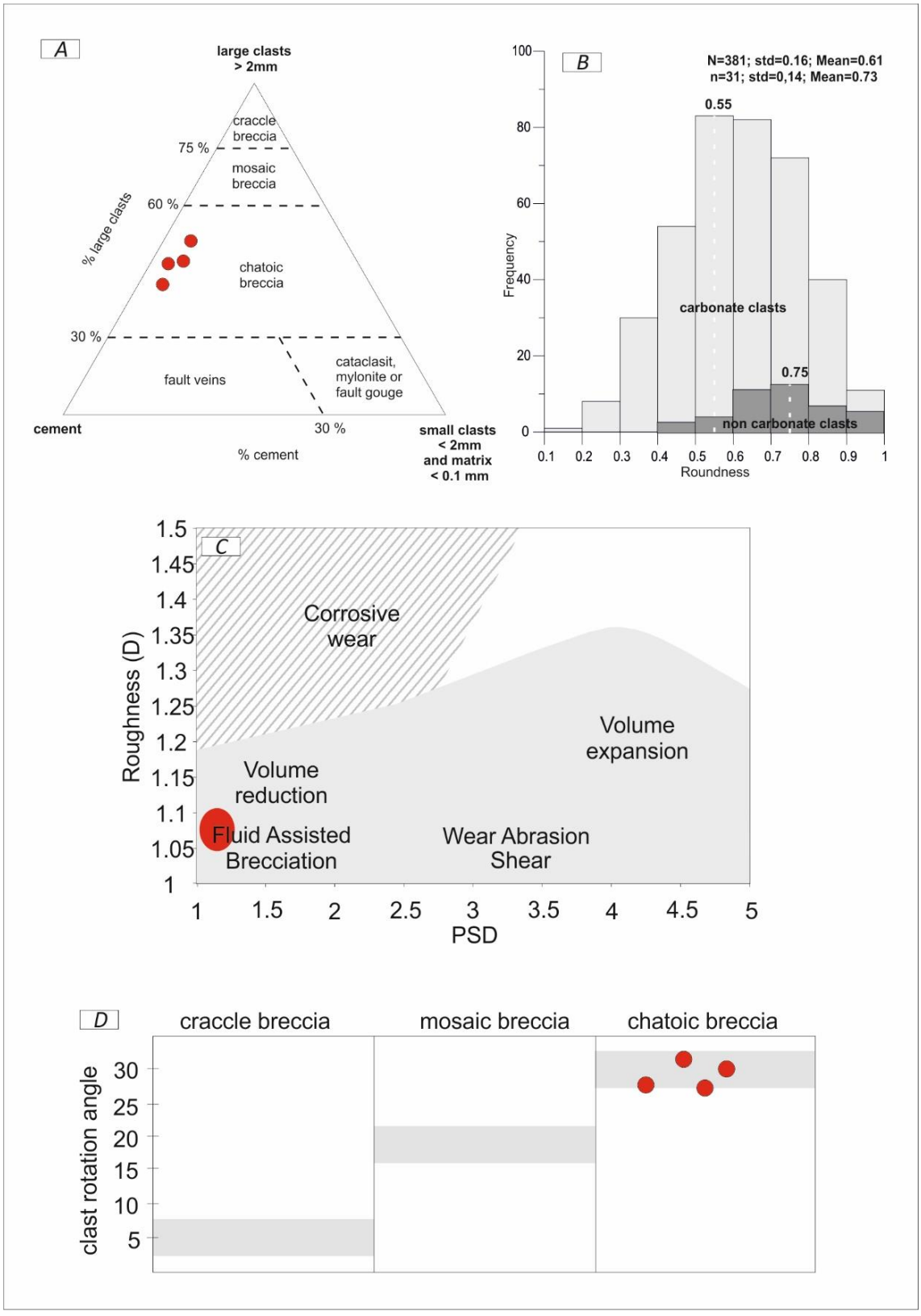

Fig. III.8: Results of PIA. Figure A and D shows the classification by Mort and Woodcock 2008 diagrams, B: shows the distribution of roundnes paramater by rock type categories, and C, shows the potentially generating processes, by Jébrak 1997

3.4.2.2. Matrix and cement phases

The matrix mostly consists of carbonate rock clasts and quartz, but calcite, anatase, feldspar and muscovite mineral fragments are present as well.

Two different types of cement phases are defined by CL microscopy. There is a fine crystalline phase in the matrix with a bright purple luminescent colour. Around the purple phase, there are numerous individual calcite crystals with dull orange luminescent colour and a very bright orange overgrowth (Fig. III.9). Based on the SE images, the purple phase seems to be a type of kandite mineral, which seems to be authigenic based on the SEM observations.

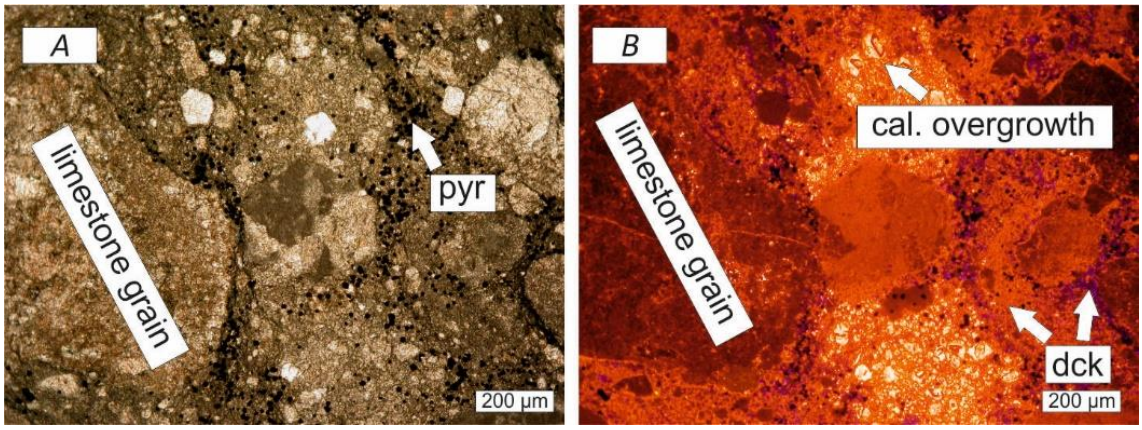

Fig. III. 9: Different calcite cement phases or overgrowths observed in the breccia. A: optical microphoto and on CL images. (All microphotos were taken in planar light.) Abbrevations: pyr: pyrite, dck: dickite.

3.4.2.3. Microstructure

Only the F1 and F4 fracture generations are detectable in the breccia zones, whereas F2 and F3, which contain a large amount of bitumen, do not seem to be evolved in this lithology. The F1 generation is only detectable inside the carbonate clasts, while the F4 generation cuts the entire matrix. F4 fractures exhibit chaotic spatial distribution; they follow the surfaces of the larger clasts. Both microfracture generations (F1, F4) have a notable secondary porosity by dissolution.

Microstylolite systems have not developed in the breccia zones, but the pressure solution is significant along the clast boundaries resulting in a stylobreccia texture.

3.4.2.4. Phase analysis

Based on the XRD measurements, the most common minerals in the matrix of the breccias are dickite (40–50%), illite±muscovite (25–35%) and quartz (20%). Subordinately, pyrite, anatase and goethite are detected as accessories.

3.4.2.5. Mineral Chemistry

Three XRF maps were recorded from different regions of the matrix for the following elements: Si, Al, Fe, Mn, P, S, Ni, Co, Ba, Sr, Ce, and Pb. Based on the element maps, none of these elements shows fabric selective distribution. The isotopic composition of a calcrete pebble is $\delta^{18}O$: -6.5 (‰V-PDB) and $\delta^{13}C$: ~6.0 (‰V-PDB), while that for the limestone is $\delta^{18}O$: ~3.5 (‰V-PDB) and $\delta^{13}C$: 2.0 (‰V-PDB) (±0.2‰) (Fig. III.10).

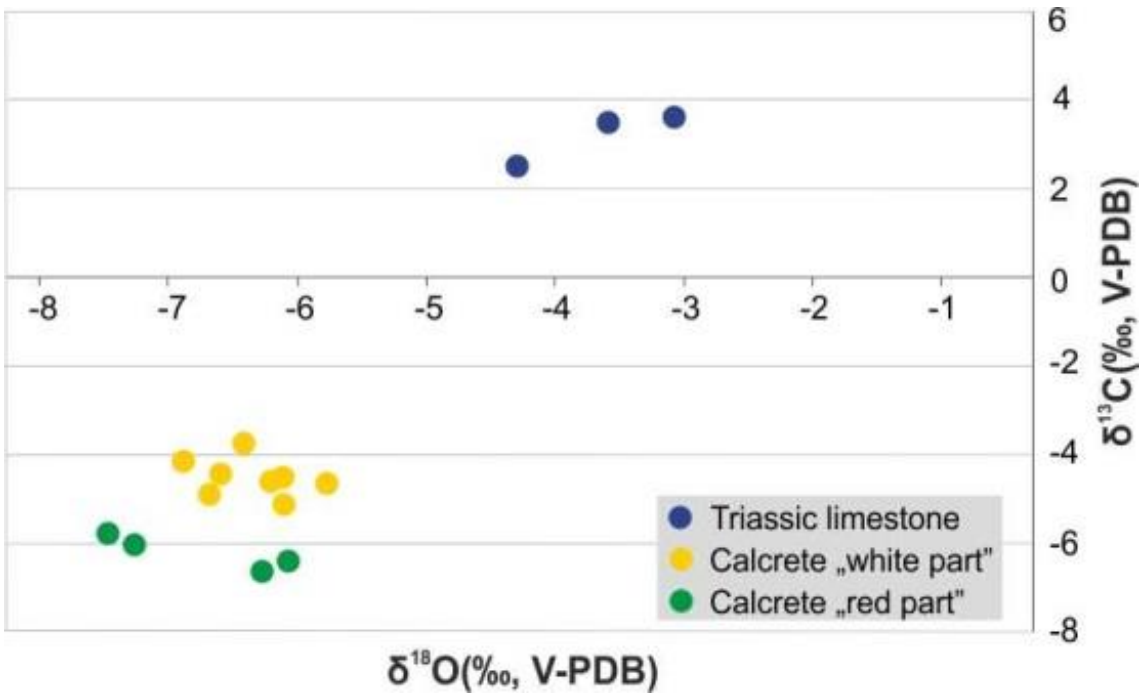

Fig. III. 10: Isotopic composition of the measured samples.

3.5. Discussion – Petrological characteristics of the main rock types

3.5.1. Limestone

Based on the core analysis, there are three different carbonate rock types in the reservoir. Among them, the most widespread is Type A limestone, which is an oncoidal, peloidal grainstone. Due to the small amount of core samples, the exact classification of the rock types into lithostratigraphic units is very uncertain. Based on the geographical position of the investigated formations, the study area should belong to the Mid-Hungarian Mega Unit, but previous report (Benedek 2009) and data from the neighbouring fields suggest that it is more likely a part of the Triassic Kisfennsík Limestone Formation or the Berva Limestone Formation in the Bükk Unit. As our results do not give any clear evidence to the contrary, the carbonate rocks in the studied reservoir are considered as a Bükk type limestone similarly to the available Mol Report (Benedek 2009).

Tidal flat, lagoonal and reefal environments have been reconstructed for the Kisfennsík Limestone in the Bükk Mts. (Velledits et al. 1999). The beds in the Gomba Field represent a different zone of platform. High energy part of the platform is represented by the well-sorted oncoidal samples (G-1 well) and the tidal flat is represented by the algal mat and the fenestral porosity of the samples (G-3 well). The stable isotopic data show a typical Triassic carbonate platform environment (Schimpf et al. 2011).

The mineralogical compositions of the limestone samples are relatively homogeneous; the studied core sections are composed of pure calcite. The proportions of non-carbonate phases are usually less than 1%. Quartz, pyrite, layer silicate phases (illite±muscovite, dickite), anatase and goethite appear as accessory minerals.

The finely dispersed distribution of euhedral crystals in the limestone is usually not an uncommon phenomenon; quartz often appears in such a textural position in hypersaline environments. Quartz with the observed morphological and mineralogical characteristics may crystallize during pedogenesis, or very shallow diagenesis (Nash et al. 2004; Varga and Raucsik 2014). Based on the geological evolution of the study area (assuming an identical history to the Kisfennsík Limestone), pedogenesis could have affected the sediments during the Palaeocene. Other substantiating signs of pedogenesis are not observed, which is the reason for that may be the erosion.

The bimodal size distribution of the framboidal pyrites suggests two generations, but this observation is not definitely confirmed by their similar chemical compositions.

Smaller pyrite grains (<15 μm) occur near the bioclasts or near to the early cement phases; therefore, its formation is considered to be early diagenetic. A possible process that produced the pyrite may be sulphate reduction. In this case, the SO4- content of the porewater is reduced by bacteria, in the organic matter–rich environment which leads to framboidal pyrite formation in the vicinity of concentrationsn of organic matter. The larger pyrite grains (>50 μm) occur detectably near the fracture system in both the Triassic carbonates and the Eocene breccia. Based on experiments of Hallbach et al. (1993) and field observations of Sweeny and Kaplan 1973), framboidal pyrites may evolve up to ~200 ºC, while their minimum growth-temperature under laboratory conditions without involving sulphate reducing bacteria (SRB) is in the range of 65–80 ºC. This temperature may even be 40–60 ºC less than that needed under natural conditions (Maclean et al. 2008). In our case, there is no direct evidence for SRB contribution toward the generation of the larger pyrite crystals. However, based on the OM Raman measurements (Table III.3), our samples reached a higher temperature than the maximum possible formation temperature for framboidal pyrites, which can be explained by their textural position. In this case, the reduced material should not be the synsedimentary organic matter of the limestones; rather, it is the bitumen seal of the veins. Because organic matter in this position is likely a result of hydrocarbon migration, it is suggested that the carbonaceous material records the maximum temperature reached during burial, and the large pyrite crystals grew in the course of the uplift following oil migration to the reservoir.

There are several subsequent cement phases in the analysed samples. The prismatic, radial, and limpid calcite cement, enveloping the ooids and oncoids, is considered to be the first phase (Fig. III.3/b). It has low Mg-content (< 4 mol%), which may suggest a meteoric origin (Hayes and Boles 1993). Based on its textural position, this phreatic cement possibly formed during early (shallow) diagenesis close to the surface.

Radiaxial fibrous cement (RFC), which can form in different environments, is clearly in younger textural position than the above mentioned phreatic cement. New research (Richter et al. 2011) says that it could develop not only in marine phreatic zones but also in a continental vadose zone, and the resulting cement may form by both diverse biogenic and abiogenic processes. Although the most common environment of this cement type is the intertidal and upper bathyal zone up to 600 m depth (Richter et al. 2011), but this cement also has been documented to form in numerous caves (Neuser and Richter 2007; Richter et al. 2011). The position of the RFCs in the samples is not fabric selective. Based on its low Mg/Ca ratio, this calcite may also have precipitated from meteoric fluids,

which is in good agreement with the results of Wilson and Dickson (1996), who said that RFC forms from meteoric fluids instead of seawater in subtropical or tropical platforms. Based on its texture, mineral chemistry and worldwide analogues, the RFC in our samples is interpreted as early digenetic cement.

The Mg/Ca ratio of the blocky calcite cement is low, and the crystals enclose numerous tiny dolomite inclusions, which are typically only a few micrometres across. The presence of dickite in the limestone shows a burial formation temperature as high as >200 ºC (Zotov et al. 1998). This value is consistent with the calculated maximum temperature based on the typical Raman spectra of the carbonaceous material (~220±50 ºC).

The tectonic evolution of the region had to be rather complex as suggested by the subsequent brittle deformation events recorded by fractures and intense brecciation. The real age of the vein filling by calcite is unknown, but the microstructural results show that the F1, F2 and F3 fracture generations are older than the main brecciation event, while the last generation (F4) must be earlier than the process what formed the breccia structure. Furthermore, we know that the vein filling in F3 has bitumen with high Tmax, while the F4 generation calcite contains fluid phase hydrocarbon inclusions. All the data indicate that the above mentioned uplift happened after the cementation of the F3 fractures but prior to or during the F4 filling by calcite, when the formation temperature was lower than in the case of F3 (Fig. III.11). This model is supported by the micro-thermometry of the F4 generation fluid inclusions (based on 16 samples) (Fig. III.5/a). The primary fluid inclusions show a ~125 ºC homogenization temperature, which is similar to the temperature of the recent pore-fluid. The data suggest that the F4 fracture generation formed due to relaxation during the uplift phase. This fracture generation has to be part of the presently active reservoir as supported by the similarity of the spectra of the oil inclusions and the produced crude oil (Fig. III.5/b).

3.5.2. Dolomitic limestone

Limestones with dolomite content of >40% are defined as dolomitic limestone in this paper using Chilingar (1960)'s terminology. The original packstone texture of the rock type is recognizable in all the studied samples despite the destructive dolomitization. This texture is interpreted as a low energy sedimentation environment, most likely along the back reef lagoon of a carbonate platform. We interpreted the calcite pseudomorphs, implying an intensive evaporation process. Dolomitic limestone samples came from the

bottom depth of 2680 m, from the very bottom of Gomba-1 well. Continuity of the facies below this depth is not known which nevertheless may be a more significant part of the reservoir than was previously believed.

3.5.3. Breccia

Based on the results breccias occur in two different stratigraphic positions in the reservoir (Fig. III.1). The thicker horizon is located at the Triassic-Eocene unconformity, while the thinner zones are observed below the unconformity, inside the carbonate body surrounded by homogeneous limestone beds that were significantly deformed by deformation events (both brittle and ductile deformation).

The investigated breccia types are rather heterogeneous both concerning composition and structure. The most common and largest clasts consist of the above described carbonates, but there are also metamorphic and siltstone fragments. Based on the results of isotopic measurements on the calcrete-like fragments, the parent fluid of this fragment was of meteoric origin. Consequently, these fragments cannot be stromatolite fragments, but these clasts may represent pieces of calcite veins or any fresh water limestone form, e.g., a speleothem or a laminated accrete fragment. As there is no datum in the literature about a vein type similar to these fragments from the wider region, the laminated carbonate clasts are considered to be speleothems (e.g., dripstone fragments). This seems to be supported by the measured isotope values, McDermott (2001) and Verheyden et al. (2008) measured similar values in speleothemes.

The subordinate mineral grains in the matrix (quartz, anatase, feldspar and dickite) of the breccia are not typical in the above described limestones. The CL colour of the kaolinite group mineral in the matrix (purple) is problematic. Based on (Boggs and Krinsley 2008, Götze et al 2002) the colour of the kaolinite and dickite is deep blue instead of the experienced purple. The most likely reason is that, the CL spectrum is shifted due to irradiation by an intensive electron beam (Götze et al 2002). The mass proportion of the dissolution residue of the breccia is ~10 m/m%, i.e. ten times what is typical for the carbonate samples. The most probable reason for the relative increase in the insoluble residue is the decreasing carbonate content resulted by dissolution. Nevertheless, in the case of dissolution, the clasts should show a very complicated shape (Jébrak 1997), which has not been observed in the present case. That is why the occurrence of these mineral

grains should be the result of postdiagenetic brecciation rather than syngenetic, intrabasinal transportation.

The basal member of the Kosd Formation in the Bükk Unit consists of 2–25 cm sized gravels, which mainly represent the Kisfennsík Limestone (Less 2005). The breccia studied in the Gomba wells is identical to the Kosd Formation by (Benedek 2009), even if the roundness of the clasts from the Kosd Formation usually increases to the SW (towards the Gomba field) (Less 2005), which is not typical here at all. In our paper this formation is called as 'Basal Paleogene clastics' (BPC). The roundness of the carbonate clasts in (BPC) is smaller on average (0.63) than that for non-carbonate clasts (0.73) (Fig. III.8/b), which suggests that the more resistant non-carbonate clasts represent a longer distance transport thus a more distant source area, while the carbonate clasts were derived from a much closer source, most likely they did not move at all. This latter model is coherent with the presence of the well-preserved supposed speleothems in the breccia because speleothems cannot withstand transportation. In addition, the unimodal, normal distribution of the roundness data of the carbonate clasts suggests that there was only a single process responsible for their shape.

3.6. Possible interpretations of the breccia formation

Breccia texture rocks can be formed by tectonic processes (compression or extension stress field) or can be formed by syngenetic processes too (e.g. regolith or other sediments). In our case we try to define those processes which can describe the breccia formation in two different depths.

3.6.1. Hydrobreccia – cave sediment theory

Using the classification scheme of Jébrak (1997), the breccias in the Gomba field could be interpreted as hydraulic breccias based on their measured geometric parameters (Fig. III.8/c). Similar rocks are known from the wider surroundings at the Triassic-Eocene boundary (Magyari 1994), confirming that the genetics of the breccia in this study may be similar to those wide-spread around the karstic area in the Buda Mts. This locality is as close as 50 km to the west of the Gomba field. Here, based on the model of Magyari (1994), marls with high fluid content were deposited and infiltrated into to the surface of the fractured and karstified Triassic limestone in the early Eocene. Brecciation in the Buda

Hills was due to the collapse of the steep marginal cliffs of the abrasional coastline (coincident with a synsedimentary fault-scarp). It is supposed that the collapse was triggered by earthquakes and the sudden deposition of the voluminous rock fall episodically increased the pore-pressure to such an extent as to result in hydrofracturing and further brecciation. These breccias have very similar textural features to those described in the Gomba wells; both are matrix supported, there are no shear indicators in the matrix or along the rock fragments and the roundness of the grains varies.

In our concept fluvial sediments (Kosd Formation?) with high fluid content were deposited onto the karstified surface and subsided into greater depths afterwards. Because of the impermeable cover (marly and clayey sequences) the fluids infiltrated into the primary, secondary and tertiary porosity were unable to escape through the existing micro fracture system and the fluids had to cause overpressure and brecciation through hydrofracturing during the Oligocene or later (Fig. III.11).

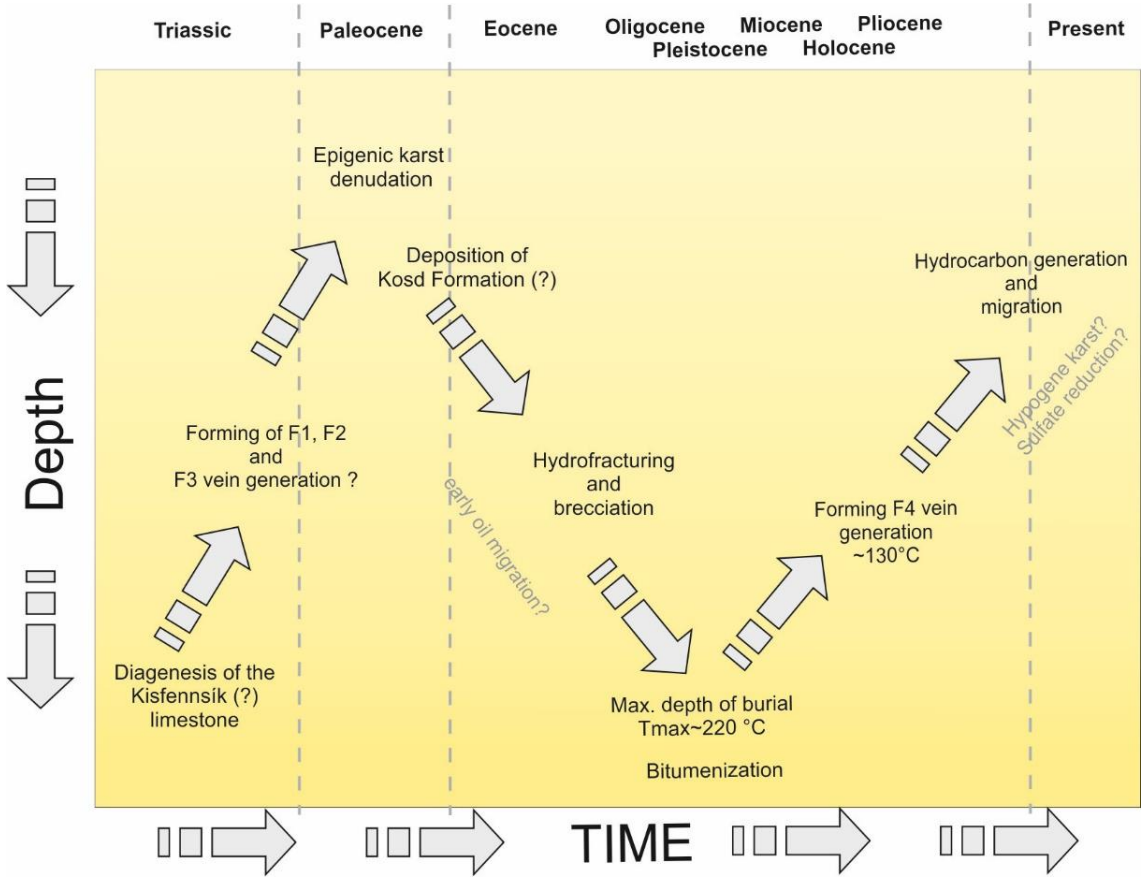

Fig. III 11: Schematic depth-time diagram of the observed diagenetic events.

In addition to the geometric parameters of the clasts (Fig. III.8), the textural position of the pyrite coating on the rock fragments supports this theory. The youngest

fingerprints of the evolution preserved in the samples are the above mentioned larger pyrites along the F4 vein generation. The maximum formation temperature of the framboidal pyrites is approximately 200 ºC. As the temperature of the maximum burial in the study area was ~220±50 ºC (based on the Raman measurements), this pyrite generation had to crystallize during an uplift event however the circumstances of this event are not known. At present the temperature of the warmest fluids in the carbonate reservoir is ~130 ºC, much lower than the Tmax value measured on the carbonaceous material. Geochemical analyses had previously confirmed that hydrocarbons are still migrating from the Triassic layers towards the Eocene conglomerates, which are also rich in pyrite (Benedek 2009). The pyrite in the basal Palogene Clastics (Kosd Formation?) has an identical textural position to that in the Triassic carbonate breccia where it coats the clasts. The similarities between these pyrites suggest that the pyrite formed due to the same process. According to our hypothesis, the framboidal pyrite zone formed at the front of the migrating hydrocarbons. In the deep zones, where the temperature was above 100–160 ºC, hydrocarbons could produce H_2S-rich fluids by thermal sulphate reduction (Machel 2001). When these fluids reached the actual (130 ºC) (or lower) temperature, framboidal pyrites formed near the migration pathways. Framboidal pyrites are usually the signs of bacterial sulphate reduction (BSR) which is normally active only up till 60 to 80 ºC (Machel 2001), but framboidal pyrites can form by replacement of greigite with pyrite in hydrothermal environment too. In this case there is not enough information about the pyrites to reconstruct the forming mechanism. Hydrogen sulphide that developed by sulphate reduction could have increased the pore volume as it is observable in the cores (Fig. III.3/a).

Hydrofracturing as a model can give an adequate interpretation for the genetics and evolution of the breccias at the Triassic-Eocene boundary but cannot explain the polymict breccia in the deeper parts of the carbonate body. Following the nomenclature of Loucks (1999), these rocks can be classified as “matrix supported chaotic breccias”. Based on recent analogies, the formation of this breccia type is possible either by cave wall collapse or fluvial transportation (White and White 1969). Both processes inevitably require a well-developed karst. Well-developed karst aquifers have a relatively large storage capacity but water flows through the system unobstructed in conduits at high velocity (up to m/h*102) (Stevanović 2015). This high flow velocity is necessary to the transportation of the coarse sediments. Based on the analogies from the Transdanubian Mega Unit and the Bükk Unit, there was intensive epigenic karstification during the Palaeocene and early Eocene, which

resulted in a dissected surface. Based on these analogies, it is presumable that the buried Gomba reservoir was karstified, at least during the Palaeocene and early Eocene, because it was in an uplifted position and there was significant precipitation during these ages (Bowen et al. 2004). Because of the small amount of breccia samples from the deeper section, it is impossible to recognize their genetics, but this rock type can be an indirect evidence of karst processes. Based on its stratigraphic position and petrographic and microstructural features, it can be suggested that the breccias in the deeper section possibly represent collapse breccia and, in part, cave sediments.

3.6.2. Regolith theory

As an alternative of the hydrobreccia model, another one, introduced by Nádor (1991, 1993) can be applied as well. Nádor (1993) investigated the paleokarst of Buda Mts., where numerous breccia outcrops occur along the Triassic-Eocene boundary. Those breccias are interpreted as a regolith that formed by tectonic events, when the area was uplifted possibly resulting in erosion of Jurassic and Cretaceous pelagic sediments during this long subaerial period. As a consequence, the underlying Triassic carbonates became exposed to meteoric waters (Nádor 1993). Due to tropical climatic conditions Late Cretaceous and early Eocene weathering may have resulted in kaolinite formation instead of dickite. The kaolinite dickite alteration is a very common process both in diagenetic environment and hydrothermal environment. Based on Ehrenberg et al. (1993), Beaufort et al (1998) the alteration works at 120–30 ^{o}C while Choo and Kim (2004) mark a higher temperature, 250–290 ^{o}C. Ehrenberg et al. (1993) says that kaolinite/dickite conversion is inhibited by the invasion of the hydrocarbons. This is in accordance with our results which show that breccia forming preceded by the hydrocarbon migration.

While the regolith theory can in part describe the breccia formation at the Triassic-Eocene boundary, it cannot explain the evolution of the deeper breccia zones at all. Most probably they form a collapse breccia and, in part, also cave sediment as detailed above.

Although there is not enough information to distinguish between the two possible scenarios concerning the breccia formation at the Triassic-Eocene boundary, mineralogical and rock fabric data suggest that the hydrobreccia concept is the most plausible explanation for the observed brecciated horizons.

3.7. Conclusions

The analysed cores suggest a complex history of the reservoir, especially concerning its karstic and structural evolution. Karstification is supposed to have been responsible for the development of the several metres thick, high permeability zone at the Triassic-Eocene boundary, which, from a genetic point of view, can be either a hydraulically fractured breccia zone or a regolith. The polymictic breccia horizons in the deeper zones can be interpreted as paleo-cave facies, collapse and/or cave sediments. While the upper breccias, independent of their genetics, represent a laterally extensive blanket-like formation, relics of the hypothetic cave are probably of linear geometry. This kind of difference may have a peculiar effect on the internal structure and so, on the hydrodynamics of the whole karstic reservoir. From this perspective, the role of the F4 fracture generation seems essential as well. Hydrocarbon fluid inclusions in the vein cementing calcite and the crude oil produced in the area are of identical composition suggesting that the F4 structure must be part of the recent fluid migration pathway. To better understand the behaviour of the rather complex fractured Gomba reservoir, interconnection between the two breccia horizons and the F4 fracture network should be modelled.

Chapter IV

Quantitative shape characterization of individual fractures and DFN modelling of the fracture network in the karstic Gomba hydrocarbon field (Middle Hungary)

Márton Bauer
Department of Mineralogy, Geochemistry and Petrology
University of Szeged, Szeged, Hungary
baumart87@gmail.com

Tivadar M. Tóth
Department of Mineralogy, Geochemistry and Petrology
University of Szeged, Szeged, Hungary
mtoth@geo.u-szeged.hu

Acta Geodaetica et Geophysica
Submitted

4.1. Introduction

The relationship between the fracture systems in limestone bodies and karst phenomena has been analysed by numerous works (e.g., Palmer 1991; Gabrovšek and Dreybrodt 2001; Kaufmann 2003a). Based on all these studies, a tight correlation exists between the connectivity and permeability of a fracture network and the rate of dissolution along these fractures. In more permeable zones, dissolution is also more effective than in low-permeability zones (Singurindy and Berkowitz 2005). In carbonate reservoirs, this phenomenon has a basic importance in terms of palaeo-fluid migration, e.g., it can control the spatial position of karstic dissolution forms (Palmer 1991; Diabat 2013; Bauer and M. Tóth 2015). Thus, if the main characteristics of the fracture network can be determined, this information can be used to help explore the details of karstic or palaeokarstic phenomena. When characterizing such a reservoir, numerous essential aspects should be evaluated, such as the localization of dissolved and cemented fracture groups, traces of palaeo-cave collapses, and features that are not drilled or are invisible in seismic surveys but may have considerable impact on the recent fluid migration geometry in the reservoir.

A significant proportion of hydrocarbons are stored in carbonate reservoirs in Hungary (Dolton 2006). The most important carbonate reservoir rocks can be found in Triassic beds in western Hungary and in the basement of the Hungarian Palaeogene basin, which mostly consists of Mesozoic carbonate rocks (Fig. IV.1). These beds are typically fractured and probably karstified. In fractured/karstified systems, hydrocarbons migrate mostly along the pathways that belong to the secondary (fractures) and even tertiary (karstic) porosity (Reimann et al. 2014; Karay and Hajnal 2015). Nevertheless, the spatial distribution of karstic voids is mainly controlled by tectonic deformation, e.g., by the formation of fracture and fault systems (Jeannin 1990; Benkovics et al. 1999; Hauselmann et al. 1999).

The Gomba field (central Hungary, Hungarian Palaeogene Basin, Fig. IV.1) is one of the most promising fields in Hungary. The productive reservoirs are located in the fractured, brecciated Triassic limestones (Kisfennsík Limestone or Berva Limestone) and in the overlying Eocene basal siliciclastic formations (Kosd Formation). The limestone formations karstified during the Palaeogene (as evidenced in outcrops in the Bükk Mts., Pelikán 2005) and were subsequently buried during the Neogene, which probably resulted in palaeo-karstic forms, such as collapse structures **(**Bauer et al. 2016).

Collapsed zones usually have a typical structure. A brecciated “core” in the middle is commonly enveloped by a fractured “disturbed zone” (Loucks 1999). In the study area, Benedek (2009) and Bauer et al. (2016) described polymictic breccia from the core material of the Gomba Field and interpreted it as a karst-related breccia or cave sediment. At present, the spatial pattern of these disturbed zones is almost unknown. Bauer et al. (2016) classified the fractures in the Triassic beds of the Gomba Field into four fracture generations based on their petrographic and microtextural features. Three of them are interpreted to be older than the karst breccia, and one of them is interpreted as younger.

The goal of our work is to explore whether there are any zones inside the reservoir where the conditions were more favourable for cave formation than in other places. A further aim is to investigate the possible connection between the micro-fracture system and the lithology in the Gomba case. In this paper, we quantify the features of individual fractures, analyse their geometric aspects and scale up the results to the well surroundings to better understand the effects of the fracture pattern and dissolution on the migration pathways.

4.2. Geological background

The Gomba Field is one of the most important hydrocarbon fields in Hungary. It was drilled for the first time by the MOL PLC in 2003. Although the production history is longer than 13 years, a detailed analysis of the petrology and microstructures of the storage rocks lacking.

The investigated area is in central Hungary and belongs to the Hungarian Palaeogene Basin (Fig. IV.1). The Hungarian Palaeogene Basin is an elongated and divided basin that evolved during the Palaeocene and Eocene. It was divided into three parts by Nagymarossy (1990). The Gomba field belongs to the southern Buda Palaeogene Unit, which is located at the boundary of the Transdanubian Range Unit (TRU) and the Mid-Hungarian Unit (MHU) (Fig. IV.1). Based on seismic data, the field is crossed by two significant fault systems, the Balaton Line and the Mid-Hungarian Line. The Balaton Line is the eastern continuation of the Periadriatic Lineament, which separates the Eastern and Southern Alps. The Mid-Hungarian Line is a major tectonic structure in the Intra-Carpathian area and was studied in detail by Géczy (1973), Kázmér and Kovács (1985), Csontos et al. (1992), Fodor et al. (1992, 1998), Csontos and Nagymarossy (1998), and Palotai and Csontos (2010). The complex tectonic history includes Oligocene–early

Miocene thrusting, middle Miocene extension, local late Miocene inversion and late Miocene–Pliocene normal faulting, as well as left-lateral wrenching across the zone (Csontos and Nagymarossy 1998). These structural elements enclose the main part of the Palaeogene Total Petroleum System, which is one of the six total petroleum systems in the Pannonian Basin Province (Dolton 2006).

In the Palaeogene Total Petroleum System, the source rocks are typically the euxinic Tard Clay (upper Eocene to lower Oligocene) and the Kiscell Clay (lower Oligocene). The Tard and Kiscell anoxic clays in northern Hungary have an average TOC content of 0.5–1.0%, with local concentrations of 0.8–1.8% and as high as 4.5% (Kókai 1994; Milota et al. 1995). Their kerogens are mostly of types I and II, but type III kerogen is also present in the upper part of the sequence (Dolton 2006). Typically, fine-grained rocks and structural and sedimentary traps close the system.

In the Gomba Field, the main storage rock formations are the basal Palaeogene clastics (Eocene Kosd Sandstone) and the Triassic Kisfennsík or Berva Limestones (Benedek 2009; Bauer et al. 2016) (Fig. IV.2). The Kosd Formation is the first member of the Palaeogene sedimentary cycle in the Palaeogene Basin (Priabonian) but was also deposited during the Lutetian. The formation consists of a mixture of variegated sediments: predominantly red, subordinately yellow clays, sands, gravels, and dolomite and limestone debris (Less 2005). While the Kosd Formation has a very significant and well-known lateral extent in the northern part of Hungary, the extent of the Kisfennsík Limestone is smaller and less known. From the surface, it is described only in the Bükk Mountains, and the westernmost occurrence is in the Gomba Field (Benedek 2009; Bauer et al. 2016).

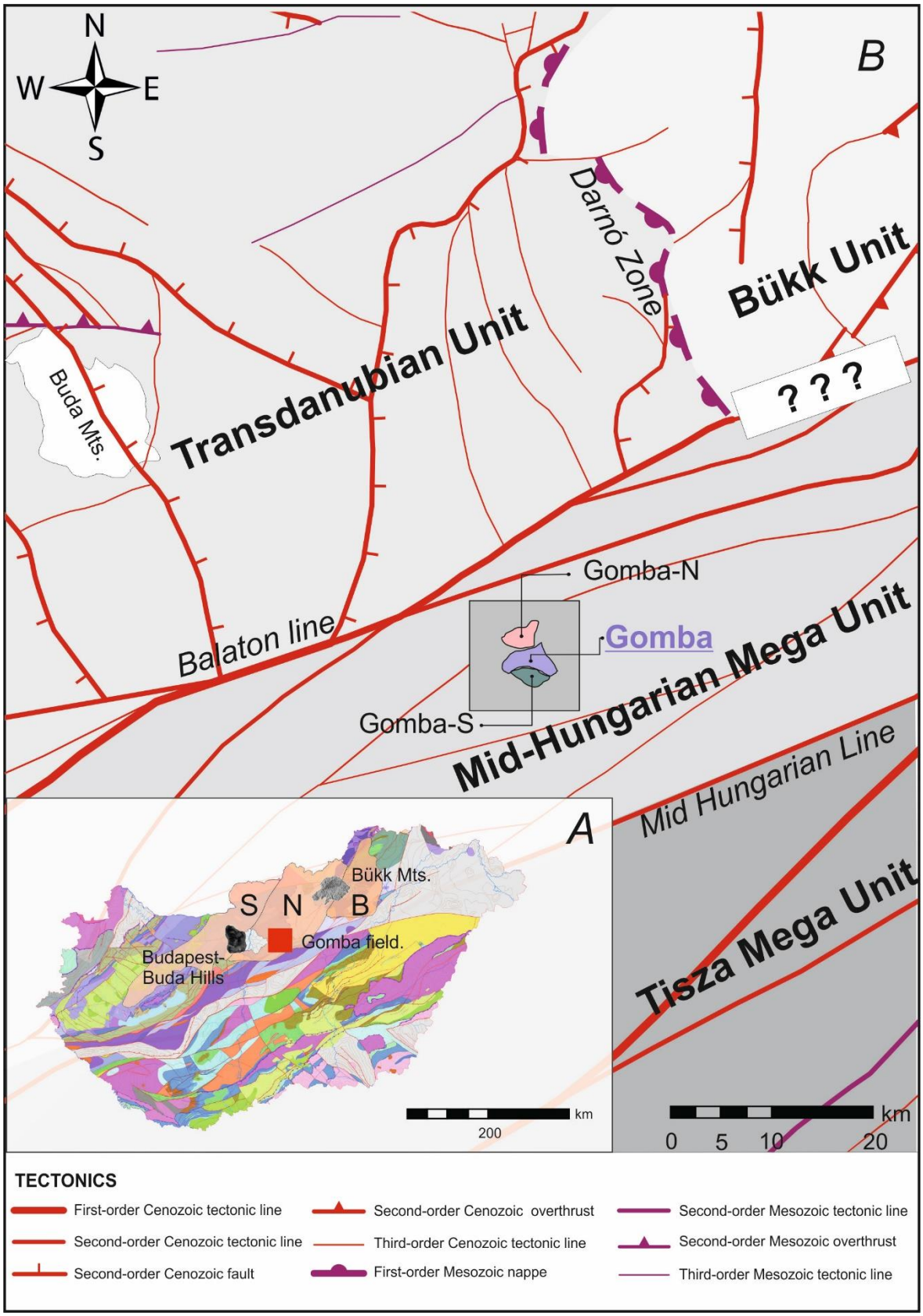

Fig. IV.1 Pre-Cenozoic basement of the investigated area (based on Haas et al. 2010). A: Location of the investigated area and the subdivisions of the Palaeogene sediments. S=South Buda Palaeogene, N=North Buda Palaeogene, B=Bükk Palaeogene (based on Nagymarosy 1990). The figure shows the Mesozoic pre-Cenozoic basement rocks (purple, blue and light green). B: The known tectonic lines in the vicinity of the Gomba field.

In the Bükk Mountains, the Kisfennsík Limestone is predominantly composed of light-grey, whitish-yellow limestone of carbonate platform facies. Tidal flat, lagoonal and reefal environments can be reconstructed in the carbonate platform sequence of the Kisfennsík block. It is mainly thick-bedded or massive, containing subordinate finely bedded parts and occasionally cyclic loferites. Syngenetic brecciation is relatively frequent (Pelikán 2005). In the Gomba Field, 7 wells penetrated the basement. Based on the cores and thin section observations, the basement is composed of grainstone and packstone limestone and subordinately of partly dolomitized dolomitic platform limestone (Fig. IV.2). Both of these limestone types consist of oncoids and peloids and have negligible clay contents (Bauer et al. 2016). Most of the analysed carbonate rocks are strongly fractured and dissolved. Based on the well-logs, the carbonates are thickly bedded in the study area. These results further show that the upper few tens of metres of the Triassic beds at the Triassic/Eocene unconformity have significant porosity and permeability. However, it was impossible to drill this zone and obtain core samples because of total mud loss. The closest cores to the unconformity consist of polymictic breccia, which can be interpreted as a result of hydro-fracturing and palaeo-karst processes (Bauer et al. 2016) or as a regolith similar to that recognized in the Buda Mts. (c.f. Nádor 1993). In the deeper region of the reservoir, there are similarly textured polymictic breccia zones, which are interpreted as palaeo-karst breccia, collapse breccia and/or palaeo-cave sediment (Bauer et al. 2016).

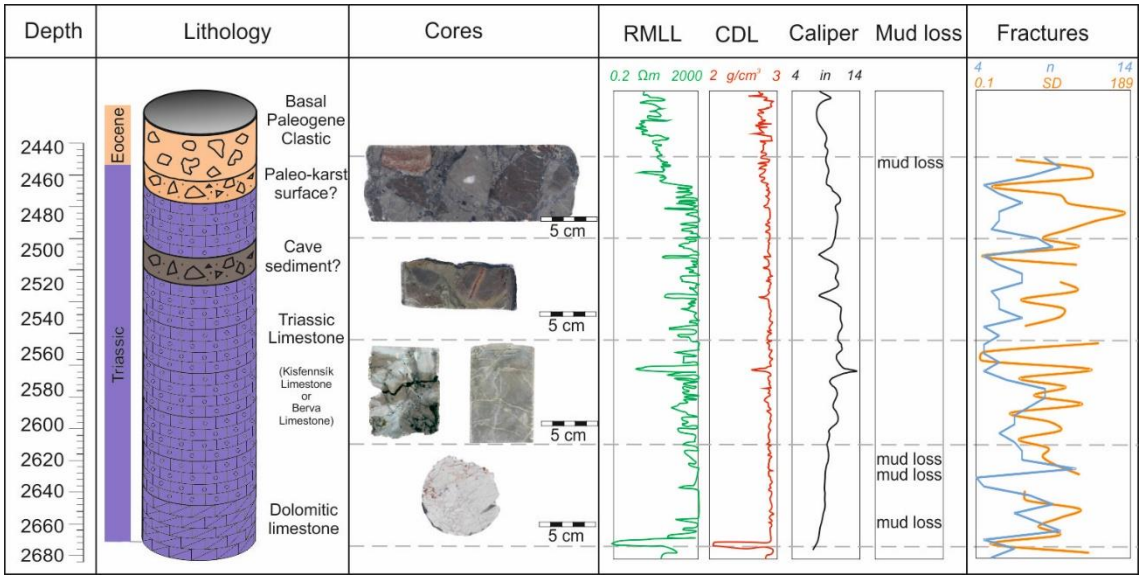

Fig. IV. 2 Idealized stratigraphy of the Gomba-1 borehole with the wire logs and the significant mud losses (Wire logs are measured by MOL PLC, Benedek 2009). For details, see text.

Based on the FMI and CBIL (acoustic borehole televiewer) data and the available cores, both the carbonate and the breccia zones are heavily fractured **(**Benedek 2009). Microstructural evaluation of the core material revealed four different fracture generations, but three of them are totally filled with calcite cement. Three fracture sets formed before the brecciation and epigene karstification, while the final one developed after or during these processes (Bauer et al. 2016). The youngest vein generation is partly filled with calcite cement as well, but it has free storage capacity as well. According to the model of Benedek (2010), the hydrocarbons migrated to the main Eocene reservoir rocks through the Triassic beds. Thus, the final fracture generation must be an active migration pathway even at present.

The Gomba field is actually a compartmentalized reservoir. The field is divided into three parts: Gomba-North, Gomba, and Gomba-South. The Gomba-North part has a different type of oil (higher density) than the central Gomba and Gomba-South regions, for reasons that remain unclear. Similar to faults and lithology, fracture networks can also compartmentalize a reservoir.

4.3. Methods

Certain well-logging methods can measure the position and orientation of fractures but are unable to characterize them based on qualitative parameters, such as fracture shape, fracture connection relationships, etc. These parameters can nevertheless be derived from thin sections or digitized core images. Therefore, to characterize the fracture network in the studied carbonate rocks, data were collected at two scales. The individual fracture shape has been analysed in thin sections, while other quantitative data (fracture density and orientation) have been analysed at the well-log scale. The combination of both data sets was then used to build a discrete fracture network (DFN) model (Fig. IV.3).

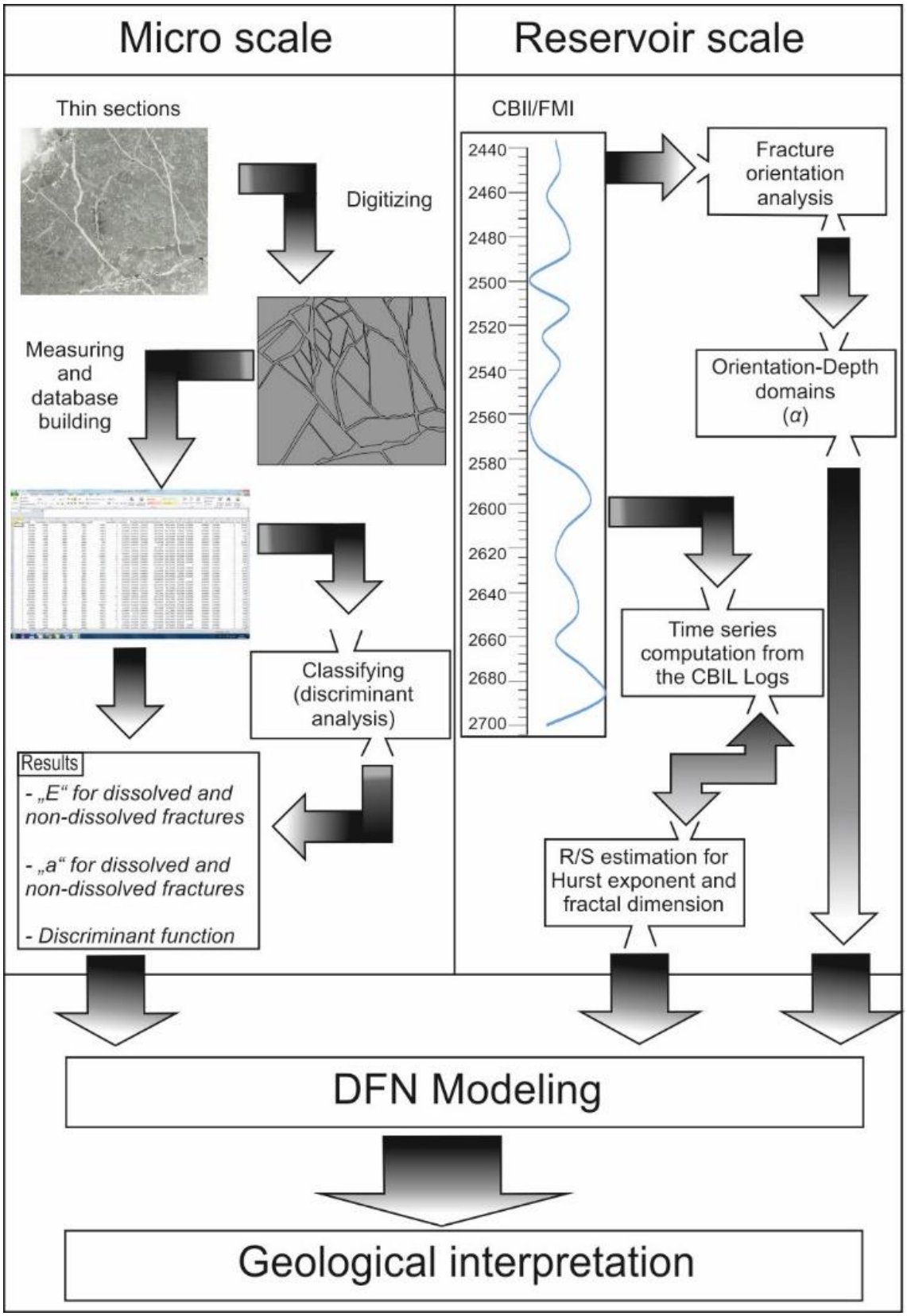

Fig. IV.3 Method of input data generation for DFN modelling. For details, see text.

4.3.1. Micro-scale – Preparation of input files, digitalization, and data processing

Twenty-one thin sections were chosen from the Gomba-1, Gomba-3 and Gomba-6 wells from different depths. The samples were mostly limestones (17), and some were breccia (4). The area of the polished thin sections was 5x5 cm^2. The input files for image analysis were taken by an Epson X6000 dia scanner working with a parallel Nikol position at 6000 dpi resolution. The digital images were then traced manually on-screen in the CorelDraw graphics package to delineate fracture types. The traced images were analysed by using the ImageJ software (Rasband 1997-2006), and Olympus Stream Essential 1.9 was additionally used to calculate the geometric parameters.

During the image analysis, the fractures have been classified into two types: dissolved and non-dissolved. The basis of this categorisation was the shape of the fracture walls. Fracture walls with a purely tectonic origin usually have a primitive shape, whereas an acid solution can complicate this simple form (Feng et al. 2013). Therefore, the simplest shaped fractures were assigned to the non-dissolved category, while the most complicated ones were assigned to the dissolved category. There is a transitional category, which contains the fractures that are neither clearly dissolved nor non-dissolved.

4.3.1.1. Measured parameters

As basic geometric parameters, the area, perimeter and length of each fracture trace were measured on the thin sections. Furthermore, geometric features were identified to accurately differentiate between the dissolved and non-dissolved fractures; therefore, convexity, roundness, aspect ratio, Feret diameter and sphericity parameters were measured too. The measured and calculated parameters, their abbreviations and calculation formulae are summarized in Table IV.1.

Abbreviation	Name	Calculation formula
α, β	fracture orientation	dip, dip direction
a	aperture	Mean of diameter and Feret diameter
A	area	The number of pixels that cover the shape
P	perimeter	Pixel number of the perimeter
L	length	Pixel number of a line
C	convexity	Area relative to the area of the measurement object's convex hull.
S	sphericity	Sphericity is approximately the squared ratio of width and length.
F_min	minimum Feret	Minimal diameter is the shortest distance between any two points along the selection boundary.
F_max	maximum Feret	Feret's diameter is the longest distance between any two points along the selection boundary, also known as maximum caliper.
PA	perimeter/length	$PA = \frac{\text{perimeter}}{\text{area}}$
R	roundness	$R = 4 * \frac{\text{area}}{\pi * \text{major axis}^2}$
AR	aspect ratio	$AR = \frac{\text{minor axis length}}{\text{major axis length}}$
E	elongation	$E = \frac{\text{longest distance from the centrum}}{\text{shortest distance from the centrum}}$
D	fractal dimension	box-counting method
E	exponent of length distribution	$N=(L)F*L^{-E}$

Table IV.1: Abbreviations and formulae of the used geometric parameters

The fracture length distribution was calculated independently for the limestone and breccia reservoir rocks. It is generally understood that length data follow some non-symmetrical distribution, i.e., the number of small fractures exceeds the number of large ones. Following the model applied most frequently (Yielding et al. 1992; Min et al. 2004), it is the power law type distribution

$$N(L) = F*L^{-E} \quad (1)$$

that best describes the behaviour of the fracture sizes. Because the number of classes on the frequency distribution function (k) may have a great influence on the shape of the histogram, this number was defined as

$$k = 2 * INT(\log_2(max(L)) \quad (2)$$

prior to fitting the analytical curve.

Measuring fracture aperture is a very uncertain task. In many cases, the distance between the opposite fracture walls could not be measured correctly because of the irregular and rough walls. A frequently applied method is to measure the diameter in at least three points (typically four or five) at different sections and to identify a geometric parameter that can describe the aperture in 2D. This parameter is the Feret diameter (Feret 1931), defined as the distance between two parallel tangential lines rather than planes. Hereafter, aperture (*a*) is defined as the average of the minimal Feret (F_min) and maximal Feret (F_max) values.

4.3.1.2. Data processing

Data processing started with analysing the outliers of the data sets, which appear to be due to sampling uncertainty. Outliers mostly originate from the sampling methods: fracture size can be smaller than the detection limit or the fractures length can be longer than the thin section size. Outliers were handled by boxplot charts of the area parameter in SPSS 22.0 software.

Characterization of the dissolution state of the individual fractures was computed by discriminant function analysis. During this statistical approach, the Wilk's lambda stepwise method was applied. The grouping variable was the classification category (dissolved or non- dissolved) and the independents were all of the measured parameters in addition to the following calculated variables: Diameter/Area, (Feret/Area)*100, Feret/Diameter, Perimeter/Sphericity, Elongation/Perimeter, Aspect Ratio/Perimeter, Aspect Ratio/Area, and Feret/Perimeter.

4.3.2. Reservoir scale – Fracture density and fracture orientation

The investigated wells were not drilled with core for the full length. Therefore, even if the digitized thin sections characterize the fracture network at a very good resolution, they represent the reservoir only along a few tens of metres and cannot provide any information about the whole fracture system. To analyse the entire fracture network, CBIL and FMI data were used to calculate the fracture density and to describe the fracture orientation (dip and dip angle).

Well-log methods are often used to study fractured reservoirs (Bean 1996; Marsan and Bean 1999) because they can provide valuable information at the reservoir scale. Borehole image logs (e.g., FMI) and diverse core imaging processes result in deterministic data sets of fractures with exact spatial positions (Tezuka and Watanabe 2000; Yang et al. 2004). The series of intersection points between the fracture network and the borehole can be further analysed mathematically as a time series that is well characterized by its Hurst exponent. According to M. Tóth (2010), the fractal dimension *(D)* of the fracture network can be calculated from the Hurst exponent *(H)* of the fracture intersection point series, as was applied in our analysis. The Hurst exponents were calculated by using R/S analysis in Benoit 1.0 software. According to M. Tóth (2010), based on the *H* values estimated for at least 200 point-long series, the fractal dimension of fracture midpoints can be computed by using a simple linear equation. In this way, the variation in fracture density (measured as fractal dimension) along the well becomes measurable. For more mathematical details of fracture density estimation using well-log data, see M. Tóth (2010).

Orientation values for the fracture network modelling were derived directly from the FMI logs.

4.3.3. Fracture network simulation

The analysis of geometric parameters of fracture sets provides an opportunity to make a simulation of a discrete fracture network (DFN) for the whole study area. There are numerous DFN simulators available (e.g., FracMan, RMS, and Connect Flow). The RepSim code is used here and has been applied to solve several 3D fracture network

simulation problems before (M. Tóth et al. 2004; Vass et al. 2009; Bauer and M. Tóth 2015). Among many others, one significant difference among the DFN simulation software programs is the fracture centre allocation approach. Many of them allocate the fracture centres uniformly (e.g., Dershowitz and Einstein 1988) or following Poisson point process (Priest and Hudson 1976), while some of them also take into consideration the scale invariance of the fracture networks and allocate the fracture centres fractally with a given fractal dimension (e.g., Hewett 1995).

The RepSim code is based on fractal geometry. It follows the box-counting algorithm to locate fracture midpoints in 3D using the calculated *D*, while *E* and orientation data are used for generating fractures around them. By evaluating the simulated fracture network, this code can also calculate the spatial position of the interconnected fracture sets.

4.4. Results

4.4.1. Micro-scale

4.4.1.1. Individual fracture geometry

Each individual fracture (152) was evaluated using the above methods. Most cases represent fractures in limestone because the limestones are much more fractured than the breccias. Fractures in the breccia mostly occur inside the individual limestone clasts, but in some places, the youngest fracture generation (F4 in Bauer et al. 2015) crosscuts both the breccia matrix and the limestone clasts. Based on the histograms of the measured parameters (Fig. IV.4.B/1-3), there is no significant difference in the fracture geometry between the breccia and limestone rock types. Hence, hereafter, we do not distinguish between the rock types based on this aspect.

There are numerous quantitative differences between the non-dissolved (Fig. IV.4.A/1) and dissolved fractures (Fig. IV.4.A/2). One of the most prominent differences concerns the logarithm of area. The dissolved fractures have much larger areas in 2D than the non-dissolved ones (Fig. IV.4.B/1). There are significant differences in aspect ratio (Fig. IV.4.B/2), elongation (Fig. IV.4.B/3) and convexity too. All of these variables have much smaller values for dissolved fractures than for non-dissolved ones. The

elongation/Feret values and the ln(Feret) values are higher for the dissolved fractures than for the non-dissolved ones. The sphericity values do not show any significant difference.

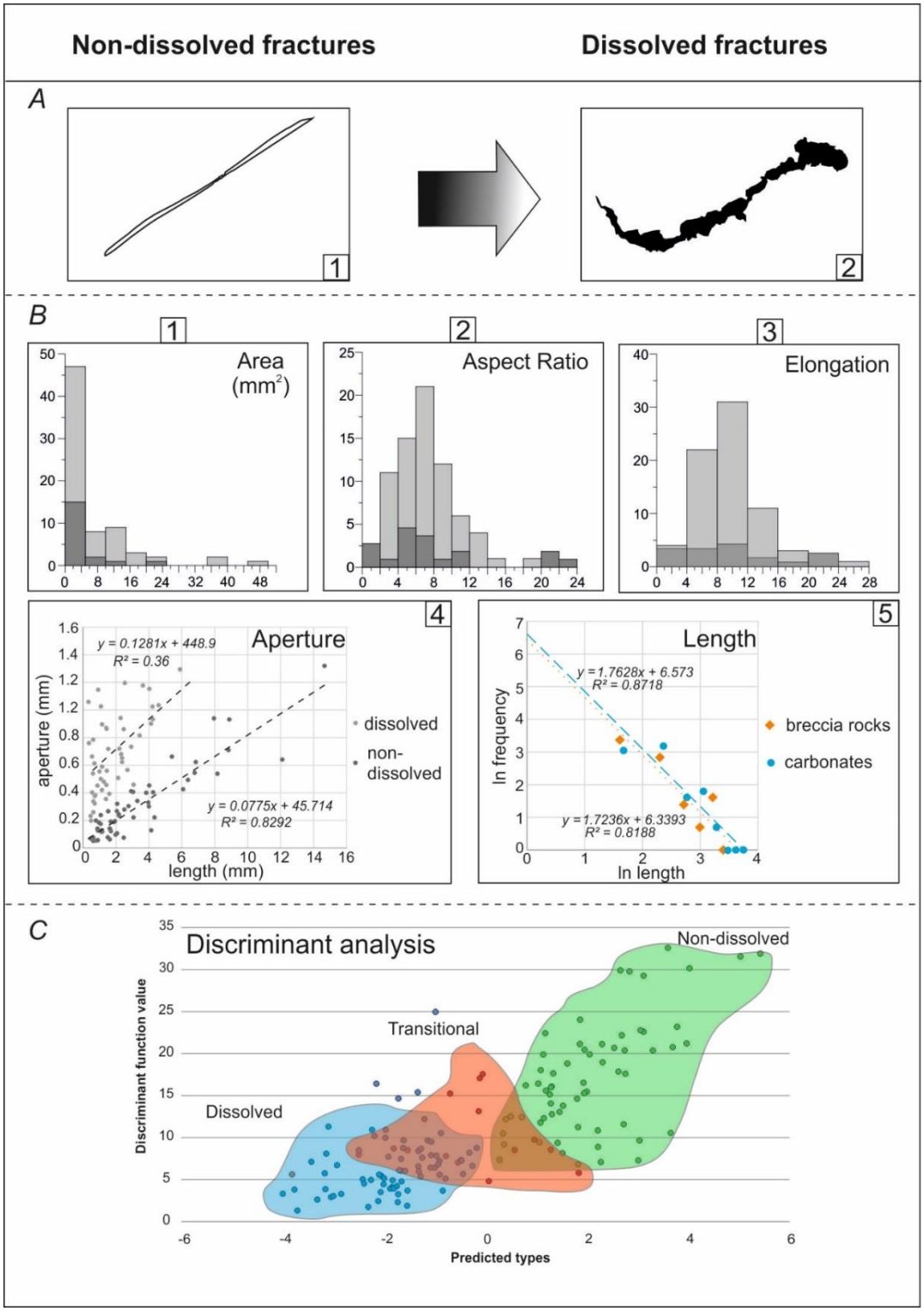

Fig.IV. 4 Results of the individual fracture geometry measurements. A: A one-to-one example of the dissolved and non-dissolved fracture shapes. B: The main geometric parameters. In the histograms, light-grey values represent the dissolved fractures, and dark-grey values represent the non-dissolved fractures. C: The result of the discriminant analysis. The green zone represents the non-dissolved fractures, the blue represents the dissolved fractures, and the red represents the transitional fractures that are neither dissolved nor totally non-dissolved.

4.4.1.2. Results of the fracture type classification

Based on these observations, a classification function was computed to characterize and separate the two types of fractures. During the digitization, 72 cases were classified as clearly dissolved fractures, and 64 cases were classified as clearly non-dissolved fractures, while 16 cases were not classified. As a result of the discriminant function analysis, the main classifying parameters are PA, C, S, ln(L), ln(P) and ln(F_min) in the following unstandardized discriminant function

$$F(D) = 72.6\,PA + 15.17\,C + 9.4S + 5P + 4.1L - 2.2A - 4.2F\_min - 40.88 \qquad (3)$$

With this function, dissolved and non-dissolved fractures become clearly distinguishable (Fig. IV.4.C), and ungrouped cases are also classified.

4.4.1.3. Length and aperture distribution calculation

The length distribution of the fractures is one of the most important numerical features of a fracture network (M. Tóth and Vass 2011), and it can be easily different for each rock type in a given reservoir. Therefore, we analysed the fracture length distribution separately for breccia and limestone. Based on these calculations, the breccia has a smaller number of fractures, but the fractures have the same length distribution as those in the limestone (Fig. IV.4.B/5). The *E* values of the breccia and limestone are rather close to each other, being -1.76 and -1.72, respectively.

The aperture distribution is significantly different for the dissolved and non-dissolved fractures (Fig. IV.4.B/4). The average aperture of non-dissolved fractures is 0.30 mm, while the average aperture of dissolved fractures is 0.72 mm (Table IV.2). The regression lines between aperture and length for the two cases are shown in Fig. IV.4.B/4. The slopes of these lines are similar for dissolved and non-dissolved fractures, but the dissolved fractures have much higher and much more scattered values. Moreover, the trend computed for the dissolved fractures via linear regression does not intercept the Y axis at the origin, illustrating the clear role of dissolution.

Non-Dissolved		*Dissolved*	
Mean	301.51	Mean	723.82
Std. Deviation	34.51	Std. Deviation	42.20
Median	221.92	Median	680.07
Variance	255.98	Variance	312.99
Skewness	42471.00	Skewness	-0.58
Kurtosis	1.83	Kurtosis	0.41
Range	1266.80	Range	1273.95
Minimum	52.35	Minimum	198.18
Maximum	1319.15	Maximum	1472.13
N	55.00	N	55
Confidence intervall (95.0%)	69.20	Confidence intervall (95.0%)	84.61

Table IV.2. Results of the Exploratory Data Analysis of the two fracture types.

4.4.2. Reservoir scale

FMI data representing both the carbonate and the karst breccia zones are available from two wells. The data contain more than 300 individual fractures in each well that can be transformed to point series for mathematical treatment (M. Tóth 2010). The data sets show that the spatial distribution of the fracture density is heterogeneous with depth and so can be characterized by different fractal dimension values for different intervals. The fracture density (*D*) parameters for DFN modelling were calculated every 25 m along the wells. The applied length distribution (*E*) and the fractal dimension (*D*) for the 25 m intervals are summarized in Table IV.3. The applied aperture function was 0.124*L+728 for the dissolved model and 0.077*L+45 for the non-dissolved model (c.f. Fig. IV.4.B/4).

Borehole: Gomba-1				Borehole: Gomba-3		
Depth interval (m)	*D*	*E*		*Depth interval (m)*	*D*	*E*
2475-2500	1.75	-1.7		2490-2510	1.00	-1.1
2500-2525	1.70	-1.7		2510-2530	1.10	-1.7
1525-2550	1.50	-1.7		2530-2550	1.90	-1.7
2550-2575	1.42	-1.7		2550-2570	1.45	-1.7
2575-2600	1.23	-1.7		2570-2590	1.72	-1.7
2600-2625	1.10	-1.7				
2625-2650	1.38	-1.7				
2650-2675	1.62	-1.7				

Table IV.3. The applied values for the DFN model building.

Based on the previous microstructural evaluation (Bauer et al. 2015), there are 4 different fracture generations in the area, which may have different orientations. Although the amount of fractures associated with each generation is unknown, the FMI data sets can be used to check whether there is any variability in the fracture dip direction and dip angle along the wells. Although there is no significant difference in the dip direction, the coefficient of variation in the fracture dip angle varies widely along both wells. There are some depth zones where the fracture dip angles do not vary at all (values close to zero), while high values in other places suggest chaotic behaviour in the fracture orientation (Fig. IV.5). There are some zones where the variation coefficient of the dip angle changes significantly. In the case of Gomba-1, there are significant changes in the density and the calliper data at the depth of ~2560–2570 m, total mud loss occurred at ~2620 m, Total Gamma increases and the density decreases at 2640, and total mud loss and a fall in the drill bit occurred at 2680 m during the drilling. In the case of Gomba-3, there is a high positive permeability anomaly at the depth of 2500 m, and the gamma increases and the resistivity and neutron density decrease at 2540–2560 m (see Fig. IV.2).

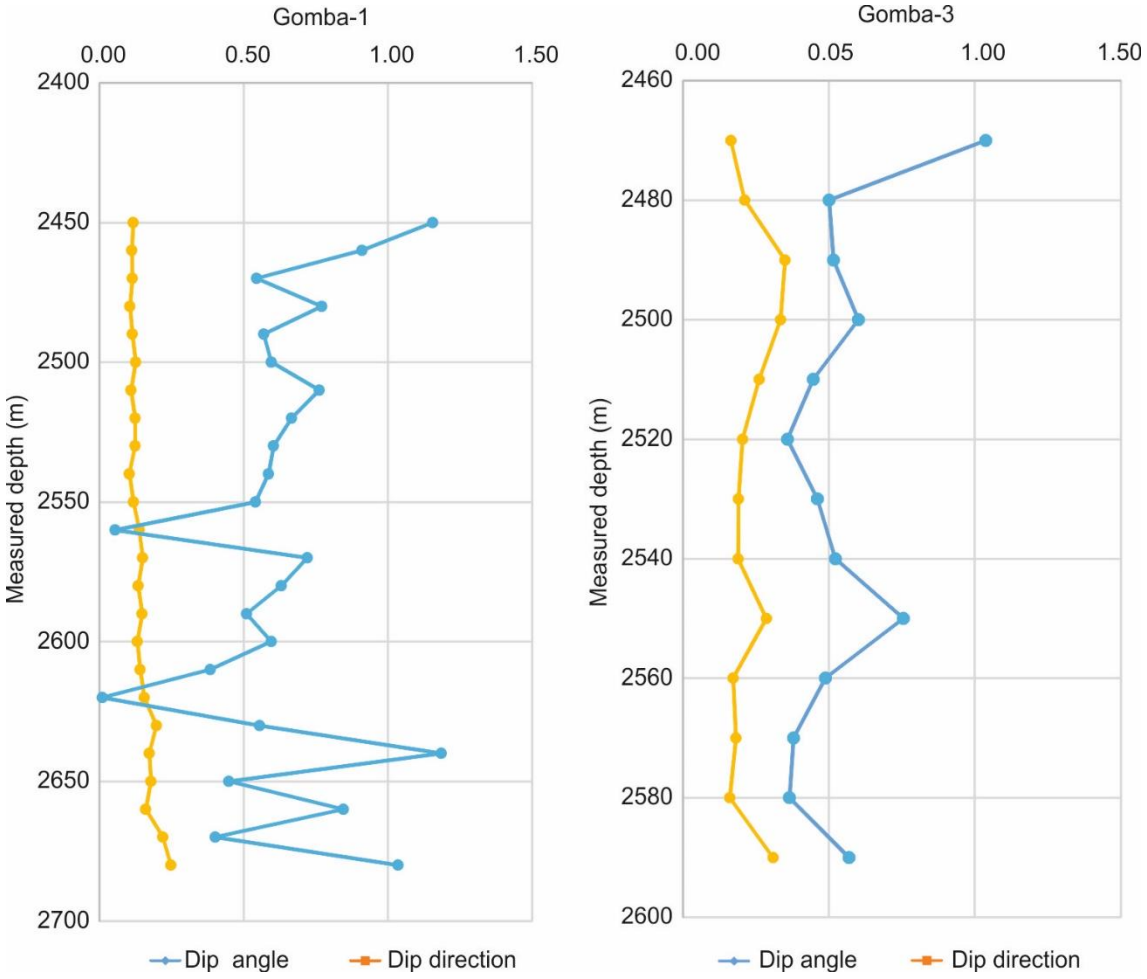

Fig. IV.5 Variation coefficient of the fracture dip angle and dip direction (based on FMI/CBIL logs). (see Fig. IV.2)

4.4.3. Fracture network simulation

Based on the different characteristics of the individual fractures, two types of models were computed for the well surroundings. First a model was constructed to represent the fracture network prior to the dissolution effect of karstic processes, and a second model was constructed to account for the effect of dissolution. The main input parameters (E, D, α, and β) were the same for the two cases, but the non-dissolved model used the aperture function calculated for the non-dissolved individual fractures, and the post-karstic model used the dissolved aperture function (Fig. IV.4.B/4). Simulations were run for a 100*100 m area surrounding each well and repeated ten times in order to analyse the model uncertainty. For both wells, the simulated fracture length interval was 1–10 m. The final DFN model consists of ~370,000 individual fractures in the case of Gomba-1 and ~100,000 fractures in the case of Gomba-3 well.

One of the most important features of fracture networks is how coherent they are, so how many fractures define the connected sub-systems. This feature can be characterized by the size distribution of the communicating fracture groups. In the case of the Gomba-1 well, the size distribution is clearly asymmetric (Fig. IV.6). There are two specific size scales: the groups containing more than 10^5 fractures and groups containing 10^2–10^3 fractures. The two groups appear separately in the Gomba-1 well (Fig. IV.7). The largest fracture groups can be found between 2450–2510 metres (Upper zone) and below 2600 metres (Lower zone). The upper fracture group contains approximately 50% of all of the simulated fractures, while the lower one contains slightly less, approximately 30% of them. Near the two large fracture groups, some smaller clusters occur as well, but they typically appear between 2510–2600 metres (Middle zone).

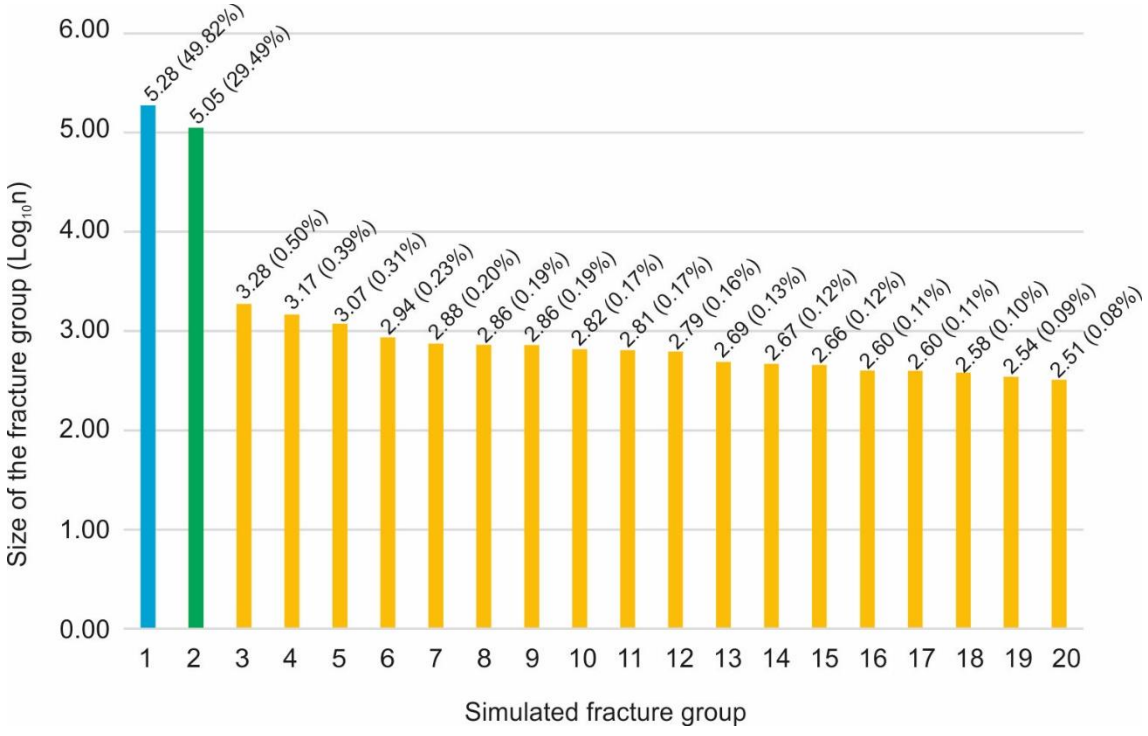

Fig. IV.6 Size distribution of the simulated fracture groups in the Gomba-1 well (n=the number of the connected fractures in a fracture group). The total fracture number is 378,000. The blue column represents the largest fracture group in the upper zone, the green one represents the large fracture group in the Lower zone, and the orange columns appear in the middle zone and near the two large groups.

The fracture network surrounding the Gomba-3 well is basically similar to that of Gomba-1. In this case, the fracture groups can be sorted into two isolated size categories as well. There are also groups containing more than 10^5 fractures and others containing only 10^2–10^3 fractures. Nevertheless, there is an important difference between the two wells. In the case of Gomba-3, the upper 60 metres of the Triassic unit is not fractured, and only

insignificant sized fracture groups occur in this section (10^1 connected fractures). Below this zone, a quite large fracture group appears and contains approximately 30% of all fractures (2535–2555), while further down, between 2570–2590 metres, another significant group appears with 13% of all fractures. Between the two highly fractured zones, only small fracture groups appear.

Another important feature of a stochastically simulated fracture network is the stability of the size distribution and locations of the largest groups during repeated simulations. In the case of both wells, 10 independent runs resulted in essentially identical outputs, demonstrating that the fracture group structure is stable.

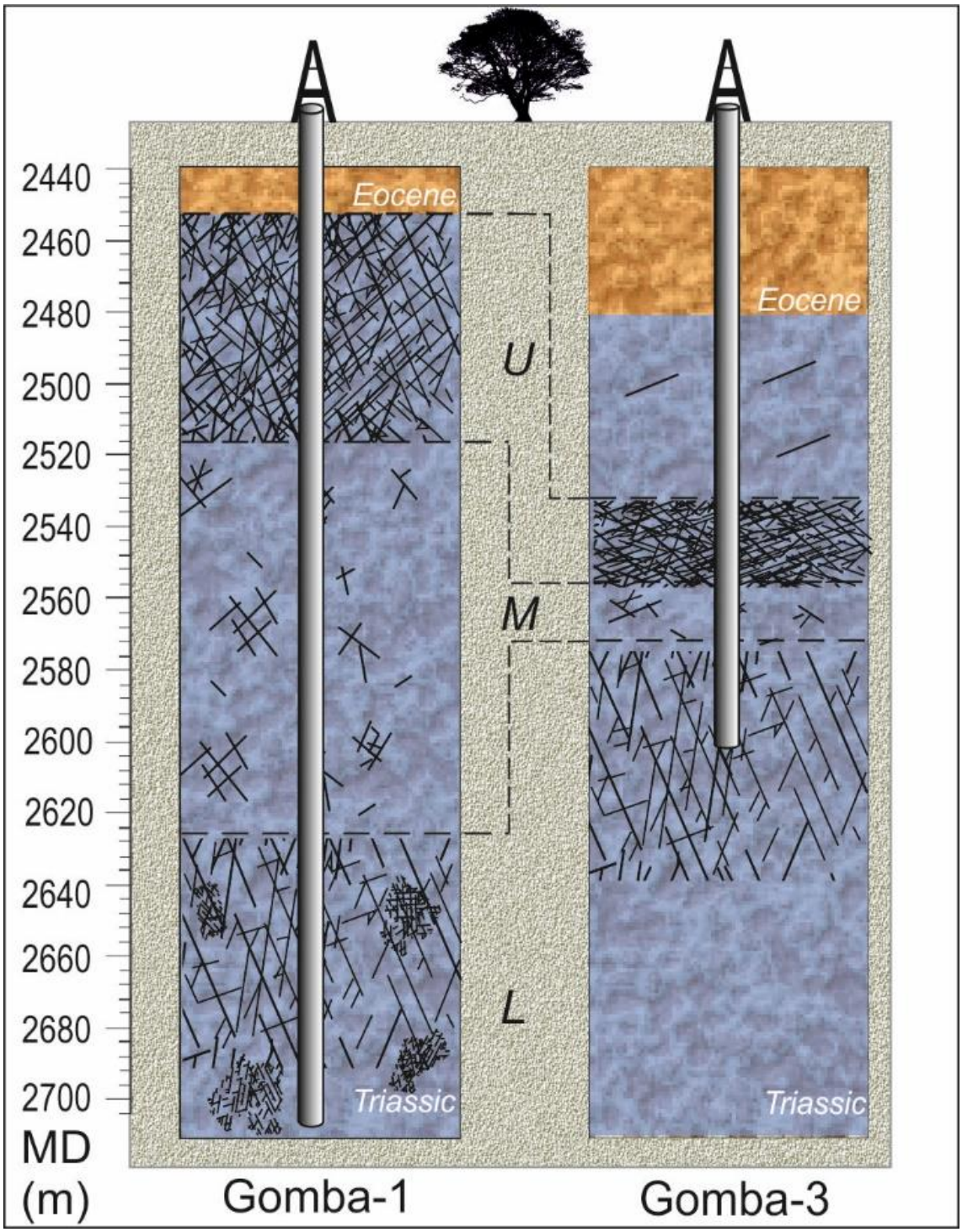

Fig. IV.7 Results of the DFN models. The fracture networks of the two boreholes mainly follow the same structures. There is a large coherent fracture group in the upper zone of the modelled interval (U). Below this, a weakly fractured zone follows with fewer and isolated fracture groups (M). Finally, there is a zone where a relatively large fracture group appears. There are also some middle-sized fracture groups that do not create an interconnected fracture network (L). (U: Upper zone, M: Middle zone, L: Lower zone)

4.5. Discussion

Based on the detailed geometry analysis of the fractures, many of the fractures show dissolution marks (increase in area, convexity, etc.). Dissolution of the fractures is independent of lithology; it occurs in similar proportion in both the breccia and limestone specimens.

DFN models created from the calculated quantitative data (length distribution, aperture, fracture density) and the fracture orientations (dip angle and dip direction) show three typically different fracture zones. The upper zone contains numerous fractures, which form one significant coherent fracture system. The middle zone contains very few fractures, which do not form a coherent fracture system; instead, small separated fracture groups are present. In addition, there is a lower zone, which consists of a large number of individual fractures that form a large fracture group, but there are also numerous small groups that do not create a geometrically permeable, coherent fracture system.

Based on our results, the fracture network of the Gomba field is heterogenic. In the case of the Gomba-1 borehole, the depth segments of 2452–2520 m and 2620–2680 m are much more fractured than the other sections. At depths of approximately 2450, 2570 m and 2640 m, the variation coefficient of the dip angle is high (c.f. Fig. IV.5), suggesting highly scattered fracture directions. In other intervals (2540-2620 m), the variation coefficient is close to zero, suggesting close to parallel fractures. In both of these cases, uncommon fracturing processes appear to have occurred, independent from the local palaeostress field. Highly varied fracture directions may be indicative of the presence of karstic breccia, while parallel fractures probably imply cave roof collapse.

Previous studies suggest that several dissolution events influenced the carbonate storage rocks of the reservoir (Bauer et al. 2016) and resulted in the formation of the dissolved fractures. This effect can be identified based on their geometry. While the non-dissolved fractures are elongated and have small apertures, the dissolved ones usually have a more complicated and asymmetric shape (Fig. IV.4.A). Using more geometric parameters, the two groups can be clearly distinguished (Fig. IV.4.C). Applying the discriminant function along the longest continuous core section (Gomba-1, 2492–2498 m) shows that there are differently dissolved segments even in a highly fractured part of the reservoir (Fig. 8).

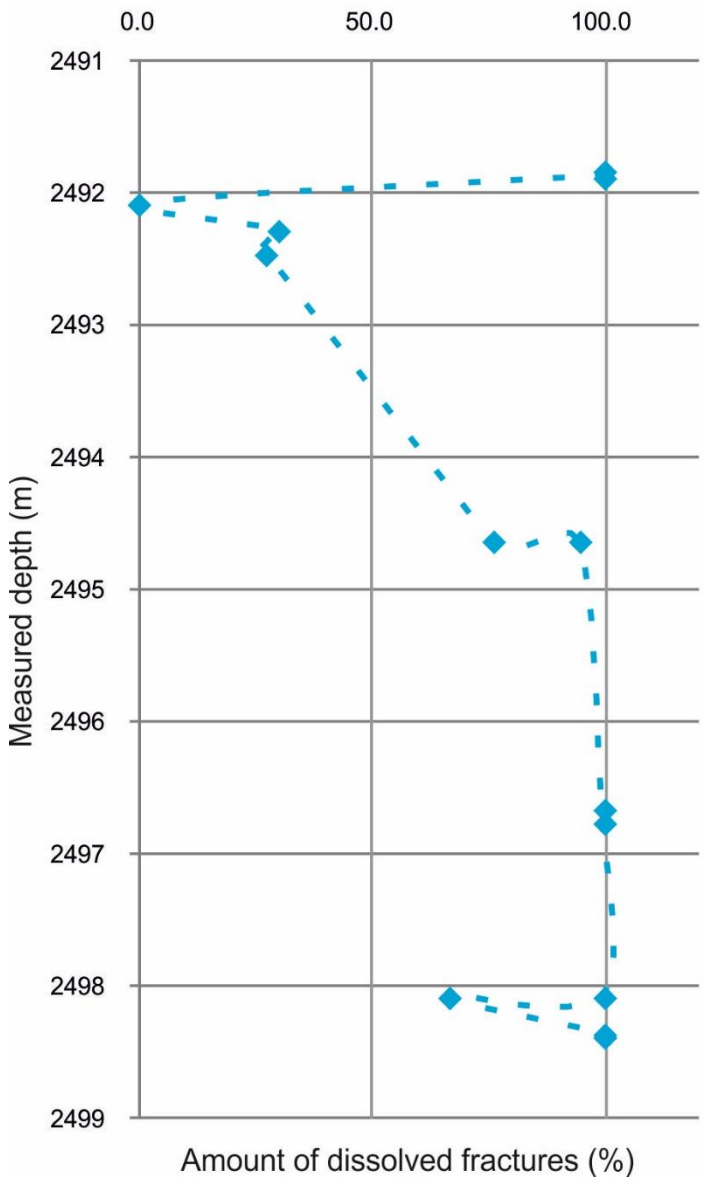

Fig. IV.8: The ratio of the dissolved and not-dissolved fractures in the longest continuous core section in the Gomba-1 well based on the discriminant function.

Although apertures increase, the fracture length distribution does not change as a result of the dissolution, and it follows the typical power-law function with the same parameters for the two fracture groups. As a result of dissolution, the strong correlation between aperture and length disappeared; the correlation coefficient between length and aperture is very weak (0.36), with an anomalously large a/L ratio ($1.2*10^{-1}$), while the same values for non-dissolved fractures are 0.82 and $7*10^{-2}$.

It is known that the investigated area began to be buried along the main structure lines during the middle Eocene (Csontos and Nagymarosy, 1998). This process, together with the Mesozoic deformation events and the Cenozoic renewal of the Mesozoic faults, created the micro-fracture system, which was simulated by the DFN models. According to

earlier studies (e.g., Bauer et al., 2015), the main geometric factor in cave formation is fracture network connectivity and not only the amount of the individual fractures. Based on the above DFN model (c.f. Fig. 7), it is not likely that cave systems could form between 2520 and 2620 m in the case of the Gomba-1 well and between 2475–2530 and 2550–2570 m in the Gomba-3 well because the fracture system is not well-developed enough to allow a high volume of karst water to migrate. In contrast, the modelled upper and lower zones are likely to have a well-developed cave system. This is also confirmed by the total mud loss at 2680 m and the fact that the drilling tool was blow off between 2679 and 2681 m, which is a clear sign of open voids.

A significant portion of the non-dissolved fractures reached apertures of 5–10 mm, which, in addition to fracture connectivity, is a basic requirement for cave formation (White, 1988). As the area was exhumed during the Palaeogene (Kecskeméti 1998; Less 2005), the karstic rocks came into contact with aggressive meteoric fluids, and karstic processes occurred. As a consequence, the fracture network in the Upper and Lower fractured zones allowed the formation of massive caves and the transport of surface sediments into the fracture network. The chaotic textured breccia identified inside the Triassic carbonate beds is possibly further proof for karstification. A similar formation is interpreted as fossil allochthonous cave sediment by Osborne (2001). These sediments are present in certain depth intervals (e.g., in Gomba-3: 2570–2575, 2580 m) in both wells and indicate the positions of previous caves. The presence of caves is also supported by the freshwater-limestone fragments in the breccia (e.g., Gomba-1, 2492 m, Bauer et al. 2016), which are the result of $CaCO_3$ dissolution and re-precipitation. The freshwater-limestone fragments appear in the fine-grained matrix of the breccia. The breccia also contains substantial amounts of dickite (Bauer et al. 2016), the high-temperature polymorph of kaolin minerals. Kaolinite is a common mineral in karstic soils and cave sediments and develops through the weathering of clay minerals in surface soils in tropical environments. All these data suggest that the sediments of the cover layers infiltrated into the contemporaory cave and were preserved, thereby recording a characteristic feature of epigene karstification.

In fractured and karstified rock bodies, only a small part of the former void system is preserved as open voids after subsidence. Due to burial, collapses occur often and form well-defined structures. As reported by Loucks (1999), in collapsed caves, a “core zone” that represents the former cave hole and the infiltrated sediments develops. It is surrounded by a “disturbed zone”, where the bedding of the host rock is recognizable, but many

fractures are present due to the collapse. Based on the FMI data, the two most fractured depth intervals in Gomba-1 contain significant variation in the individual fracture orientations. The average dip direction of the upper zone can be characterized as 157°, whereas that of the lower zone can be characterized as 219°. The dip angles are 54° and 61°, respectively. Figure 5 shows that the variation coefficient of dip angles and the dip directions significantly change in some zones. The fractures in most of these zones are characterized by chaotic fracture orientations, which certainly do not denote one fracture generation and instead can be interpreted as the fracture system of the "disturbed zone" facies of a palaeo-cave according to Loucks (1999). In the Gomba-1 well, there are two depth intervals with significant anomalies in the fracture orientation. Both of them are observable on the master log (unpublished report by MOL PLC). In the upper one (2560 m), the calliper values increase, and the CDL (density) and RMLL (resistivity) values strongly decrease (Table IV.4). Based on the DFN models, in this depth, a previous cave cannot be assumed. Instead, the well-log anomalies relate to an isolated fracture group. In the lower one (2680 m), the wire logs do not show significant anomalies, but significant mud loss was observed during the drilling, and this is an obvious sign of high porosity.

Gomba-1					
Depth	**Modell type**	**Log and drilling event**	**Fracture dip angle relative variance**	**Breccia or known cavern**	**Can it be paleocave?**
2450	Coherent	Low TG, low resistivity, high density	High	Yes	Karst related Unconformity
2560 - 2570	Isolated	High caliper, low densitiy and resistivity	Low	Not known	NO
2620	Coherent	Total Mud loss	Low	Not known	YES
2640	Coherent	High TG, low resitivity, low density	High	Not known	YES
2680	Coherent	Total Mud loss, Drilling bit blows off	High	Yes	YES

Gomba-3					
Depth	**Modell type**	**Log and drilling event**	**Fracture dip angle relative variance**	**Breccia or known cavern**	**Can it be paleocave?**
2475	Isolated	Low TG, low resistivity, high density	High	Not known	Karst related Unconformity
2540-2550	Coherent	High TG, low resistivity and density	High	Not known	YES
2555-2570	Coherent	High TG, low resistivity and density	Low	Yes	YES

Table IV.4: Relationship between the DFN models, wire logs, drilling events, the FMI/CBIL data, and the known cave sediments or caverns

Based on Table IV.4, the presence of a previous cavity system, i.e. a cave, can be assumed below 2620 m in the Gomba-1 well and below 2540 m in the Gomba-3 well. The structural position and thickness of the upper, fractured zone of the Gomba-1 well are rather similar to those in Gomba-3, suggesting a near-surface branch of a previous cave. The breccia horizon drilled at the top of the fractured upper zone of the Gomba-1 well (Fig. 7) likely formed due to surface karstic processes (Bauer et al., 2016) following exhumation of the cave due to erosion. Karstic caves evolve in fractured rocks (e.g., Palmer 1991; Diabat 2013), but the spatial appearances of caves can be very different (White 1988; Palmer 1991). Based on more than 500 individual modern samples, cave

geometries can be classified into four main categories: branchwork, network, anastomotic and ramiform and spongework caves (Palmer 1991) (Fig. IV.9).

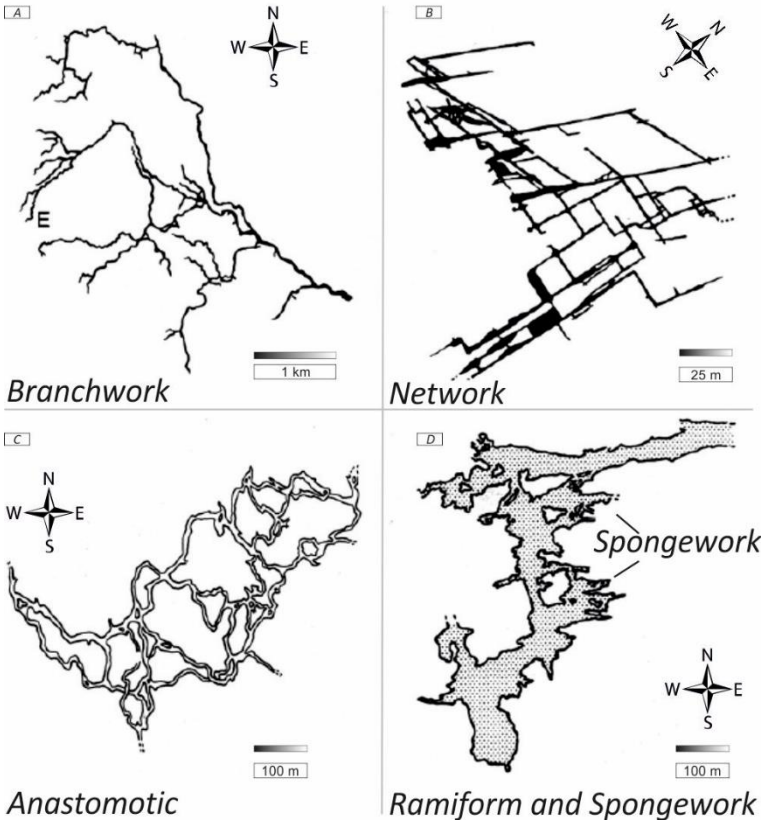

Fig. IV.9. The four fundamental cave morphologies (based on Palmer 1991). Approximately 57% of all caves are branchwork caves. This cave type exhibits one or more entrances (sinkholes) and springs. Aggressive fluids penetrate the karst at discrete points. Large rooms form only at passage intersections where collapses and cave sediments are common.

Approximately 57% of all caves are categorized as branchwork caves. The specific features of this cave type include hundreds of metres in vertical extent, 10^2–10^5 m in total length, dripstone and other speleothem formations and infiltration and accumulation of surface sediment with different grain sizes. In the studied case, the laminated fresh-water limestone fragments and the fine-grained sediments are the results of epigene karstification. Based on these observations, it is likely that the presumed palaeo-cave in the Gomba field had a branchwork pattern. Although the presence of epigenetic sediments is characteristic both for the branchwork and anastomic cave types, the branchwork type is much more frequent.

The most typical feature of branchwork type caves is the well-separated recharge zones (sinkholes), the spatial positions of which are influenced by the surface morphology and the fracture system of the rocks (e.g., Western Mecsek, Hungary; Bauer and M. Tóth 2015). Recharge and leakage zones are more likely to develop along well-connected

fracture systems than in the non-fractured areas. Usually, variously sized conduits may develop between the recharge and the leakage areas. During the evolution of the cave system, each first-order branch serves as a conduit for water fed by a discrete recharge source. Water converges into high-order passages that become fewer and generally larger in the downstream direction (Palmer 1991). The main structures (e.g., faults) designate the typical directions of the high-order passages.

The spatial distribution of the open voids and collapsed zones are not random. They are actually remnants of a palaeocave and likely follow the main tectonic structures. In the studied case, the strike of all main structural lines is NE–SW; hence, the collapsed zones of the palaeo-cave crosscut by drillings probably continue in this direction. Although the fracture groups are geometrically isolated in both modelled wells, they are probably part of the same previous cave system. Thus, the highly fractured zones throughout the reservoir may be better hydraulically connected in the NE-SW direction than any other directions.

Unfortunately, there is not enough information to determine the age of the karstification. Nonetheless, it is very likely that the epigene karst phase started during the Palaeocene, when the Mesozoic basement was exhumed. The hydrocarbon generation started only ~5 million years ago (Benedek 2009), when the area started to intensively subside. Because the presence of an extended cave system can be assumed in the area, in addition to the structural hydrocarbon traps, karst-related traps must also occur in the field. These are related to the modelled coherently fractured zones representing the previous cave system and the unconformity zone at the Triassic-Eocene boundary, which probably represents an exhumed branch of the cave system. It is probable that there are also small isolated caverns in the less fractured zones that are not part of the communicating fluid reservoir. Ancient cave passages, collapses, and high primary porosity cave sediments are probably below 2600 m in the case of Gomba-1 and below 2540 m in the case of Gomba-3.

4.6. Conclusion

The reservoir rocks in the Gomba field are composed mostly of fractured carbonate beds, which have been modified by karstic and palaeokarstic phenomena. Based on image analysis, the individual fractures show very complex geometry. Fractures can be classified into two classes: one class features large 2D areas (in thin section), large apertures, complicated shapes, little elongation and small aspect ratios. The members of the other class feature large elongation and high aspect ratios and have simple shapes and small

aperture values. The first class is interpreted as dissolved fractures, while the second is interpreted as non-dissolved fractures.

Analysing the FMI and CBIL data, some zones were identified in which the distribution of the fracture dip direction becomes chaotic or even strikingly uniform. These zones are interpreted as palaeokarstic zones. Based on microscopic 2D data and the FMI/CBIL information, DFN models were computed for the surroundings of two boreholes. These models show that the fractures do not form a coherent network. Instead, there is an upper fracture system and a lower fracture system, but there is no fractured connection between them. According to modern cave morphologies, the discrete fracture groups likely formed a branchwork type cave with a NE–SW orientation. In this direction, the modelled fracture groups were probably connected by dissolution and cave formation.

Chapter V
Conclusions

5.1. Summary of the results

Before the material included in this dissertation no published information has been available on the Gomba hydrocarbonate reservoir. Everything we knew about the lithology and structure of the reservoir came from the internal reports of MOL PLC. These reservoir rocks can mainly be linked to the Eocene Kosd Formation as well as to the fractured Triassic Kisfennsík Limestone Formation that can be found in the Mesozoic basement. The production history already known at the beginning of the research showed that the fractures are likely of high significance on the production. Also, the idea arose that the hydrodynamics of the reservoir is affected by karstic dissolution but no petrological information was at hand.

In this dissertation I basically dealt with the lithology and fracture system of the Gomba reservoir. Still, as a first step, I have analysed the fracture system of a well-known karstic area and also the connection among the spatial positions of karstic forms so as to draw general conclusions on how karstification and the fracture system are linked (Chapter II).

I could find close relationship between the direction of cave passages, the cave entrance postions and the spatial frequency of fractures in the researched area (West-Mecsek Karst). DFN-models that were constructed based on geometrical data coming from on-site measurements show that the aquifer (karstic water reservoir) can be divided into fractured and non-fractured parts. Data resulting from the applied methods greatly reflect what is known in speleology, geomorphology and hydraulics, so we believe that the method applied is suitable for the research of deeply buried karstic areas, such as the Gomba reservoir as well.

In Chapter III we were dealing with the petrography and petrology of the Triassic formations in the Gomba hydrocarbon reservoir. Under the evidence of core samples we were able to separate three rock types, such as limestone, dolomitic limestone and chaotic textured breccia. We have found that the dolomitic limestone got formed through the recrystallization of the limestone and the two rock types are not separated along a fault zone. We interpreted the breccia as regolith that can be linked to karstification or as a

hydraulic breccia based on its texture. Moreover, in the lower zones there are polimictic breccias as well, known from cores and chips, the formation of which cannot be explained by these formation processes. Textural and mineralogical results point to the fact that the lower breccia horizons can be treated as former cave sediments, so we have found lithological proof for contemporoary karstification. Based on mineralogical, petrological and geochemical data we sketched the possible development of the area. Following the carbonate formation in the Triassic, the first main stage was Paleocene exhumation, erosion and karsticifaction. Burial started in the Eocene after the basal clastic rocks formed and finaly the area started partially to uplift. Coevally hydrocarbons migrated through karstified zones and the fracture network (Fig. III.11).

We have examined the fractures and vein filling minerals at mezo (core) and micro (thin section) scale (Chapter III). We defined four vein-generations; three of what do not show traces of dissolution while the youngest one (F4), which is even younger than the breccia formation, so also younger than karstification, does. We have found hydrocarbon inclusions exclusively in the calcite fillings of the F4 fracture, which contain HC that, as UV spectroscopic measurements show, is consistent with the oil produced nowadays. That way we have proved that a certain part of HC migration is currently going on along the dissolved fractures.

In Chapter IV we have examined the particular fractures of the Gomba reservoir from geometrical aspect, and similarly to the simulations mentioned in Chapter II, we have executed fracture system simulations based on the obtained data. Finally, we have compared the fracture system with other available information like petrological, wire-log and drilling data. During the survey of the individual fractures we have described the digitalized fractures with their geometrical features (area, perimeter, convexity, sphericity, axial ratio, etc). The obtained database allowed us to compute a function that is able to discriminate dissolved and not-dissolved fractures, using parameters that are easy to measure. Relying upon these findings we have demonstrated that there exists segmentation with a pronounced transition between the dissolved and non-dissolved fractures on the available bore core section. This type of heterogeneity can be investigated on larger scale too; FMI/CBIL data show that the distribution of the fractures as to vertical extent is heterogeneous. They show significant deviation and the prominent anomalies often correspond with the drilling anomalies and also with the anomalies of the well-logs.

DFN-models created using the data of the two scales (thin section and macro scale; CBIL/FMI) proposes non-coherent fracture systems both in the case of Gomba-1 and

Gomba-3 wells. The breccia section under the Triassic-Eocen unconformity is the most connected fracture system in case of Gomba-1 (2450–5210 m), while the same interval is not connected in case of Gomba-3 (2475–2520 m). In case of Gomba-1 we can render larger connected fracture system probable below 2600 m, while in case of Gomba-3 we can find a relatively fractured zone below 2575 m. Only isolated, smaller fracture groups can be rendered probable in the intermediate vertical sections in case of both wells.

Referring back to Chapter II, the simulated fracture system suggests the rock body was suitable for formation a pervasive cave system. Therefore it seems probable that the falling in of the drilling bit during the drilling (Gomba-1 2680 m) as well as the total mud loss do not simply hint at isolated caverns but rather at an intact section of a former cave system. The formation of a branchwork-type cave system is most likely as literature says. The results of Chapter II imply that the microfracture network follows the direction of the main structural lines so we can assume that the caverns may be of NE-SW direction laterally in the Gomba field.

Chapters III and IV show that the Triassic carbonate rocks of the Gomba HC field are of all probability, paleokarstic formations. The Gomba field fits well in the paleokarstic classification systems mentioned in Chapter I: under James and Choquette (1988) it definitely belongs to the category of regional paleokarsts, the long-term exposure may have gone through during the paleogene exhumation. Under Esteban (1991) the Gomba area is a paleokarst associated with the unconformity of 3-4th order. Mazullo and Chilingarian (1966) have separated 7 types of karstic reservoirs based on published karstified carbonate reservoirs of various ages from around the world. In the Gomba field the most probable one is the „Buried Hill" type. It is typical of this particular type that karstification creates porosity or significantly increase it if it already exists and raises permeability and also, that the geomorphology of the buried rock is greatly affected by karstic erosion.

5.2. Outlook

It is clear from the dissertation that there are plenty of unanswered questions concerning the Gomba paleokarst, so further surveys are necessary. If there has been any other karstification event before or after the proved epigene karstification phase is still a question. That once a homogeneous karstification has gone through in the whole area is of high probability, and this process could have resulted in a developed cave system of

several kilometres, like in the Buda Hills (Kriván 1959, Nádor and Sásdi 1991, Nádor 1993, Győri et al. 2011). To prove this, first we should examine the chemical composition of the aqueous fluid inclusions.

To interpret the reservoir parameters is not the topic of this dissertation, still utilizing the parameters that have been used to the DNF simulation; there is an opportunity to estimate fractured porosity and permeability, even with the help of RepSim software. Chapter II demonstrates that the latter can show significant anisotropy in case of fractured carbonate bodies, which can have a decisive effect on dissolution-cementation processes and eventually on the fluid-storing ability (Singurindy and Berkovitz 2005).

Further interpretation of seismic survey can greatly assist the spatial expansion of our results. It is mainly the collapses and the disturbed zones around the collapses (e.g. Loucks 1999) which can reach sizes that can be recognized in seismic surveys. Although there is a good quality 3D seismics at our disposal, this is a rather problematic task as the Gomba paleokarst is very deep underground. Despite this fact lots of studies were released which localize paleokarstic objects, mostly through amplitude analysis (e.g. Zuo et al. 2009, Bili et al. 2016).

There are numerous areas both in Hungary and abroad the study of which can make use of the methods we have applied. These are basically the Hungarian Paleogene Basin, the Little Plain as well as the less known fluid reservoirs of considerable geothermic potential in the precenozoic basement in the Mid Hungarian Unit or even in the Great Plain. I believe that the image analysing and statistical methods applied to determine the rate of dissolved and non-dissolved fractures is apt to be used in any field and, if we have enough samples, it is suitable to make useful conclusions. The RepSim program can also be applied to simulate the fracture system in any karstic/paleokarstic area even with highly dissolved fractures.

Chapter IV says that a relation can be rendered probable between certain wire-log anomalies (total gamma, resistivity, density) and the paleokarstic events in the surveyed region. Still, this relation is by no means inevitable, though other scientist describe similar observations (e.g. Mazullo and Chiligarian 1996). As such anomalies can be caused by other geological processes as well I do not think that these coincidences would indicate paleokarstic zones without any trace of doubt.

Summary

1. Introduction and Aims

Karstic and paleokarstic fluid reservoirs are of extremely heterogeneous structure and have a major share both in the area of hydrocarbon production and of geothermal energy utilization. The fracture system forms the main storage spaces and the migration pathways in the usually layered or bedded carbonate formations, which are further subdivided by possible cavities or collapses but smaller dissolved caverns can also significantly increase pore space.

Carbonate bodies that can be suitable for hydrocarbon storage or have undergone karstification are easy to find in several places in the Precenozoic basement of Hungary. The Gomba hydrocarbon reservoir, which can be found in the Paleogene Basin, can also be related to fractured limestones. The area started to be studied in the late 1990s, while production began in the early 2000s. No geological and geophysical information accumulated since then got published so we know them only from the internal reports of MOL PLC. There are many karstic areas in Hungary what are used in the drinking water supply (e.g. Tata, Tatabánya, Miskolc and Orfű) too.

One of the dissertation goals is to recognize the relationship between the fracture network and the macro-karstic forms (caves, dolinas) in a nearsurface karstic area of Mecsek Mts. near Orfű. Another main dissertation aim was the petrological description of the carbonate body of the Gomba hydrocarbon reservoir, with special regard to the fracture system that determines possible karstification stages. The last main aim was to explore the depth intervals underwent karstification with the help of fracture system simulations as well as to point out zones where no major cavity system was able to develop.

The work includes two parts. The first section treats the relationship between the geometric parameters of a fracture network and the karstic forms, while the second one is related to the Gomba field fracture network and petrology.

2. Applied methods

Resulting from the peculiarities of the study areas slightly different methodology seemed to serve the purpose in the two areas examined. Nevertheless, the working process was the same in both cases: petrological description, fracture parametrization, DFN simulation and eventually making conclusions.

As for the Mecsek area petrological description was based on literature thanked to the ample references, in the case of Gomba field the petrological reinterpretation of the cores seemed necessary. So I have examined the available rock samples of both Gomba-1 and Gomba-3 both on macroscopical and thin section scales. Besides optical microscopic analyses also Scanning Electron Microscopic, X-ray Powder Diffraction, X-ray Fluorescent, Raman Spectrometry, UV-spectroscopic, cathode-luminescent, fluid inclusion as well as stable isotopic measurements were carried out.

In case of exposed breccia sections texture analysis was done with image analysis methods on thin section scale using Olympus Stream Essential and ImageJ softwares. We have measured the size, the average axial direction of the clasts, the proportion of the clasts and matrices and also sphericity.

What differed most in the methods applied in the two areas was fracture parametrization. If on surface, samples were provided by rock exposures of various sizes (0.1–2.0 m^2), in case of the Gomba field samples were taken from CBIL/FMI logs measured during drillings and from the cores themselves. In both cases we have examined the length distribution of the fractures (E), aperture of the fractures (a), and fracture density which have been described by fractal dimension (D). In case of the Mecsek sample area we have derived any parameter from digitalized rock exposures (11 samples altogether, 1727 fractures). While in the case of the Mecsek area we have calculated the D parameter by box-counting, in drillings (Gomba samples) we have derived D from the Hurst-exponent determined from the interpreted CBIL/FMI data.

When studying the Gomba samples I have also examined the individual fractures by image analysis. As we had a large database of fracture geometrical results we had the opportunity to carry out multivariate statistical processing on the data through which I targeted the grouping of dissolved and non-dissolved fractures. Finally I have prepared fracture- network models using RepSim software. Then I have compared the structure of the models with the known lithological structure and with the technical problems that

occurred during the drillings. I also managed to point out the zones where major cavity-formation is rendered possible around the wells and vertical sections where we cannot expect major cave systems.

3. New scientific results

The research presented in the dissertation has provided the following new scientific results:

1. In the Mecsek study area I have pointed out two fracture zones communicating through fractures with a non-fractured zone between them. The sinks in one fractured zone (e.g. Trió-cave, Gilisztás-cave, Szuadó-cave) are hydraulically connected with the spring in the other fractured zones (Vízfő-cave). The hydraulic connection between the two areas can mainly be explained by the flow along the bedding surfaces.

2. Through studying the Mecsek area I have shown that the microfracture network is able to divide an area interpreted hydraulically unified into parts where the hydraulic connection definitely does not go through the fracture system. This also means that regions can be separated within an aquifer where solution is able to create connected subsurface cave systems and also parts where the formation of major cave systems is hindered. All parameters (as climate, soil thickness, surface morphology, lithology etc.) may be the same, the formation of karstic cavities in a particular aquifer is not of the same probability.

3. 3. I have separated three rock types in the Triassic sequence of the Gomba reservoir. The most frequent rock type is a limestone with oncoidal grainstone, wackestone texture, which also served as precursor of a dolomitic limestone resulting from the fabric-selective recrystallization. The limestone is overlain by a breccia body of varying thickness and chaotic texture. Both composition of the breccia matrix (high content of dickite and quartz) and of the breccia framework grains (carbonates, metamorphic rocks and claystones) and also the textural parameters render tectonic origin out of question. Mineralogical, geochemical and image analysis results show that the breccia formation is linked to karstification and is genetically hydraulic and/or regolith.

4. Based on the characteristics of fracture fillings and the mineral composition I have concluded that the Gomba reservoir must have experienced higher temperatures in the past than nowadays (125 °C). The Raman thermometry results of the organic material in the fractures as well as the presence of dickite and framboidal pyrites show that the maximum temperature of the burial can be estimated as ~220 °C.

5. Regarding the fracture system of the Gomba field, I have separated 4 fracture generations. I have found oil inclusions in the calcite fillings of the youngest fracture system – younger than the breccia formation – characterized by identical UV-spectra with the oil produced nowadays. That way I was able to prove that the fracture system is an active part of the recent hydrocarbon migration. Additionally, I have also found bitumen fillings in the older fracture generations what indicate a previous hydrocarbon migration phase.

6. The image analysis of the individual fractures indicates that the shape of several fractures has been greatly modified due to dissolution. The application of the discrimination function to separate the dissolved and non-dissolved fractures numerically made it possible to calculate the extent of dissolution. I have pointed out that non-dissolved fractures formed even in the most fractured parts of the rock which could not have taken part in the coeval flow system.

7. In case of the Gomba field I have proved the existence of a karstification event. This event is suggested by the presence of cavity crossed during the drilling, by the fresh-water limestone clast found among the breccia clasts the texture of which is mostly similar to that of a dripstone, by the high number of dissolved fractures, by the dissolution traces on the cores, and also by the significant amount of dickite in the breccia matrix which is the polytype modification of kaolinite produced by the tropical weathering conditions during sedimentation.

8. In case of the reservoir in the surrounding of the Gomba-1 and Gomba-3 wells the fracture network does not constitute a consistent fracture system. In the case of both wells two major fracture sub-systems are separated by a non-fractured zone. Therefore, as in the Mecsek, areas can be assigned which structurally determine the zones where major cave systems could be formed and where they could not. Each

depth interval suitable for cave formation contains some trace of paleo-caves (e.g. cave sediment, open cavity, extreme/total mud loss). Based on geological setting and published analogues from literature the contemporary cave-system must have been an epigenetics, branchwork-type cave, with NE–SW main passages.

Összefoglalás

1. Bevezetés és célok

A karsztos és paleokarsztos fluidum tárolók rendkívül heterogén szerkezeti egységek, melyek világszerte jelentős részesedéssel bírnak mind a szénhidrogén termelés, mind pedig a geotermikus energia hasznosítás területén. Az általában rétegzett vagy pados karbonátos képződményekben a fő tárolási tereket és áramlási pályákat a törésrendszer alakítja ki, melyet tovább tagolnak az esetleges barlangi üregek, vagy kollapszusok, de a kisebb méretű oldásos üregek, kavernák is számottevően növelhetik a pórusteret.

Magyarország prekainozoos aljzatában számos helyen találhatóak olyan karbonát testek, melyek alkalmasak lehetnek szénhidrogén tárolásra, illetve a földtörténet során valamikor karsztosodhattak. A Paleogén Medencében található gombai szénhidrogén telep is repedezett mészkövekhez köthető, melyekben karsztosodáshoz kapcsolható folytonossági hiányok találhatóak. A terület kutatása a 90-es évek végén kezdődött meg, míg a termelés a kétezres évek elején. Az eltelt időszak alatt felhalmozódott geológiai és geofizikai ismeretek nem kerültek publikálásra, így kizárólag a MOL Nyrt. belső jelentéseiből ismertek.

A dolgozat fő célja, a gombai szénhidrogén telep karbonátos kőzettestének petrológiai jellemzése, különös tekintettel az esetleges karsztosodási fázisokat meghatározó törésrendszerre. További célja, hogy az egyedi törésekből épített törésrendszer-szimulációk alapján a karsztosodásra alkalmas mélységtartományokat felderítse, illetve meghatározzon olyan zónákat, ahol fejlettebb üregrendszer nem alakulhatott ki. Szintén célja a disszertációnak a Nyugat-Mecseki karszt repedésrendszere és karsztos formakincse közötti kapcsolat megismerése. Mivel ez a terület felszínközeli és több évtizedes szerteágazó kutatási múlttal bír, így a kapott eredmények jól korrelálhatók más ismeretekkel. Az ilyen formán validálható eredmények fontos következményekkel bírhatnak a gombai szénhidrogén rezervoár repedésrendszerének vizsgálatában is.

A disszertáció két részből áll. Az első szakasz a törés paraméterek (hosszúság, nyitottság, sűrűség) és a karsztos formák kapcsolatával foglalkozik az orfűi Vízfő-forrásbarlang példáján, a második pedig a gombai szénhidrogén rezervoár kőzettanát és repedésrendszerét elemzi.

2. Alkalmazott módszerek

A mintaterületek sajátosságából fakadóan némileg különböző módszertan alkalmazása volt célravezető a két vizsgált területen, ugyanakkor az alkalmazott munkafolyamat mindkét esetben azonos: kőzettani jellemzés, törés parametrizálás, DFN szimuláció, végül a következtetések levonása.

A mecseki mintaterület esetében a petrológiai jellemzés – köszönhetően a jelentős mennyiségű irodalmi forrásnak – irodalmi adatok alapján történt. A gombai terület esetében azonban célszerű volt a fúrómagok petrográfiai újra értelmezése is, így mind makroszkópos, mind vékonycsiszolati léptékben vizsgáltam a Gomba-1 és Gomba-3 fúrás rendelkezésre álló kőzetmintáit. Az optikai mikroszkópos elemzés mellett Pásztázó Elektron Mikroszkópos, Röntgen diffrakciós, Röntgen fluoreszcens, Raman spektroszkópiás, UV-spektroszkópiás és katód lumineszcens, fluidum zárvány, valamint stabil izotóp összetétel vizsgálatok is történtek. A maximális hőmérséklet megbecslésére Raman spektroszkópiai alapú szenes anyag termométert alkalmaztunk (Beyssac et al. 2002, Rahl et al. 2005).

A feltárt breccsás szakaszok esetében a szöveti vizsgálatot képelemzési módszerrel végeztük el vékonycsiszolatokon, melyhez Olympus Streem Essential és ImageJ szoftvereket alkalmaztunk. A vizsgálat során mértük a klasztok méretét, a klasztok átlagos tengelyirányát, a klasztok és a mátrix arányát és a klasztok kerekítettségét is.

A legnagyobb eltérés a két területen alkalmazott módszerben a törésparametrizálás esetén volt. A felszíni esetben változó méretű (0,1–2,0 m^2) kőzetkibukkanások, míg a gombai területen a fúrásban mért CBIL/FMI logok, illetve maguk a fúrómagok szolgáltatták a mintákat. Mindkét esetben vizsgáltuk a törések hosszúság eloszlását (E), a törések nyitottságát (a), és a törés sűrűséget, melyet a fraktál dimenzióval jellemeztünk (D). A mecseki mintaterület esetében minden paramétert digitalizált kőzetkibukkanásokról származtattunk (összesen 11 minta, 1727 db törés). Amíg a mecseki terület esetében a D paramétert box-counting módszerrel számítottuk, addig a fúrásokban (gombai minták), az értelmezett CBIL/FMI adatsorból meghatározott Hurst kitevőből származtattuk a D értéket.

A gombai minták esetében az egyedi törések alakját is vizsgáltam képelemzési módszerekkel. A törésgeometriai eredmények nagyméretű adatbázisa lehetővé tette az adatok többváltozós statisztikai feldolgozását, melynek elsődleges célja az oldott és nem oldott törések csoportosítása volt. Végül a kapott adatokból töréshálózati modelleket készítettem a RepSim szoftver segítségével, melyek szerkezetét összevetve az ismert

litológiai felépítéssel, valamit a fúrás során felmerült technikai problémákkal (pl. teljes iszapveszteség), sikerült kimutatni olyan zónákat a vizsgált kutak környezetében, ahol jelentősebb üregesedés valószínűsíthető, illetve olyan mélység tartományokat, ahol fejlettebb üregrendszer nem várható.

3. Új tudományos eredmények

A dolgozatban bemutatott kutatás az alábbi új tudományos eredményeket szolgáltatta:

1. A mecseki terület esetében két kommunikáló törészónát és a két térrész között egy nem repedezett zónát mutattam ki. Az egyik repedezett zónában található víznyelő barlangok (pl. Trió-barlang, Gilisztás-barlang, Szuadó-barlang) a másik repedezett zónában található forrással (Vízfő-forrás barlang) hidraulikai kapcsolatban állnak, így bizonyos, hogy a két terület között a hidraulikai kapcsolat nem a törések, hanem főként réteglapok menti áramlással zajlik.

2. A mecseki mintaterület vizsgálata alapján kimutattam, hogy egy hidraulikailag egységesként értelmezett karbonátos vízgyűjtőt a mikrotöréshálózat képes olyan részterületekre tagolni, melyek között a hidraulikus kapcsolat bizonyosan nem a törésrendszeren keresztül történik. Mindez azt is jelenti, hogy egy vízgyűjtő területen elkülöníthetőek olyan térrészek, ahol az oldódás képes összefüggő felszín alatti üregrendszert kialakítani és olyanok, ahol a fejlett üregrendszerek kialakulása gátolt. Tehát nem azonos valószínűséggel keletkeznek karsztos üregek egy adott vízgyűjtőn, még akkor sem, ha minden más paraméter (pl. klíma, talajvastagság, felszín morfológia, litológia, stb) azonos is.

3. A gombai rezervoár triász rétegsorában három kőzettípust különítettem el. A leggyakoribb kőzettípus a grainstone, wackestone szövetű onkoidos mészkő, melynek feküjét a mészkő szövetszelektív átkristályosodásával keletkezett dolomitos mészkő alkotja. A mészkő fedője a kaotikus szövetű, változó vastagságú breccsa. A breccsa mátrixának összetétele (magas dickit és kvarc tartalom), valamint a breccsát alkotó szemcsék összetétele (karbonátok, metamorf kavicsok és agyagkövek), valamint a szöveti paraméterek mind kizárják a tektonikus eredetet.

Az ásványtani, geokémiai és képelemzés eredmények alapján a breccsa kialakulása karsztosodáshoz kötött, hidraulikus és/vagy regolit genetikájú.

4. Az érkitöltések vizsgálata, valamint az ásványos összetétel alapján arra következtetésre jutottam, hogy a gombai rezervoár a régmúltban bizonyosan magasabb hőmérsékleti tartományba került, mint a mai állapot (125 °C). A törésekben található szerves anyag Raman termometriai mérési eredménye, valamint a mintákban található dickit jelenléte a betemetődés maximális hőmérsékletét ~220 °C-nak mutatja.

5. A gombai terület repedésrendszerének vizsgálata során 4 törésgenerációt különítettem el, melyek közül a legfiatalabb, a breccsa képződésénél is fiatalabb törésrendszer kalcit kitöltéseiben a napjainkban termelt olajjal azonos UV-spektrummal jellemezhető olajzárványokat azonosítottam, így bizonyítottam, hogy a törésrendszer aktív eleme a recens szénhidrogén migrációnak. Az idősebb törésgenerációk bitumen kitöltést tartalmaznak, mely egy korábbi szénhidrogén migrációt jeleznek.

6. Az egyedi törések képelemzési vizsgálata alátámasztja, hogy számos törés alakja az oldódás hatására számottevően módosult. Az oldott és nem oldott törések numerikus elkülönítésére számított diszkriminancia függvény alkalmazásával az oldódás mértéke megbecsülhetővé vált. Kimutattam, hogy a vizsgált mészkőtest legintenzívebben töredezett szakaszain is találhatók nem oldott törések, melyek ez alapján nem vettek részt az egykori áramlási rendszerben.

7. A gombai területen igazoltam egy karsztosodási esemény meglétét, melyet alátámaszt a fúrás során harántolt üreg jelenléte, a különböző mélységekben megjelenő polimikt breccsa, a breccsa klasztjai között feltárt cseppkő szövetű édesvízi mészkő töredék, a jelentős számú oldott törés, a fúrómagokon található oldódási nyomok, valamint a breccsa mátrixában található jelentős dickit tartalom, mely a trópusi mállás eredményeként létrejövő kaolinit magasabb hőmérsékletű változata.

8. A gombai rezervoár esetében, a Gomba-1 és Gomba-3 kutak környezetében a töréshálózat nem alkot összefüggő törésrendszert. Mindkét kút esetében két összefüggő, nagyméretű törésrendszert választ el egy nem töredezett zóna. A mecseki területhez hasonlón itt is lehatárolhatóak olyan területek, melyek szerkezetileg predesztinálják azokat a zónákat, ahol kialakulhattak fejlettebb üregrendszerek, illetve ahol nem. A barlangképződésre alkalmas mélységintervallumok mindegyike tartalmaz valamilyen paleobarlangra utaló nyomot (pl. barlangi üledék, nyitott üreg, extrém nagy/teljes iszapveszteség). A földtani környezet és irodalmi analógiák alapján az egykori barlangrendszer egy epigén, patakos (branchwork) típusú barlang volt, melynek fő járatai ÉK-DNy irányt vehettek fel.

Acknowledgements

I would like to express my sincere gratitude to my consultants, *Dr. Tivadar M. Tóth* and *Dr. Béla Raucsik* for their overall professional guidance and most useful pieces of advice.

I would like to say thanks to each and every colleague in the *Department of Mineralogy, Geochemistry and Petrology in the University of Szeged* because they were able to create an athmosphere where thinking together was an everyday matter as well as to the *Institute for Geography and Earth Sciences* who has supported me by granting a pre-doctoral scholarship. I am also grateful to *MOL PLC.* who made the rock samples and survey reports necessary to my research available to me.

I would like to thank *Dr. Bernadett Bajnóczi* for the CL measurements and for *Dr. Andrea Raucsikné Varga* who has supported the stabile isotopic measurements. I would like to thank *János Ország*, Dr. *Károly Barta and Tamás Tarnai* for their advice during the Mecsek research.

I am indebted to *Beáta Csépe-Muladi and Zoltán Csépe* for the so much hours they spent with answering my questions and dealing with my requests concerning the research. Last, but not least, I would like to thank my mother, *Pozsár Katalin,* for her help with English and also *Petra Sebestyén and Dr. Ágnes Cserkész-Nagy* for their professional advice and constant encouragement.

References

Allègre, C. J., Le Mouel, J. L., Provost, A. (1982): Scaling rules in rock fracture and possible implications for earthquake prediction. Nature, 297, 47–49.

Árkai, P. (1983): Very low- and low grade alpine regional metamorphism of the Paleozoic and Mesozoic formations of The Bükkium, NE-Hungary. Acta Geologica Hungarica, 26, 1–2, 83–101.

Bada, G., Horváth, F., Dövényi, P., Szaffián, P., Windhoffer, G., Cloetingh, S. (2007): Present-day stress field and tectonic inversion in the Pannonian basin. Global and Planetary Change, 58, 165–180.

Barabás A., Barabás-Stuhl, Á. (2005): Geology of the Lower Triassic Jakabhegy Sandstone Formation, Hungary, SE Transdanubia. Acta Geologica Hungaica, 48, 1–7.

Barton, C. C., Larsen, E. (1985): Fractal geometry of two-dimensional fracture networks at Yucca Mountain, Southwestern Nevada. Fundamentals of Rock Joints: Proceedings of the International Symposium on Fundamentals of Rock Joints, 77–84.

Barton, C. C. (1995): Fractal analysis of scaling and spatial clustering of fractures. In: Barton, C. C., La Pointe, P. R. (eds): Fractals in the Earth Sciences. Plenum Press, New York, 168.

Bauer, M., M. Tóth, T. (2015): Modeling microfracture geometry to asses the function of a karst system (Vízfő spring catchment area, Western Mecsek Mountains, Hungary). Geologica Croatica, 68, 1, 11–23.

Bauer, M., M. Tóth, T., Raucsik, B., Garaguly, I. (2016): Petrology and Paleo-karst features of the Gomba hydrocarbon reservoir (Central Hungary). Central European Geology, *In-press*.

Bauer, S., Liedl, R. (2000): Modelling of karst development considering conduit-matrix exchange flow. Calibration and Reliability in Groundwater Modelling (Proceedings of the ModelCARE 99 Conference held at Zurich, Switzerland, September 1999) IAHS Publ., Zürich10–15.

Bauer, S., Liedl, R., Sauter, M. (2002): Modelling of karst genesis at the catchment scale influence of spatially variable hydraulic conductivity. Acta Geologica Polonica, 52, 13–21.

Bauer, S., Liedl, R., Sauter, M. (2003): Modelling of karst aquifer genesis — influence of exchange flow. Water Resources Research, 39, 10, 1285.

Bean, C. J. (1996): On the cause of 1/f-power spectral scaling in borehole sonic logs. Geophysical Research Letters, 23, 3119-3122.

Bear, J. (1972): Dynamics in porous media. Elsevier, New York, 1-392.

Beaufort, D., Cassagnabere, A., Petit, S., Lanson, B., Berger, G., Lacharpagne, J. C., Johansen, H. (1998): Kaolinite to Dickite reaction in sandstone reservoirs. Clay. Min., 33, 297–316.

Benedek, L. (2009): Gomba mező geológiai újrafeldolgozása és művelési terve. MOL plc. Report, Budapest, 1–210.

Benkovits, L., Csontos, L., Mansy, J. L., Bergerat, F. (1997): Folding in the Abaliget road Cut. Acta Geologica Hungarica, 40, 4, 425–440.

Benkovics, L., Obert, D., Bergerat, F., Mansy, J. L., Dubois, M. (1999): Brittle tectonics and major dextral strike- slip zone in the Buda karst (Budapest, Hungary). Geodinamica Acta, 12, 3–4, 201–211.

Beyssac, O., Goffé, B., Chopin, C., Rouzaud, J. N. (2002): Raman spectra of carbonaceous material in metasediments: A new geothermometer. Journal of Metamorphic Geology, 20, 859–871.

Billi, A., Valle, A., Brilli, M., Facenna, C., Funiciello, R. (2007): Fracture controlled fluid circulation and dissolutional weathering in sinkhole-prone carbonate rocks from central Italy. Journal of Structural Geology, 29, 385–395.

Blenkinsop, T. G. (1991): Cataclasis and processes of particle size reduction. Pure and Appl. Geophys., 136, 1-33.

Bodnar, R. J. (1993): Revised equation and table for determining the freezing point depression of H2O-NaCl solutions. Geochimica et Cosmochimica Acta, 57, 683–684.

Boggs, S. (2009): Petrology of sedimentary rocks. Cambridge University Press, Cambridge, New York, 600 p.

Boggs, S., Krinsley, D. (2008): Application of cathodoluminescence imaging to the study of sedimentary rocks. Cambridge University Press, New York, 1–165.

Bons, P. D. (2000): The formation of veins and their microstructures. Journal of the Virtual Explorer, 32.

Bons, P. D., Elburg, M. A., Gomez-Rivas, E. (2012): A review of the formation of tectonic veins and their microstructures.Journal of Structural Geology43, 33–62.

Borghi, A., Renard, P., Jenni, S. (2012): A pseudo-genetic stochastic model to generate karstic networks. Journal of Hydrology, 414–415, 516–529.

Bowen, G. J., Wassenaar, L. I., Hobson, K. A. (2004): Global application of stable hydrogen and oxygen isotopes to wildlife forensics. Oecologia, 143, 337–348.

Campos, I., Balankin, A., Bautista, O., Ramírez, G. (2005): Self-affine cracks in a brittle porous material. Theoretical and Applied Fracture Mechanics, 44, 2, 187–191.

Candelaria, M. P., Reed, C. L. (1992): Paleokarst, karst related diagenesis and reservoir development: Examples from Ordovician-Devonian age strata of West Texas and the Mid-Continent. Blackie and Son Ltd., 92–33, 239, 202.

Chiles, J., De Marsily, G. (1993): Stochastic models of fracture systems and their use in flow and transport modeling. In: Bear, J., Tsang, C. F., De Marsily, G. (eds): Flow and contaminant transport in fractured rock. Academic Press, 169–236.

Chilingar, G. V. (1960): Notes on classification of carbonate rocks on basis of chemical composition. Journal of Sedimentary Petrology, 30, 157–158.

Choo, O. C., Kim, S. J. (2004): Dickite and other kaolin polymorphs from an Al-rich clay deposits formed in volcanic tuff, southeastern Korea. Clays & Clay Min., 52, 749–759.

Choquette, P. W., Pray, L. C. (1970): Geologic nomenclature and classification of porosity in sedimentary carbonates. AAPG Bulletin, 54, 2, 207–250.

Coplen, T. B. (1996): Guidelines for reporting certain isotopic values relevant to ground-water studies. Ground Water, 34, 3, 338.

Curl, R. L. (1986): Fractal dimensions and geometries of caves. Mathematical Geology, 18, 8, 765–783.

Czigány, Sz., Lovász, Gy. (2006): A mecseki karszt térképezésének újabb eredményei (New results of the mapping on the karstic area of Mecsek Mountain – in Hungarian). Közlemények a Pécsi Tudományegyetem Földrajzi Intézetének Természetföldrajzi tanszékéről, 28, 3–14.

Csontos, L., Nagymarosy, A., Horváth, F., Kovács, M. (1992): Tertiary evolution of the Intra-Carpathian area: A model. Tectonophysics, 208, 221–241.

Csontos, L., Nagymarosy, A. (1998): The Mid-Hungarian line: A zone of repeated tectonic inversions. Tectonophysics, 297, 1–4, 51–71.

Csontos, L., Benkovits, L., Bergerat, F., Mansy, J. L., Wórum, G. (2002): Tertriary deformation history from seismic section study and fault analysis in former European Tethyan margin (The Mecsek-Villány Mountains area, SW Hungary). Tectonophysics, 357, 81–102.

De Dreuzy, J. R., Davy, P., Bour, O. (2002): Hydraulic properties of two-dimensional random fracture networks following power law distributions of length and aperture. Water Resources Research, 38, 12, 121–129.

Dershowitz, W. S., Einstein, H. H. (1998): Characterizing rock joint geometry with joint system models. Rock Mech. Rock Eng., 1, 21–51.

Diabat, A., Ahmad, F., Hammouri, N., Obeidat, M. (2013): Karst development related to extensional fracture network at Bany-Kanana area, northern Jordan. Arab J. Geosci., 8, 4999–5014.

Dolton, G. L. (2006): Pannonian Basin Province, Central Europe (Province 4808) – Petroleum geology, total petroleum systems, and petroleum resource assessment. U.S. Geological Survey Bulletin, 2204, B, 47.

Dreybrodt, W., Gabrovšek, F. (2000): Dynamics of the evolution of a single karst conduit. In: Klimchouk, A. B., Ford, D. C., Palmer, A. N., Dreybrodt, W. (eds): Speleogenesis: Evolution of karst aquifers. National Speleological Society, USA, 184–193.

Dreybrodt, W., Gabrovšek, F., Perne, M. (2005): Condensation corrosion: A theoretical approach. Acta Carsologica, 34, 2, 317–348.

Dunham, R. J. (1962): Classification of carbonate rocks according to depositional texture. Am. Assoc. Petrol. Geol. Mem., 1, 108–121.

Ehrenberg, S. N., Aagard, P., Wilson, M. J., Fraser, A. R., Duthie, D. M. L. (1993): Depth dependend transformation of kaolinite to dickite in sandstones of the Norwegian continental shelf. Clay. Min., 28, 325–352.

Ehrenberg, S. N., Nadeau, P. H. (2005): Sandstone vs. carbonate petroleum reservoirs: A global perspective on porosity-depth and porosity-permeability relationships. AAPG Bulletin, 89, 4, 435–445.

Esteban, M. (1991): Palaeokarst: practical applications.- in V. P. Wright, M. Esteban, & P. L. Smart, eds., Palaeokarst and palaeokarstic reservoirs. University of Reading, Postgraduate Research for Sedimentology, PRIS Contribution, 152, 89–119.

Esteban, M., Budai, T., Juhász, E., Lapointe, P. (2009): Alteration of Triassic carbonates in the Budai Mountains - a hydrothermal model. Central European Geology, 52, 1, 1–29.

Feng, K., Cao, J., Hua, K., Peng, X., Chen, Y., Wang, Y., Wang, M. (2013): Dissolution and its impacts on reservoir formation in moderately to deeply buried strata of mixed siliciclastic and carbonate sediments, northwestern Qaidam Basin, northwest China. Marine and Petroleum Geology, 39, 124–137.

Feret, L. R. (1931): La Grosseur des Grains des Matieres Pulverulentes. Association Internationale pour l'Essai des Materiaus, 2, D, 428.

Filipponi, M., Jeannin, P., Tacher, L. (2009): Evidence of inception horizons in karst conduit networks. Geomorphology, 106, 86–99.

Flook, A. G. (1978): Use of dilation logic on the Quantimet to achieve fractal dimension characterization of texture and structured profiles. Powder Technology, 21, 295–298.

Fodor, L., Magyari, Á., Kázmér, M., Fogarasi, A. (1992): Gravityflow dominated sedimentation on the Buda paleoslope (Hungary): Record of Late Eocene continental escape of the Bakony unit. Geol. Rundsch., 81, 3, 695–716.

Fodor, L., Jelen, B., Márton, E., Skaberne, D., Car, J., Vrabec, M. (1998): Miocene-Pliocene tectonic evolution of the Slovenian Periadriatic Line and surrounding area – implication for AlpineCarpathian extrusion models. Tectonics, 17, 5, 690–709.

Fritz, R. D., Wilson, J. L., Yurewicz, D. A. (1993): Paleokarst related hydrocarbon reservoirs. SEPM Core Workshop, 18, 275.

Gabrovšek, F., Dreybrodt, W. (2001): A model of the early evolution of karst aquifers in limestone in the dimensions of length and depth. Journal of Hydrology, 240, 206–224.

Gabrovšek, F., Romanov, D., Dreybrodt, W. (2004): Early karstification in a dual-fracture aquifer: The role of exchange flow between prominent fractures and a dense net of fissures. Journal of Hydrology, 299, 1–2, 45–66.

Géczy, B. (1973): Plate tectonics and paleogeography in the East-Mediterranean Mesozoic. Acta Geol. Acad. Sci. Hung., 17, 421–428.

Gila, Cs. (2000): Barlangjárat-jelleg vizsgálata vízfestéses eljárással a Nyugat-mecseki karszton (Diploma thesis characterization of the caves in the Western Mecsek by tracing methods-In Hungarian). University of Szeged Department of Physical Geography and Geoinformatics, Szeged, 26.

Goldstein, R. H., Reynoldsm, T. J. (1994): Systematics of fluid inclusions in diagenetic minerals SEPM Short Course 31. Society of Sedimentary Geology, 203.

Götze, J., Plötze, M., Götte, Th., Neuser, R. D., Richter, D. K. (2002): Cathodoluminescence (CL) and electron paramagnetic resonance (EPR) studies of clay minerals. Mineralogy and Petrology, 76, 195–212.

Gudmundsson, A., Berg, S. S., Lyslo, K. B., Skurtveit, E. (2000): Fracture networks and fluid transport in active fault zones. Journal of Structural Geology, 23, 2–3, 343–353.

Gudmundsson, A. (2001): Fracture dimensions, displacements and fluid transport. Journal of Structural Geology, 22, 9, 1221–1231.

Győri, O., Poros, Zs., Mindszenty, A., Molnár, F., Fodor, L., Szabó, R. (2011): Budai-hegységi paleogén karbonátos kőzetek diagenezistörténete (Diagenetic history of the Palaeogene carbonates, Buda Hills, Hungary). Földtani Közlöny, 141, 4, 341–361.

Haas, J., Budai, T., Hips, K., Konrád, Gy., Török, Á. (2002): Magyarországi triász fáciesterületek szekvencia-rétegtani elemzése (Sequence stratigraphy of Triassic facies areas in Hungary). Földtani Közlöny, 132, 1, 17–43.

Haas, J. (2004): Magyarország Geológiája – Triász. Elte Eötvös Kiadó, Budapest, 1-306.

Haas, J., Budai, T., Csontos, L., Fodor, L., Konrád, Gy. (2010): Pre-Cenozoic geological map of Hungary 1:500 000. MÁFI, Budapest

Halbach, P., Pracejus, B., Marten, A. (1993): Geology and mineralogy of massive sulfide ores from the central Okinawa trough, Japan. Economic Geology, 88, 8, 2210–2225.

Häuselmann, P., Jeannin, P. Y., Bitterli, T. (1999): Relations between karst and tectonics: The case-study of the cave system north of Lake Thun (Bern, Switzerland). Geodinamica Acta, 12, 377–388.

Hayes, M. J., Boles, J. R. (1993): Evidence for meteoric recharge in the San Joaquin Basin, California provided by isotope and trace element chemistry of calcite. Marine and Petroleum Geology, 10, 135–144.

Hewett, T. A. (1995): Fractal methodes for fracture charactherization. In: Yarus, J. M., Chambers, R. L. (eds): Stochastic Modeling and Geostatistics. Principles, Methodes and Case Studies. – AAPG Computer Applications in Geology, No. 3. AAPG, Tusla, 249-260.

Jacquet, O., Siegel, P., Klubertanz, G., Benabderrhamane, H. (2004): Stochastic discrete model of karstic networks. Advances in Water Resources, 27, 7, 751–760.

Jakucs, L. (1971): A karsztok morfogenetikája. Akadémiai Kiadó, Budapest, 46.

Jeannin, P. Y. (1990): Neotectonique dans le karst du N-O du lac de Thoune (Suisse). Karstologia, 15, 41–54.

Jébrak, M. (1997): Hydrothermal breccias in vein-type ore deposits: A review of mechanisms morphology and size distribution. Ore Geology Reviews, 12, 111–134.

Karay, Gy., Hajnal, G. (2015): Theory and practical implementations of modelling groundwater flow in fractured rocks. Mérnökgeológia-Kőzetmechanika, 2015, 1-10.

Kaufmann, G. (2003a): A model comparison of karst aquifer evolution for different matrix-flow formulations. Journal of Hydrology, 283, 1–4, 281–289.

Kaufmann, G. (2003b): Modelling unsaturated flow in an evolving karst aquifer. Journal of Hydrology, 276, 1–4, 53–70.

Kaufmann, G., Braun, J. (1999): Karst aquifer evolution in fractured rocks. Water Resources Research, 35, 3223–3238.

Kaufmann, G., Braun, J. (2000): Karst aquifer evolution in fractured, porous rocks. Water Resources Research, 36, 1338–1391.

Kaufmann, G., Romanov, D. (2008): Cave development in the Swabian Alb, south-west Germany: A numerical perspective. Journal of Hydrology, 349, 302–317.

Kaufmann, G., Romanov, D., Hiller, T. (2010): Modeling three-dimensional karst aquifer evolution using different matrix-flow contributions. Journal of Hydrology, 38, 3–4, 241–250.

Kecskeméti, T. (1998): Magyarország epikontinentális eocén képződményeinek rétegtana. In: Bérczi, I., Jámbor, Á. (eds): Magyarország geológiai képződményeinek rétegtana. MÁFI, Budapest, 403-417.

Keith, B. D., Wickstrom, L. H. (1991): The Lima – Indiana trend – reservoir characterization. AAPG Bulletin, 75, 606.

Kókai, J. (1994): Exploration history and future possibilities in Hungary. In: Popescu, B. M. (eds): Hydrocarbons of eastern central Europe, Habitat, exploration and production history. Springer-Verlag, Berlin, 147–173.

Kókai, J., Pogácsás, G. (1991): Tectono-stratigraphical evolution and hydrocarbon habitat of the Pannonian Basin. In: Spencer, A. M. (eds): Generation, accumulation and production of Europe's hydrocarbons: Special Publication of the European Association of Petroleum Geoscientists No. 3p. Springer-Verlag Berlin Heidelberg, Berlin, 1–380.

Koltai, G., Ország, J., Tegzes, Z. (2010): Radontransport mesaurments in Mecsek Mountains. Karst Development, 1, 18–30.

Konrád, Gy., Sebe, K. (2010): Fiatal tektonikai jelenségek új észlelései a Nyugat-Mecsekben és környezetében (New details of young tectonic phenomena in the Western Mecsek Mts. and their surroundings -in Hungarian). Földtani Közlöny, 140, 2, 135–163.

Korpás, L., Juhász, E. (1990): Paleokarszt földtani modellek . Karszt és Barlang, 2, 105–116.

Korvin, G. (1992): Fractal models in the Earth sciences. Elsevier, Amsterdam, 396.

Kovács, S., Szederkényi, T., Haas, J., Buda, Gy., Császár, G., Nagymarosy, A. (2000): Tectonostratigraphic terranes in the pre-Neogene basement of the Hungarian part of the Panonian area. Acta Geol. Hung., 43, 3, 225–328.

Kraus, S. (1982): A Budai-hegység hévizes barlangjainak fejlődéstörténete (Evolution of the hydrotermal caves in the Buda Mountains). Karszt és Barlang, 1, 29–34.

Kriván, P. (1959): Mezozóos karsztosodási és karsztlefedési szakaszok, alsóbartoni sziklásparti jelenségek a Budai-hegységben A szubgresszió fogalma. Földtani Közlöny, 89, 4, 393–401.

Lahfid, A., Beyssac, O., Deville, E., Negro, F., Chopin, C., Goffé, B. (2010): Evolution of the Raman spectrum of carbonaceous material in low-grade metasediments of the Glarus Alps (Switzerland). Terra Nova, 22, 5, 354–360.

Less, Gy. (2005): Paleogene. In: Pelikán, Gy. (eds): Geology of the Bükk Mountains. Hungarian Geological Society, Budapest, 204–210.

Lipmann, L., Kiss, K., Móga, J. (2008): Az Abaliget- Orfűi Karszt karsztos felszínformáinak vizsgálata térinformatikai módszerekkel (Investigation of the karstic phenomenon near Orfű and Abaliget by GIS methods- In Hungarian). Karsztfejlődés, 13, 151–166.

Loucks, R. G. (1999): Paleocave carbonate reservoirs: Origins, burial-depth modifications, spatial complexity, and reservoir implications. AAPG Bulletin, 83, 11, 1795-1834.

Loucks, R. G., Mescher, P. K., McMechan, G. A. (2004): Three-dimensional architecture of a coalesced, collapsed-paleocave system in the Lower Ordovician Ellenburger Group, central Texas. AAPG Bulletin, 88, 5, 545–564.

Lovász, Gy. (1971): Adatok az Abaligeti- karszt geomorfológiai és hidrológiai jellemzéséhez (Data for the characterization of the hydrology and geomorphology of the Abaliget karst - In Hungarian). Földrajzi Értesítő, 47, 3, 283–296.

Lucia, F. J. (1968): Sedimentation and paleogeography of the El Paso Group. In: Stewart, W.J. (eds): Delaware basin exploration: West Texas Geological Society Guidebook N.68-65. West Texas Geological Society, Texas, 61–75.

Lucia, F. J. (1995): Lower Paleozoic cavern development, collapse, and dolomitization, Franklin Mountains, El Paso, Texas. In: Budd, D. A., Saller, A. H., Harris, P. M. (eds): M63: Unconformities and porosity in carbonate strata. AAPG, Austin, 279–300.

Lucia, F. J. (1996): Structural and fracture implications of Franklin Mountains collapse brecciation. In: Stoudt, E. L. (eds): Precambrian-Devonian geology of the Franklin Mountains, West Texas-Analogs for exploration and production in Ordovician and Silurian karsted reservoirs in the Permian basin. West Texas Geological Society, Texas, 117–123.

Lucia, F. J., Charles, K., G. W. Vander, S. (1992): Characterization of a karsted, high-energy, rampmargin carbonate reservoir: Taylor-Link West San Andres Unit, Pecos County, Texas. The University of Texas Report of Investigations No. 208, Austin, 46.

Lun, Z., Jianxin, L., Kongchou, L., Zifei, F., Heng, S., Xubin, C. (2010): Development and genetic mechanism of complex carbonate reservoir fractures: A case from the Zanarol Oilfield, Kazakhstan. Petroleum Exploration and Development, 37, 3, 304–309.

M. Ahr, W. (2008): Geology of carbonate reservoirs: the identification, description, and characterization of hydrocarbon reservoirs in carbonate rocks. Wiley, Hoboken, 1–277.

M. Tóth, T. (2003): Mészkő területek repedésrendszerének modellezési lehetőségei (Modeling possibilities of limestone areas- In Hungarian). In: Kiss A., Mezősi, G., Sümeghy Z. (eds): Ünnepi tanulmányok Keveiné Bárány Ilona professzor asszony tiszteletére. University of Szeged, Szeged, 447–455.

M. Tóth, T. (2010): Determination of geometric parameters of fracture networks using 1D data. Journal of Structural Geology, 32, 7, 878-885.

M. Tóth, T., Hollós, Cs., Szűcs, É., Schubert, F. (2004): Conceptual fracture network model of the crystalline basement of the Szeghalom Dome (Pannonian Basin, SE Hungary). Acta Geologica Hungarica, 47, 1, 19–34.

M. Tóth, T., Vass, I. (2011): Relationship between the geometric parameters of rock fractures, the size of percolation clusters and REV. Mathematical Geosciences, 43, 1, 75–97.

Machel, H. G. (2001): Bacterial and thermochemical sulfate reduction in diagenetic settings – old and new insights. Sedimentary Geology, 140, 143–175.

MacLean, L. C., Tyliszczak, T., Gilbert, P. U., Zhou, D., Pray, T. J., Onstott, T. C., Southam, G. (2008): A high-resolution chemical and structural study of framboidal pyrite formed within a low-temperature bacterial biofilm. Geobiology, 6, 5, 471–480.

Magyari, Á. (1994): Késő-Eocene hidraulikus breccsásodási jelenségek a Budai-hegység déli részén. Földtani Közlöny, 124, 1, 89–107.

Mandelbrot, B. B. (1983): The fractal geometry of nature. Freeman, New York, 468.

Mandelbrot, B. B. (1985): Self-affine fractal dimension. Physica Scripta, 32, 257–260.

Marsan, D., Bean, C. J. (1999): Multiscaling nature of sonic velocities and lithology in the upper crystalline crust. Geophysical Research Letters, 26, 275–278.

McDermott, F., Mattey, D. P., Hawkesworth, C. J. (2001): Centennial- scale Holocene climate variability revealed by a high-resolution speleothem δ18O record from SW Ireland. Science, 294, 1328–1331.

McKinney, C. R., McCrea, J. M., Epstein, S., Allen, H. A., Urey, H. C. (1950): Improvements in mass spectrometers for the measurement of small differences in isotope abundance ratios. Rev. Sci. Instrum., 21, 724.

Milota, K., Kovács, A., Galicz, Zs. (1995): Petroleum potential of the north Hungarian Oligocene sediments. Petroleum Geoscience, 1, 81–87.

Min, K. B., Jing, L., Stephansson, O. (2004): Determining the equivalent permeability tensor for fractured rock masses using stochastic REV approach: Method and application to the field data from Sellafield, UK. Hydrogeology Journal, 12, 497–510.

Mort, K., Woodcock, N. H. (2008): Classification of fault breccias and related fault rocks. Geological Magazine, 145, 3, 435–440.

Nádor, A. (1991): A Budai-hegység paleokarsztjai és fejlődéstörténetük. Ph.D. Dissertation. Eötvös Loránd University, Budapest, 1–171.

Nádor, A. (1993): Paleokarsts and long-term karst evolution of the Buda Mountains, Hungary. Bulletin de la Société Géographique de Liège, 29, 139–143.

Nádor, A., Sásdi, L. (1991): A Budai-hegység paleokarsztjai és fejlődéstörténetük I Termális hatást nem tükröző paleokarsztok. Karszt és Barlang, 1, 3–10.

Nagymarosy, A. (1990): Paleogeographical and paleotectonic outlines of some IntraCarpathian Paleogene basins: – Geologický Zborník. Geologica Carpathica, 41, 3, 259–274.

Nash, D. J., Mclaren, S. J., Webb, J. A. (2004): Petrology, geochemistry and environmental significance of silcrete-calcrete intergrade duricrusts at Kang Pan and Tswaane, central Kalahari, Botswana. Earth Surf. Process. Landforms, 29, 1559–1586.

Neuser, R. D., Richter, D. K. (2007): Non-marine radiaxial fibrous calcites – examples of speleothems proved by electron backscatter diffraction. Sedimentary Geology, 194, 149–154.

Nieto-Samaniego, A. F., Alaniz-Alvarez, S. A., Tolson, G., Olescho, K., Korvin, G., Xu, S. S., Perez-Venzor, J. A. (2005): Spatial distribution, scaling and self similar behavior of fracture arrays in the Los Planes fault Baja, California Sur, Mexico. Pure and Applied Geophysics, 162, 805–826.

Olsen, J. E. (1993): Joint pattern development: Effects of subcritical crack growth and mechanical crack interaction. Journal of Geophysical Research, 98, 12251–12256.

Ortega, O. J., Marrett, R. A., Laubach, S. E. (2006): A scale-independent approach to fracture intensity and average spacing measurement. AAPG Bulletin, 90, 2, 193–208.

Osborne, R. A. L. (2001): Petrography of lithified cave sediment. Proceeding of the13th International Congress of Speleology, Brasilia, 1, 101–104.

Ouillon, G., Castaing, C., Sornette, D. (1996): Hierarchical geometry of faulting. Journal of Geophysical Research, 101, 5477–5487.

Palmer, A. N. (1991): Origin and morphology of limestone caves. Geological Society of America Bulletin, 103, 1–21.

Palotai, M., Csontos, L. (2010): Strike-slip reactivation of a Paleogene to Miocene fold and thrust belt along the central part of the Mid-Hungarian Shear Zone. Geologica Carpathica, 1, 6, 483–493.

Pardo-Iqúzuiza, E., Dowd, P. A., Xu, C., Durán-Valsero, J. J. (2012): Stochastic simulation of karst conduit networks. Advances in Water Resources, 35, 141–150.

Pelikán, P. (2005): Geology of the Bükk Mountains. Hungarian Geological Society, Budapest, 1–284.

Poros, Zs., Mindszenty, A., Molnár, F., Pironon, J., Győri, O., Ronchi, P., Szekeres, Z. (2012): Imprints of hydrocarbon-bearing basinal fluids on a karst system: Mineralogical and fluid inclusion studies from the Buda Hills, Hungary. International Journal of Earth Sciences, 101, 429–452.

Priest, S. D., Hudson, J. A. (1976): Discontinuity spacings in rock. International Journal of Rock Mechanics and Mining Sciences and Geomechanics Abstracts, 13, 5, 135–148.

Rahl, J. M., Anderson, K. M., Brandon, M. T., Fassoulas, C. (2005): Raman spectroscopic carbonaceous material thermometry of low grade metamorphic rocks: calibration and application to tectonic exhumation in Crete, Greece. Earth and Planetary Science Letters, 240, 339–354.

Rasband, W. S. (1997–2006): ImageJ, U. S. National Institutes of Health (Bethesda, Maryland, USA). Available: http://rsb.info.nih.gov/ij/, Bethesda.

Reimann, T., Giese, M., Geyer, T., Liedl, R., Maréchal, J. C., Shoemaker, W. B. (2014): Representation of water abstraction from a karst conduit with numerical discrete-continuum models. Hydrol. Earth Syst. Sci., 18, 227–241.

Renshaw, C. E., Pollard, D. D. (1994): Numerical simulation of fracture set formation: A fracture mechanics model consistent with experimental observations. Journal of Geophysical Research, 99, 9359–9372.

Richter, D. K., Neuser, R. D., Schreuer, J., Gies, H., Immenhauser, A. (2011): Radiaxial-fibrous calcites: A new look at an old problem. Sedimentary Geology, 239, 1, 23–36.

Riley, M. S. (2004): An algorithm for generating rock fracture patterns mathematical analysis. Mathematical Geology, 36, 4, 683–702.

Roehl, P. O., Choquette, P. W. (1985): Carbonate petroleum reservoirs. Springer, New York, 1–622.

Romanov, D., Gabrovšek, F., Dreybrodt, W. (2004): Modeling the evolution of karst aquifers and speleogenesis. The step from 1-dimensional to 2-dimensional modeling domains. Speleogenesis and Evolution of Karst Aquifers, 2, 1, 2–28.

Rónaki, L. (1970): Vízfő forrás és barlangjának kutatása (Researach of the Vízfő Spring and the cave behind the spring- In Hungary). Karszt és Barlang, 1, 25–30.

Rónaki, L. (2007): A Mecseki karszton történt víznyomjelzések áttekintése (Overview of the water tracing in the Mecsek Mountain – In Hungarian). Karsztfejlődés, 13, 91–103.

Schimpf, D., Kilian, R., Kronz, A., Simon, K., Spötl, C., Wörner, G., Mangini, A. (2011): The significance of chemical, isotopic, and detrital components in three coeval stalagmites from the superhumid southernmost Andes (53°S) as high-resolution palaeo-climate proxies. Quaternary Science Reviews, 30, 3–4, 443–459.

Schmid, S. M., Bernoulli, D., Fügenschuh, B., Matenco, L., Schefer, S., Schuster, R., Ustaszewski, K. (2008): The Alpine-Carpathian-Dinaridic orogenic system: Correlation and evolution of tectonic units. Swiss Journal of Geosciences, 101, 1, 139–183.

Sebe, K., Csillag, G., Konrád, Gy. (2008): The role of neotectonics in fluvial landscape development in the Western Mecsek Mountains and related foreland basins (SE Transdanubia, Hungary). Geomorphology, 102, 55–67.

Shepherd, M. (2009): Oil Field Prodctuion Geology. AAPG, Tusla, 1–350.

Shepherd, T. J., Rankin, A. H., Alderton, D. H. L. (1985): A practical guide to fluid inclusion studies. Blackie and Son Ltd., Glasgow, 239.

Sibley, D. F., Gregg, J. M. (1987): Classification of dolomite rock textures. Journal of Sedimentary Petrology, 57, 967-975.

Singurindy, O., Berkowitz, B. (2005): The role of fractures on coupled dissolution and precipitation patterns in carbonate rocks. Advances in Water Resources, 28, 507–521.

Smith, T., Guild, J. (1931): The CIE colorimetric standards and their use. Trans. Opt. Soc., 33, 73.

Spötl, C., Wennemann, T. W. (2003): Continuous-flow isotope ratio mass spectrometric analysis of carbonate minerals. Rapid Communications in Mass Spectrometry, 17, 1004–1006.

Stevanović, Z. (2015): Karst aquifers—characterization and engineering. Springer, Berlin, 1–689.

Sweeney, R. E., Kaplan, I. R. (1973): Pyrite framboid formation: Laboratory synthesis and marine sediments. Econ.Geol., 68, 618–634.

Szabó, P. Z. (1955): A fiatal kéregmozgások geomorfológiai és népgazdasági jelentősége a Déldunántúlon (Geomorphological and economic significance of the young structural deformations in SW Hungaria –In Hungarian). Dunántúli Tudományos Intézet Gyűjteménye, 4, 12–26.

Szalay, I., Dienes, E., Nemes, I. L., Schönviszky, L. (1978): A Darnó-öv szerkezeti kutatása. Annual Report of the Eötvös Loránd Geophysical Institute of Hungary, 1977, 34–41.

Szalay, I., Dudás, K., Hegedűs, E., Schönviszky, L., Taba, S. (1976): Geophysical structure investigation around the Darnó fault line. Annual Report of the Eötvös Loránd Geophysical Institute of Hungary, 1975, 26–30.

Szőke, E., Ország, J. (2006): A mecseki Rumba-barlang víznyomjelzéses vizsgálata (Research the Rumba cave by tracing methods in the western Mecsek Mts. – In Hungarian). Karst Development, 11, 275–286.

Tari, G., Báldi, T., Báldi-Beke, M. (1993): Paleogene retroarc flexural basin beneath the Neogene Pannonian Basin: A geodynamic model. Tectonophysics, 226, 1, 433–455.

Tezuka, K., Watanabe, K. (2000): Fracture network modelling of Hijiori hot dry rock reservoir by deterministic and stochastic crack network simulator (D/SC). Proceedings World Geothermal Congress, 2000, 3993–3998.

Turcotte, D. L. (1997): Fractals and chaos in geology and geophysics. Cambridge University Press, New York, 412.

Varga, A., Raucsik, B. (2014): Pedogenic calcrete records in southern Transdanubia, Hungary: A brief review with paleoenvironmental and paleogeographic implications. Central European Geology, 57, 2, 137–151.

Vass, B. (2012): Vízhozam és hézagtérfogat számítás magaskarszt forrásoknál a Tettye példáján (Well capacity and porosity calculating on the Tettye spring catchment area - In Hungarian). In: Barta, K., Tarnai, T. (eds): A Nyugat- Mecsek karsztja. Geolitera, Szeged, 69–75.

Vass, I., M. Tóth T., Szanyi, J., Kovács, B. (2009): Az aljzati kristályos hátak szerepe az Alföld fluidum áramlási és hőtranszport folyamataiban (The role of the crystallic domes of the basement in the fluid migration and thermotransport processes – In Hungarian). In: M. Tóth, T. (eds): Magmás és Metamorf képződmények a Tiszai egységben. Geolitera, Szeged, 325–341.

Velledits, F., Bérczíné, M. A., Piros, O. (1999): A Kisfennsíki Mészkő (Bükk hegység) fáciese és kora. Földtani Közlöny, 129, 4, 573–592.

Verheyden, S., Genty, D., Cattani, O., Vanbreukelen, M. (2008): Water release patterns of heated speleothem calcite and hydrogen isotope composition of fluid inclusions. Chemical Geology, 247, 1-2, 266–281.

Vermilye, J. M., Scholz, C. H. (1995): Relation between vein length and aperture. Journal of Structural Geology, 17, 3, 423–434.

Wein, Gy. (1977): A Budai-hegység szerkezete (A Budai-hegység kialakulásának története). Földtani Közlöny, 107, 3–4, 329–347.

White, E. L., White, W. B. (1969): Processes of cavern breakdown. National Speleological Society Bulletin, 31, 83–96.

White, W. B. (1988): Geomorphology and hydrology of karst terrains. Oxford University Press, New York, 1–480.

Wilson, P. A., Disckson, J. A. D. (1996): Radiaxial calcite: Alteration product of and petrographic proxy for magnesian calcite marine cement. Geology, 24, 945–948.

Witherspoon, P. A., Wang, J. S. Y., Iwai, K., Gale, J. E. (1980): Validity of cubic law for fluid flow in deformable rock fracture. Water Resources Research, 16, 6, 1016–1024.

Wu, Q., Kulatilake, P. H. S. W. (2012): REV and its properties on fracture system and mechanical properties and an orthotropic constitutive model for a jointed rock mass in a dam site in China. Computers and Geotechnics, 43, 124–142.

Yang, H. S., Kang, J. G., Kim, K. S., Kim, C. S. (2004): Groundwater flow characterization in the vicinity of the underground caverns in fractured rock masses by numerical modelling. Geosciences Journal, 8, 4, 401–413.

Yielding, G., Walsh, J. J., Watterson, J. (1992): The prediction of small scale faulting in reservoirs. First Break, 10, 449–460.

Yui, T. F., Huang, E., Xu, J. (1996): Raman spectrum of carbonaceous material: A possible metamorphic grade indicator for low-grade metamorphic rocks. Journal of Metamorph. Geol., 14, 4, 115–124.

Zhang, B., Liu, J. (2009): Classification and characteristics of karst reservoirs in China and related theories. Petroleum Exploration and Development, 36, 1, 12–29.

Zhou, Q., Xianming, X., Lei, P., Hui, T. (2014): The relationship between micro-Raman spectral parameters and reflectance of solid bitumen. International Journal of Coal Geology, 121, 1, 19–25.

Zotov, A., Galeev, M., Schott, J. (1998): An experimental study of kaolinite and dickite relative stability at 150–300 °C and the thermodynamic properties of dickite. Am. Mineral., 83, 516–524.